UNIVERSITY OF CALIFORNIA, SAN DIEGO

Identification and Characterization of IAMH1 Gene in Biosynthesis of Plant Hormone Auxin

A dissertation submitted in partial satisfaction of the
requirements for the degree
Doctor of Philosophy

in

Biology

by

Yangbin Gao

Committee in charge:

Professor Yunde Zhao, Chair
Professor Mark Estelle
Professor James W. Golden
Professor Bing Ren
Professor Martin F. Yanofsky

2015

The dissertation of Yangbin Gao is approved, and it is acceptable in quality and form for publication on microfilm and electronically:

_____

_____

_____

_____

_____

Chair

University of California, San Diego

2015

DEDICATION

To Light, which makes this world being, and to Love, which make this world living. To my family, my mentors, my friends, and to myself.

EPIGRAPH

One is the child of the divine law.

After one come two,

after two come three,

after three come all things.

—Laozi, Tao Te Ching

TABLE OF CONTENTS

LIST OF FIGURES

LIST OF TABLES

ACKNOWLEDGMENTS

Thanks to my advisor Professor Yunde Zhao for mentoring me through one of the most important and rewarding stages of my life. Thanks to my committee members, Professor Mark Estelle, Professor Jim Golden, Professor Bing Ren and Professor Marty Yanofsky for all the support when I needed them. Thanks to Xinhua Dai for keeping the lab up and running the whole time. Thanks to all other Zhao lab past and current members for the help and fun over the years. Thanks to Shaohe Wang and Mark Moyle, for the numerous *Scientific* lunches we had together.

Chapter 1 in full, is a reprint of the material as it appears in Part 1.1 in Auxin and Its Role in Plant Development, 2014. Gao, Yangbin; Zhao, Yunde. Springer, 2014. The dissertation/thesis author was a primary investigator and author of this paper.

Chapter 2 in full, is a reprint of the material as it appears in Molecular Plant, 2013, Gao, Yangbin; Zhao, Yunde. The dissertation/thesis author was a primary investigator and author of this paper.

Chapter 3 in full, is a reprint of the material as it appears in Journal of Integrative Plant Biology, 2014, Gao, Yangbin; Zhao, Yunde. The dissertation/thesis author was a primary investigator and author of this paper.

Chapter 4 in full, is a reprint of the material as it appears in Proceedings of the National Academy of Sciences, 2015, Gao, Yangbin; Zhang, Yi; Zhang, Da; Dai, Xinhua; Estelle, Mark; Zhao, Yunde. The dissertation/thesis author was a primary investigator and author of this paper.

Chapter 5, in part is currently being prepared for submission for publication of the material. Gao, Yangbin; Zhang, Da; Dai, Xinhua; Guo, Xiuhua; Zhao, Yunde. The dissertation/thesis author was a primary investigator and author of this material.

VITA

2004	Bachelor of Science, College of Life Sciences, Peking University, Beijing, P.R.China
2008-2011	Graduate Teaching Assistant, University of California, San Diego
2009-2014	Research Assistant, University of California, San Diego
2015	Doctor of Philosophy, University of California, San Diego

PUBLICATIONS

Yangbin Gao, Yi Zhang, Da Zhang, Xinhua Dai, Mark Estelle, and Yunde Zhao, Auxin binding protein 1 (ABP1) is not required for either auxin signaling or Arabidopsis development, *Proceedings of the National Academy of Science*s, 2015. 112(7): p. 2275-2280

Yangbin Gao and Yunde Zhao, Specific and heritable gene editing in Arabidopsis, *Proceedings of the National Academy of Sciences*, 2014. 111(12): p. 4357-4358.

Yangbin Gao and Yunde Zhao, Self-processing of ribozyme-flanked RNAs into guide RNAs in vitro and in vivo for CRISPR-mediated genome editing. *Journal of Integrative Plant Biology*, 2014. 56(4): p. 343-349.

Yangbin Gao and Yunde Zhao, Epigenetic Suppression of T-DNA Insertion Mutants in Arabidopsis. *Molecular Plant*, 2012. 6(2):p. 539-545.

Yangbin Gao and Yunde Zhao, Part 1.1, Auxin Biosynthesis and Catabolism, Zažímalová, Eva, Petrasek, Jan, Benkova, Eva (Eds.), *Auxin and Its Role in Plant Development*, Springer, 2014. p. 21-38. Print.

ABSTRACT OF THE DISSERTATION

Identification and Characterization of IAMH1 Gene in Biosynthesis of Plant Hormone Auxin

by

Yangbin Gao

Doctor of Philosophy in Biology

University of California, San Diego, 2015

Professor Yunde Zhao, Chair

The plant hormone auxin plays indispensable roles in every aspect of plant life. This dissertation centered on the major natural form of auxin, Indole-3-acetic acid (IAA). In Chapter 1, we reviewed the biosynthesis and degradation of auxin. In Chapter 2 we covered an unexpected finding when crossing an auxin biosynthesis mutant, *yuc1*, to a floral homeotic gene mutant, *agamous* (*ag*). The severe phenotypes of *ag* were suppressed in the F2 population, and the suppression could be stably transmitted to later generations even without the presence of *yuc1* mutation. We demonstrated that this suppression was mediated by T-DNA insertions in the two genes, and it was related to epigenetic

changes in the *ag* mutant. We also demonstrated that this phenomenon is not rare, and advised caution when interpreting results obtained from T-DNA mutants. In Chapter 3, we introduced a novel technology for improved control of guide RNA (gRNA) production when using CRISPR systems for genome editing or gene activation/suppression. We employed self-cleaving ribozymes and attached them to both ends of a gRNA sequence to enable the expression of gRNAs using RNA polymerase II promoters. We showed that the ribozyme-flanked gRNA design is functional both in vitro and in yeast, and this opens new doors for controlled gRNA expression which was not possible using RNA polymerase III promoters. In Chapter 4, we reported a surprising finding that a null mutant of an auxin-related gene *abp1* generated using our ribozyme-based CRISPR technology described in Chapter 3 did not show any developmental defects, which is contrary to previous findings that *abp1* null mutants were embryonic lethal. We continued to identify another null *abp1* mutant which also had no obvious defects under normal growth conditions, and raised questions about the previous claims that *ABP1* is an essential gene and it encodes an auxin-binding protein which may function as an auxin receptor. In Chapter 5, we described the identification and characterization of auxin-biosynthesis genes *IAMH1* and *IAMH2* involved in converting Indole-3-acetamide (IAM) into IAA. We showed that IAMH1 could hydrolyze IAM into IAA both in vitro and in vivo and this finding added another missing piece in the auxin biosynthesis pathways.

Chapter 1

Introduction to Auxin Biosynthesis and Catabolism

1.1 Background

Auxin is an essential hormone for many aspects of plant growth and development [1]. Plants have evolved a sophisticated network to control auxin levels with spatial and temporal precision in response to environmental cues and developmental signals. Indole-3-acetic acid (IAA), the main natural auxin in plants, can be produced from de novo biosynthesis. Free IAA, which is the presumed active form of auxin, can also be released from IAA conjugates including IAA esters, IAA-saccharides, and IAA-amino acids. A third probable route for producing IAA is to convert indole-3-butyric acid (IBA) to IAA using enzymes similar to those used in -oxidation of fatty acids. When auxin levels need to be lowered, plants employ several mechanisms to deactivate IAA. IAA can be quickly converted into the presumed inactive forms by reaction of the carboxyl group of IAA with amino acids, sugars, and other small molecules. The IAA conjugates may serve as a first step for the eventual complete degradation of IAA. IAA is also

inactivated by oxidation of the indole ring of IAA. For example, IAA can be converted to 2-oxindole-3-acetic acid (OxIAA). In this chapter, we discuss the progress made in the area of auxin biosynthesis and metabolism in the past few years.

1.2 De Novo Auxin Biosynthesis

De novo auxin biosynthesis is broadly divided into two categories: Tryptophan (Trp) dependent and Trp independent. Trp-independent auxin biosynthesis pathway was proposed two decades ago based on results from feeding plants with labeled Trp and Trp biosynthetic intermediates and from studies on Trp-deficient mutants [2, 3]. However, the molecular mechanisms and genes for the Trp-independent pathway are not known. Therefore, the Trp-independent pathway will not be discussed further in this chapter.

Trp has long been known as a precursor for the production of IAA in plants. Feeding plants with labeled Trp yields labeled IAA, indicating that plants have the enzymes to convert Trp to IAA [2, 3]. Many biosynthetic pathways have been elucidated using analytic biochemistry techniques in combination with labeled precursors and intermediates. For example, the biosynthetic routes for brassinolide and ethylene have been established long before the biosynthetic genes have been identified [4, 5]. However, the classic feeding and analytic biochemical approaches failed to identify the key components for Trp-dependent plant auxin biosynthesis pathways. There are several reasons for this apparent failure.

First, Trp is a precursor for many metabolites (Figure 1.1). Trp is a precursor for indole-3-pyruvate (IPA), tryptamine (TAM), indole-3-acetaldoxime (IAOx), indole-3-acetamide (IAM), indole-3-acetonitrile (IAN), and indole-3-acetaldehyde (IAAld) (Figure 1.1). *Arabidopsis* and many other plants have the capacity to produce all of the abovementioned intermediates (Figure 1.1) at a given developmental stage [6, 7]. Some

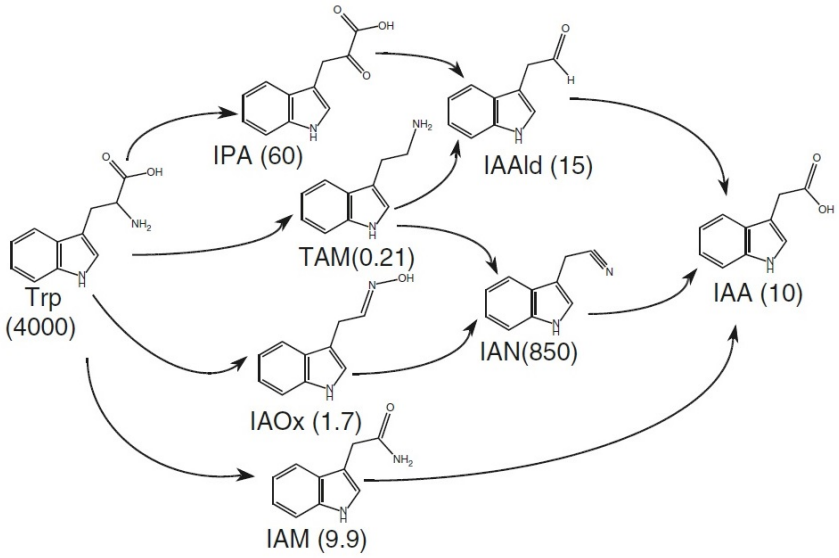

Figure 1.1: IAA Biosynthesis Pathway. Selected tryptophan metabolic intermediates. *Arabidopsis* plants produce all of the intermediates shown in the figure. The numbers in parenthesis refer to the actual concentrations in ng/g fresh weight. *IAA* indole-3-acetic acid, *IAAld* indole-3-acetaldehyde, *IAOx* indole-3-acetaldoxime, *IAM* indole-3-acetamide, *IAN* indole-3-acetonitrile, *IPA* indole-3-pyruvate, *TAM* tryptamine, and *Trp* tryptophan.

of the intermediates such as IAN exist in very high concentrations (Figure 1.1) [7]. Such a complex profile of Trp metabolism makes it difficult to identify Trp-dependent IAA synthesis intermediates. Second, some of the intermediates are intrinsically unstable in vitro and can be nonenzymatically converted to other compounds during the experimental process, therefore complicating the analysis of metabolic profiling. For example, IPA is readily converted nonenzymatically into IAA in vitro [8]. Third, most of the Trp metabolic intermediates display auxin activities during in vitro bioassays (Figure 1.2). In the presence of IAM in growth media, light-grown *Arabidopsis* seedlings have long hypocotyls and epinastic cotyledons (Figure 1.2). The IAM-induced phenotypes are identical to those observed in auxin overproduction mutants [9–11]. Therefore, the phenotypes of plants grown on IAM media are likely caused by overaccumulation of IAA in plants. *Arabidopsis* seedlings grown on IAN-containing media produce more

adventitious roots and have short primary roots [12](Figure 1.2). The IAN-induced phenotypes are very similar to those observed in plants grown on IAA-containing media, suggesting that IAN is probably converted to IAA in plants (Figure 1.2). Indeed, a genetic screen for mutants insensitive to IAN identified *Arabidopsis* nitrilase genes that encode enzymes for the hydrolysis IAN to IAA [12, 13]. Interestingly, treatments with IAN or IAM cause auxin overaccumulation in plants and high-auxin phenotypes. However, the IAM-induced phenotypes are dramatically different from those caused by IAN (Figure 1.2). It is speculated that both IAM and IAN need to be metabolized into IAA to show auxin activities as the observed phenotypic differences may be simply caused by different tissue specificities of the hydrolytic enzymes for IAM and IAN. Although it is very clear that Trp metabolic intermediates can be converted to IAA in plants, it is difficult to determine how important their contribution to the total IAA pool under natural conditions is. The fact that plants produce a large number of Trp metabolic intermediates (Figure 1.1) and that some of the Trp metabolites have auxin activities when added to growth media (Figure 1.2) made it very difficult to dissect Trp-dependent auxin biosynthesis pathways using classic analytic biochemistry techniques alone.

The main criterion for determining whether a Trp metabolite is important for de novo auxin biosynthesis is to use the deletion test. If the intermediate is important for auxin biosynthesis, we expect that plants show dramatic developmental defects similar to those observed in mutants defective in auxin transport or signaling if the plants lose the ability to make the intermediate. Recent results from a combination of analytic biochemical studies and *Arabidopsis* genetics research have established that the main auxin biosynthesis pathway in *Arabidopsis* is a simple two-step pathway that converts Trp to IAA (Figure 1.3). The pathway is highly conserved throughout the plant kingdom.

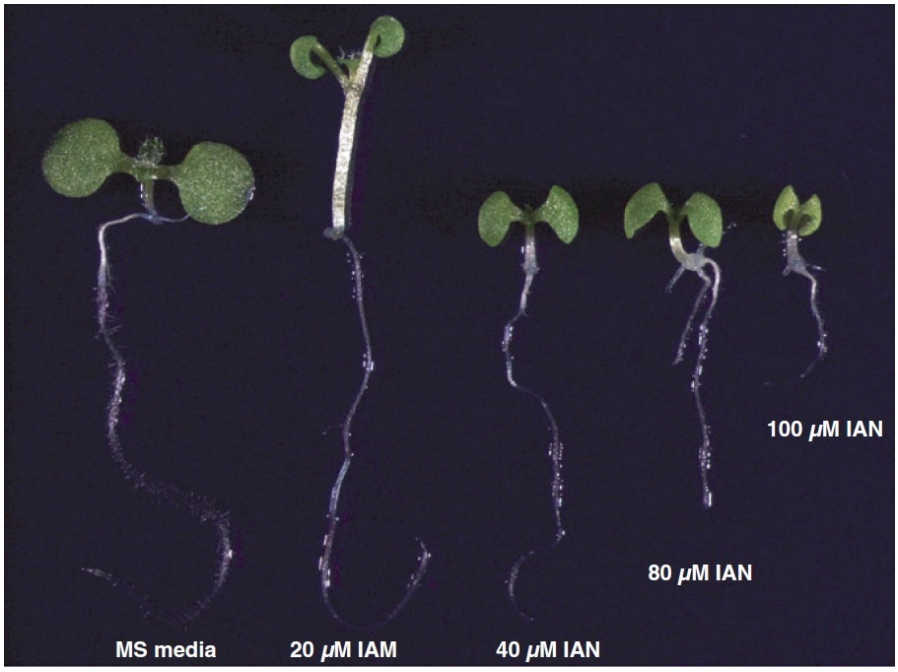

Figure 1.2: Auxin response of *Arabidopsis* to Tryptophan metabolites. Some tryptophan metabolites display auxin activities. Indole-3-acetamide (IAM) stimulates hypocotyl elongation and causes epinastic cotyledons. Indole-3-acetonitrile (IAN) inhibits primary root elongation and stimulates adventitious root initiation.

1.2.1 The TAA/YUC Pathway as the Main Auxin Biosynthesis Pathway

The YUCCA flavin-containing monooxygenases catalyze the rate-limiting step.

The YUCCA (YUC) flavin-containing monooxygenase (FMO) gene was identified as a key auxin biosynthesis gene a decade ago from an activation-tagging screen for long hypocotyl mutants in *Arabidopsis* [11]. The dominant *yucca* (later renamed as *yuc1D*) mutant was caused by the insertion of four copies of the CaMV 35S transcriptional enhancer downstream of the *YUC* gene [11]. The enhancers greatly increase the *YUC* expression levels, resulting in dramatic developmental defects. Physiological and molecular studies demonstrated that *yuc1D* is an auxin overproduction mutant [11]. Direct auxin measurements show that *yuc1D* contains 50% more free IAA than wild-type

Arabidopsis plants. Moreover, the auxin reporter DR5-GUS is greatly upregulated in *yuc1D* further supporting that *yuc1D* is an auxin overproduction mutant. It was suggested that YUC flavin-containing monooxygenases catalyze a rate-limiting step in auxin biosynthesis [11].

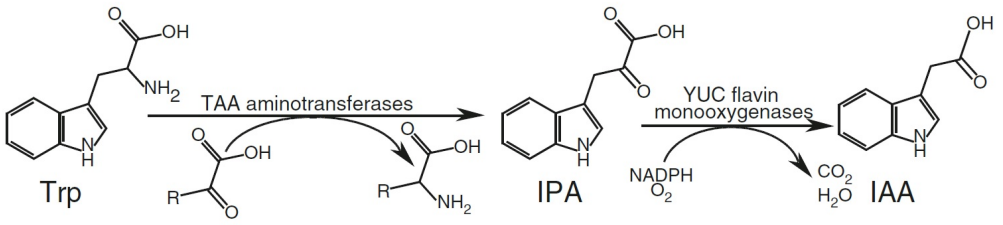

Figure 1.3: Two-step reaction from Trp to IAA. A tryptophan-dependent auxin biosynthesis pathway in plants. The TAA family of aminotransferases produces indole-3-pyruvate (IPA) from tryptophan (Trp) and the YUC flavincontaining monooxygenases catalyze the conversion of IPA into indole-3-acetic acid (IAA)

YUC was later found to be a member of a gene family with 11 genes in the *Arabidopsis* genome. The founding member was renamed as *YUC1*. Overexpression of any of the *YUC* family members leads to auxin overproduction phenotypes in *Arabidopsis*, suggesting that all of the *YUC* genes participate in auxin biosynthesis [14, 15]. The *YUC* genes have overlapping functions and inactivation of a single *YUC* gene does not cause any obvious developmental defects [14, 15]. The observed genetic redundancy among *YUC* genes may provide an explanation for why *YUC* genes had not been discovered previously by forward loss-of-function genetic screens. Detailed analyses of various *yuc* mutant combinations have demonstrated that *YUC* genes are essential for almost all of the major developmental processes including embryogenesis, seedling growth, vascular initiation and patterning, flower development, and plant architecture [14, 15]. For example, the *yuc1 yuc4* double mutants do not make tertiary veins in rosette leaves and fail to make continuous vascular boundless in flowers. Overall *yuc1 yuc4* flowers contain fewer floral organs and are completely sterile. A key piece of evidence that demonstrates the roles of *YUC* genes in auxin biosynthesis is the genetic rescue of *yuc1*

yuc4 mutants with the bacterial auxin biosynthesis gene iaaM under the control of the YUC1 promoter [14, 15].

The biochemical mechanisms of YUC-mediated auxin biosynthesis have been solved recently [16, 17]. YUC enzymes use NADPH and molecular oxygen to catalyze the oxidative decarboxylation of IPA to generate IAA (Figure 1.3). On the basis of sequence homology to the mammalian microsome FMOs, it is expected that YUCs use a flavin (FAD or FMN) as a cofactor. Expressed in and purified from *E. coli*, the *Arabidopsis* YUC6 displayed a bright yellowish colour, suggesting that YUC6 contains a flavin cofactor. HPLC and other experiments demonstrate that the cofactor in YUC6 is FAD, not FMN [17]. The YUC6-catalyzed conversion of IPA to IAA can be divided into three consecutive chemical steps: (1) reduction of FAD to FADH2 using electrons from NADPH; (2) binding of molecular oxygen to FADH2 to form the C4a-(hydro)peroxyl flavin intermediate; (3) the reaction of the C4a intermediate with IPA to produce IAA from decarboxylation of IPA (Figure 1.3 [17]. Interestingly, the reduction of YUC6 by NADPH takes place regardless of the presence of IPA. IPA also does not affect the rate of YUC6 reduction. The kinetic pattern and rate of the formation of the C4a intermediate is also not affected by IPA [17]. However, the decomposition of C4a intermediate is greatly accelerated by IPA [17]. The oxidized YUC6, reduced YUC6, and the C4a intermediate display distinct spectroscopic properties and can be monitored spectroscopically. The oxidized YUC6 shows two peaks at 376 and 448 nm in the UV-visible spectrum, while reduction of YUC6 causes the disappearance of the 448 nm peak. The YUC6 C4a-(hydro)peroxyl flavin intermediate has a maximum absorbance at 381 nm in a UV-visible spectrum [17]. The FAD cofactor in YUC6 provides a convenient handle to follow the progression of the YUC-catalyzed reactions. Besides IPA as a substrate, YUC6 can also catalyze the decarboxylation of phenyl-pyruvate (PPA) to produce phenyl-acetic acid (PAA), suggesting that YUC enzymes do not have strict

substrate specificities [17]. It is not known whether the YUC6-catalyzed conversion of PPA to PAA has any physiological significance. However, it is known that PAA displays auxin activities when added into growth media. Both YUC enzymes and mammalian FMOs share sequence homologies and form the C4a-(hydro)peroxyl flavin intermediate. Mammalian FMOs are mainly known for their ability to oxygenate soft nucleophiles such as nitrogen- or sulfur-containing molecules, whereas YUCs such as YUC6 oxygenate electrophilic substrates such as IPA and PPA [17–19]. However, mammalian FMOs recently have been shown to use electrophilic substrates as well and YUCs were previously shown to oxygenate soft nucleophiles in vitro [11, 20, 21]. The stability of the C4a intermediate is also quite different for YUCs and mammalian FMOs. The YUC6 intermediate has a half-life of about 20 s, whereas that of some FMOs from mammalian cells is more than 30 min [17–19]. It is important to use both in vitro enzymatic assays and in vivo genetic evidence to determine the physiological functions of flavin-containing monooxygenases.

In the presence of excess PPA or IPA, some uncoupled YUC6 reactions still take place and produce hydrogen peroxide. The uncouple ratio is about 4% [17]. It is not clear whether the uncoupled reaction plays any physiological role. It is conceivable that H_2O_2 produced from the uncoupled reaction may participate in deactivating YUC enzymes, providing an intrinsic mechanism for turning off auxin biosynthesis.

Genetic, physiological, and biochemical studies have unambiguously demonstrated that the YUC family of flavin-containing monooxygenases plays a key role in auxin biosynthesis. Genetic evidence suggests that the conversion of IPA to IAA is the rate-limiting and the committed step for IAA biosynthesis.

Tryptophan Aminotransferase of *Arabidopsis* (TAA) family of aminotransferases plays a key role in auxin biosynthesis

Three groups independently discovered that TAA1, the founding member of a large family of aminotransferases, is an important auxin biosynthesis enzyme [22–24]. Mutations in *TAA1*, which is also called *SAV3*, *WEI8*, and *TIR2*, alter shade-avoidance responses, cause resistance to ethylene and to the auxin transport inhibitor NPA [22–24]. Although inactivation of *TAA1* alone does not cause dramatic developmental phenotypes, simultaneously disruption of *TAA1* and its close homolog *TAR2* leads to defects in vascular pattern formation and in flower development in *Arabidopsis*. The *taa* mutants produce less free IAA compared to wild-type plants [22–24].

TAA1 and its related proteins catalyze the transfer of the amino group from Trp to pyruvate or to -ketoglutarate to produce IPA and Ala or Glu (Figure 1.3) in vitro. Therefore, it is important to keep in mind that *TAA* genes not only produce IPA but also affect the homeostasis of other -keto acids and other amino acids. It is not clear which -keto acid is the preferred in vivo acceptor of the amino group from Trp.

TAAs and YUCs were previously placed in two separate pathways [11, 22, 23]. But several recent genetic studies have demonstrated that YUCs and TAAs participate in the same pathway [16, 25, 26]. The *yuc* mutants and *taa* mutants share many similarities. For example, *yuc1 yuc2 yuc4 yuc6* quadruple mutants have dramatic vascular and floral defects, which are also observed in *taa1 tar2* double mutants [14, 22]. In fact, all of the characteristics of *taa* mutants can be phenocopied by inactivating certain combinations of *YUC* genes [26]. Overexpression of *YUC* genes leads to auxin overproduction phenotypes, which are dependent on the presence of functional *TAA* genes [26]. Furthermore, *taa* mutants are partially IPA deficient, whereas *yuc* mutants accumulate IPA, suggesting that *TAA* genes participate in IPA production and that YUCs use IPA as a substrate [16, 26]. Finally, recent biochemical studies on the catalytic mechanisms of YUC flavin

monooxygenases provide the final proof of the TAA/YUC two-step pathway as the main auxin biosynthesis pathway [16, 17, 27].

The TAA/YUC pathway is widely distributed throughout the plant kingdom. *YUC* genes from maize [28], rice [29–32], tomato [33], petunia [34], strawberry [35], and other species [36, 37] have been functionally characterized and they all participate in auxin biosynthesis. The *TAA* genes in maize have also been shown to participate in auxin biosynthesis [38]. The committed step for auxin biosynthesis is catalyzed by the YUC flavoproteins. Thus the YUC-catalyzed reaction has to be tightly controlled. It has been shown that *YUC* genes are only expressed in discrete groups of cells [14, 15]. Such tight control of YUC transcription provides a mechanism for temporal and spatial regulation of auxin production.

1.2.2 Other Trp-Dependent Auxin Biosynthesis Pathways

Trp is metabolized into several other indolic compounds (Figure 1.1), some of which show auxin activities when applied to plants (Figure 1.2). The physiological roles of the indolic compounds other than IPA in auxin biosynthesis are still ambiguous. That a compound can be metabolized into IAA both in vitro and in vivo does not mean that the compound is actually an important contributor to auxin biosynthesis in plants. Further genetic analysis of the genes responsible for generating the Trp metabolic intermediates (Figure 1.1) is needed to assess the roles of the compounds in auxin biosynthesis.

IAM pathway.

Arabidopsis and maize have detectable amount of IAM [7], which is the key intermediate in the bacterial auxin biosynthesis pathway characterized in *Agrobacterium* and *Pseudomonas* two decades ago [10, 39]. In plant pathogenic bacteria, Trp is oxidized by the iaaM Trp-2-monooxygenase to IAM that is subsequently hydrolyzed by iaaH to produce IAA. Unlike the bacterial IAM pathway, the genes and enzymes responsible

for producing IAM in plants have not been identified. It appears that plants do not have genes with high sequence homology to the bacterial iaaM gene. Therefore, IAM may be synthesized using a different mechanism. It is possible that IAM may be synthesized from IAA as a way to control free IAA levels. Conversion of IAA to IAM may be accomplished using mechanisms similar to glutamine biosynthesis.

Hydrolysis of IAM occurs in plants as feeding plants with IAM leads to elevated auxin levels and high-auxin phenotypes (Figure 1.2). It is proposed that a group of hydrolases, which are homologous to the bacterial hydrolase iaaH, plays a role in converting IAM to IAA [40, 41]. It is still inconclusive whether IAM is an important auxin biosynthesis intermediate in plants because IAM-deficient mutants have not been identified.

TAM pathway.

Tryptamine is presumably produced by Trp decarboxylase, but the enzymes responsible for the reaction in *Arabidopsis* have not been characterized. Sequence homology-based prediction may not lead to the correct identification of the genes. TAM was a proposed substrate for the YUC flavin monooxygenases [11, 36], which have now been shown to catalyze the conversion of IPA to IAA in vitro and in vivo. However, all of the flavin-containing monooxygenases form the C4a-(hydro)peroxyl flavin intermediates, which are the catalytically active intermediates. The C4a intermediate can do both nucleophilic and electrophilic reactions, depending on the reaction conditions. For example, mammalian FMOs have long been recognized for their roles in xenobiotic metabolism by reacting with soft nucleophiles such as nitrogen-containing compounds [19]. It has also been shown that Human FMOs can catalyze a BaeyerVilliger type reaction, in which the C4a intermediate reacts with an electrophilic carbonyl carbon [21]. To date, it has not been ruled out that TAM is an important intermediate in auxin biosynthesis; however, biosynthesis and metabolism of TAM are not well understood.

IAN pathway.

IAN is very abundant compared to other Trp metabolites (Figure 1.1). IAN stimulates adventitious root development and inhibits primary root elongation (Figure 1.2). The conversion of IAN to IAA is catalyzed by nitrilases. Inactivation of nitrilase genes leads to resistance to exogenous IAN, but the nitrilase mutants do not display obvious developmental defects observed in known auxin signaling and transport mutants [12, 13]. *Arabidopsis* genome contains four copies of the nitrilase gene. The developmental consequences of disrupting all four nitrilase genes have not been investigated, partially due to the fact that two of the copies are immediately adjacent to each other on the same chromosome. Therefore, it is still an open question whether IAN plays a significant role in auxin biosynthesis.

The routes for IAN production are not well understood either. It has been reported that metabolism of indolic glucosinolate yields IAN [42]. However, maize does not produce glucosinolates, but still produces IAN, suggesting that other routes can produce IAN. It has been suggested that IAN may also be produced from other indolic compounds such as IAOx [7].

IAAld pathway.

IAAld was previously proposed as an intermediate in the IPA pathway for auxin biosynthesis [1]. In plants, it is now known that IAAld is not an intermediate in the IPA pathway [16, 26] as IPA is converted to IAA by the YUC flavin-containing monooxygenases without producing IAAld [17]. In some IAA-producing bacteria, IAAld is produced from IPA by IPA decarboxylases [43]. IAAld can be further oxidized into IAA by aldehyde oxidases. In *Arabidopsis*, genes homologous to the bacterial IPA decarboxylases appear not to play a role in auxin biosynthesis. Inactivation of *Arabidopsis* aldehyde oxidases does not disturb auxin homeostasis, suggesting that it is very likely that IAAld does not contribute significantly to de novo auxin biosynthesis [16]. However, IAAld

can also be oxidized by aldehyde dehydrogenases, which have not been characterized in *Arabidopsis*.

IAOx pathway.

IAOx has only been detected in *Arabidopsis* and related species [16]. Monocots such as rice and maize do not have detectable levels of IAOx [16]. In *Arabidopsis*, CYP79B2 and CYP79B3 convert Trp directly to IAOx [44, 45]. Overexpression of *CYP79B2* in *Arabidopsis* leads to long hypocotyl and epinastic cotyledons, a phenotype that is also observed in *YUC* overexpression lines, suggesting that IAOx can be a precursor for IAA biosynthesis [45]. IAOx is also a precursor for indolic glucosinolate biosynthesis [9,46]. When the genes encoding glucosinolate biosynthesis enzymes are mutated, more IAOx is fluxed into IAA biosynthesis, causing auxin overproduction phenotypes [9,46]. For example, the *sur1* and *sur2* mutants that are defective in glucosinolate biosynthesis overproduce auxin, which leads to the development of long hypocotyls and numerous adventitious roots.

It appears that *CYP79B2* and textitB3 are the only genes responsible for producing IAOx in *Arabidopsis*. The *cyp79b2 cyp79b3* double mutants appear to completely abolish the biosynthesis of IAOx and the double mutants have no detectable amount of IAOx [7]. The double mutants have subtle growth defects when grown at high temperature, but have no obvious phenotypes under normal growth conditions [45]. Therefore, it is believed that IAOx is not an essential intermediate for auxin biosynthesis. Nor is IAOx a universal intermediate for auxin biosynthesis.

In summary, after three decades molecular genetics studies in *Arabidopsis*, the picture of de novo auxin biosynthesis has become clearer. The two-step Trp-dependent pathway catalyzed by TAAs and YUCs is the main auxin biosynthesis pathway that plays essential roles in almost all of the main developmental processes. In retrospect, *Arabidopsis* probably is not the best model for auxin biosynthesis studies for two main

reasons. First, the *Arabidopsis* glucosinolate biosynthesis pathway really complicated the analyses of IAA biosynthesis because the glucosinolate biosynthesis intermediate IAOx can be converted into IAA. The aforementioned glucosinolate mutants such as *sur1* and *sur2* had dramatic auxin overproduction phenotypes [9, 46]. Second, the genetic redundancy within *YUCs* and *TAAs* in *Arabidopsis* made it difficult for loss-of-function studies. The single *Arabidopsis yuc* or *taa* mutants do not show dramatic auxin phenotypes. Only the multiple mutants of *taa* or *yuc* display dramatic developmental defects [14, 15, 22]. In contrast, some monocots such as maize offer a relatively simpler system for analyzing auxin biosynthesis. Maize does not produce indolic glucosinolate [7]. Furthermore, inactivation of a single *YUC* gene or *TAA* gene in maize leads to dramatic developmental phenotypes, whereas inactivation of at least two *YUC* genes or *TAA* genes in *Arabidopsis* is needed to cause main developmental defects [28, 38].

1.3 IAA Production from Non-De Novo Pathways

Besides de novo in loco synthesis and transportation from neighboring cells, free IAA can also be made available by releasing IAA from its conjugated forms or from indole butyric acid (IBA) [47]. In fact, the majority of IAA in plants exists in the conjugated forms, which are proposed to serve as a storage pool. It is known that IAA can be conjugated via ester bonds with simple alcohols and with sugars such as glucose and myo-inositol or via amide bonds with amino acids, peptides, or proteins. Free IAA can be produced when the conjugates are hydrolyzed. Hydrolysis of conjugates provides plants with a potentially faster way to modulate free IAA levels than de novo biosynthesis. For example, in the germinating seeds of maize, large amount of IAA is released from the endosperm from its ester form to support the growth of developing seedlings [48]. Some of the enzymes responsible for hydrolyzing IAA-sugar or IAA-amino acids have been

characterized and they show different substrate specificities and are developmentally regulated [49–53].

1.3.1 Conversion of IBA to IAA

IBA has long been used in agriculture for promoting root initiation/growth from plant cuttings. *Arabidopsis* plants accumulate detectable amount of IBA. However, it is not understood how IBA is synthesized in plants. IBA is known to inhibit primary root elongation and stimulate lateral root formation. Genetic screens for *Arabidopsis* mutants resistant to exogenous IBA have identified many loci (*ibr*, IBA resistant). The majority of the *ibr* loci encode enzymes related to -oxidation of fatty acids or biogenesis of peroxisome, where -oxidation takes place. The genetic data suggest that the observed auxin activities of IBA depend on the conversion of IBA to IAA [54, 55]. However, it has not been completely ruled out that IBA itself has some biological activities [56].

The physiological roles of IBA-derived IAA are difficult to determine because the enzymes responsible for IBA to IAA conversion may also participate in other pathways such as fatty acid metabolism. Recent characterization of mutations resistant to IBA leads to the discovery that disruption of *ENOYL-COA HYDRATASE2* (*ECH2*) gene causes defects in IBA responsiveness, but appears not to affect sugar and fatty acid metabolism. Further analysis of *ech2* and other *ibr* mutants demonstrated that IBA-derived IAA plays important roles in root hair development and cotyledon cell expansion [55, 57].

1.3.2 Release of Free IAA from IAA Conjugates

IAA conjugates with ester-link to sugars and small alcohols or amide-link to amino acids and peptides have been identified in plants. The various conjugates may serve as a storage form of IAA and can release free IAA when needed. The most studied case

of releasing free IAA from conjugates is the hydrolysis of IAA-amino acid conjugates. Among the 20 potential amino acid conjugates, 19 (except IAA-Arg) were tested for their ability to release free IAA in a bioassay based on root elongation in *Arabidopsis* [52]. It was shown that IAA-Ala, -Leu, -Phe, -Asn, -Gln, -Glu, -Gly, -Met, -Ser, -Thr, and -Tyr inhibited root elongation by more than 50% at 40 μM, suggesting that these amino acid conjugates can be hydrolyzed to release free IAA. In contrast, IAA-Asp, -Cys, -His, -Ile, -Lys, -Pro, -Trp, and -Val appeared not a source for free IAA [52]. Genetic screens for *Arabidopsis* mutants resistant to IAA-Leu and IAA-Ala identified a family of hydrolases including *IAALeu Resistant 1* (*ILR1*), *IAAAla resistant* (*IAR3*), and the *ILR1-like protein* (*ILL2*) responsible for releasing free IAA from the IAA-amino acid conjugates [50–53]. The *ilr1 iar3 ill2* triple mutants are resistant to several IAA-amino acid conjugates and have shorter hypocotyl and fewer lateral roots than wild-type plants, suggesting that releasing free IAA from conjugates plays important roles in IAA homeostasis and plant development [53].

1.4 Deactivation of IAA

The active form of IAA is believed to be free IAA. The carboxyl group in IAA is essential for its auxin activities. IAA is inactivated by complete oxidation, a process that is still not well understood. IAA can also be taken out of action by forming various conjugates with alcohols, sugars, and amino acids [47].

1.4.1 Synthesis of IAA Conjugates

Great progresses have been made in recent years towards understanding the enzymes responsible for synthesizing IAA esters and amide conjugates. In maize, synthesis of IAA-ester with sugar starts with the formation of IAA-glucose that is

preceded by activation of glucose by the formation of glucose-UDP that is then joined with IAA. IAA-glucose is further converted to other IAA-sugar ester conjugates that are mostly believed to be a storage form of IAA [58–60]. The formation of methyl IAA by the IAMT1 methyl transferase has been implicated in regulating leaf development in *Arabidopsis* [61].

In *Arabidopsis*, 20 amidosynthases encoded by the large *Gretchen Hagen 3* (*GH3*) family of genes conjugate IAA as well as some other plant hormones such as jasmonic acid and salicylic acid with amino acids to form amide conjugates [62–64]. *GH3* genes are among the early-induced genes by auxin treatments [62]. Originally discovered as being able to adenylate IAA in vitro, GH3 amidosynthases are later shown to be responsible for synthesizing IAA-amino acid conjugates. The adenylyl-IAA serves as the activated intermediate and readily reacts with some amino acids [64]. Some of the IAA-amino acid conjugates can be hydrolyzed to release free IAA, while some of the conjugates appear non-hydrolyzable in vivo [52]. The latter group of IAA-conjugates may serve as a way to inactivate IAA. For example, once IAA-Asp is formed, it would not be hydrolyzed and the conjugated IAA is consequently permanently deactivated. IAA-Asp is also known as a target for oxidative degradation. GH3 proteins have also been shown to play roles in response to environmental stimuli such as light and wounding processes, possibly through the regulation the formation of IAA, jasmonic acid, and/or salicylic acid conjugates [47]. Interestingly, some of the IAA conjugates possesses antagonist effects against IAA. Externally applied IAA-Trp effectively antagonizes the inhibitory effects of IAA treatment in *Arabidopsis* roots [65, 66]. IAA-peptide and IAA-protein conjugates have also been discovered [67], indicating that IAA may serve as a small molecular tag, but their functions are still unclear.

1.4.2 IAA Degradation via Oxidation

IAA starts the oxidative degradation either with decarboxylation on the side chain or with oxidation of the indole ring. Very little is known regarding oxidative degradation of IAA. It has been reported that peroxidase may be involved in the oxidative decarboxylation of IAA [68]. Oxidative intermediates including OxIAA have been discovered in plants [69–72]. In *Arabidopsis*, other IAA metabolites such as N-(6-hydroxyindol-3-ylacetyl)-phenylalanine (6-OH-IAA- Phe), N-(6-hydroxyindol-3-ylacetyl)-valine (6-OH-IAA-Val), and 1-O-(2-oxoindol-3-ylacetyl)-beta-d-glucopyranose (OxIAA-Glc) have been observed with OxIAA-Glc being the main oxidative product. Recently, it was reported that in *Arabidopsis* roots, OxIAA is the major catabolic product of IAA [73]. Because OxIAA has little auxinic effects, irreversible oxidation of IAA into OxIAA effectively removes the IAA from the auxin pool. Another recent discovery in rice shed light on the genes underlying the conversion of IAA to OxIAA [27]. Rice plants with a mutation in the *Dioxygenase for Auxin Oxidation* (*DAO*) gene have elevated free IAA levels in anthers and ovaries and are defective in anther dehiscence, pollen fertility, and seed development [27]. The *dao* mutants also do not have detectable level of oxIAA, and the purified DAO protein expressed in *E. coli* could convert IAA to oxIAA in vitro [27]. The new findings mark the beginning of understanding the molecular and genetic mechanisms underlying IAA oxidation and the roles of oxidative degradation of IAA in auxin homeostasis.

1.5 Acknowledgments

Chapter 1 in full, is a reprint of the material as it appears in Part 1.1 in Auxin and Its Role in Plant Development, 2014. Gao, Yangbin; Zhao, Yunde. Springer, 2014. The dissertation/thesis author was a primary investigator and author of this paper.

Chapter 2

Epigenetic Suppression of T-DNA Insertion Mutants in *Arabidopsis*

2.1 Abstract

T-DNA insertion mutants have been widely used to define gene functions in *Arabidopsis* and in other plants. Here, we report an unexpected phenomenon of epigenetic suppression of T-DNA insertion mutants in *Arabidopsis*. When the two T-DNA insertion mutants, *yuc1-1* and *ag-TD*, were crossed together, the defects in all of the *ag-TD* plants in the F2 population were partially suppressed regardless of the presence of *yuc1-1*. Conversion of *ag-TD* to the suppressed *ag-TD* (named as *ag-TD** did not follow the laws of Mendelian genetics. The *ag-TD** could be stably transmitted for many generations without reverting to *ag-TD*, and *ag-TD** had the capacity to convert *ag-TD* to *ag-TD**. We show that epigenetic suppression of T-DNA mutants is not a rare event, but certain structural features in the T-DNA mutants are needed in order for the suppression to take place. The suppressed T-DNA mutants we observed were all intronic T-DNA mutants and the T-DNA fragments in both the trigger T-DNA as well as in the suppressed T-DNA

shared stretches of identical sequences. We demonstrate that the suppression of intronic T-DNA mutants is mediated by trans-interactions between two T-DNA insertions. This work shows that caution is needed when intronic T-DNA mutants are used.

2.2 Introduction

Agrobacterium-mediated plant transformation is achieved when the T-DNA (Transfer DNA) fragment from the modified Ti plasmids is integrated into chromosomes in plant cells. T-DNA transformation can be used as a tool for insertional mutagenesis and also serves as an efficient vehicle for delivering target genes into plant cells. T-DNA fragments randomly insert into a plant genome during transformation and, when a T-DNA insertion is inserted in an exon or an intron, it often leads to the inactivation of the gene. As part of the different functional genomic initiatives in *Arabidopsis*, a number of T-DNA insertional mutagenesis have been conducted and currently we have access to large libraries of sequence-indexed T-DNA insertion lines in *Arabidopsis* [74–76]. The T-DNA insertion mutants are tremendous resources for the determination of gene function and the elucidation of metabolic/signaling pathways. T-DNA mutants in *Arabidopsis* have become the first choice for many scientists because (1) the mutants are easily accessible through the *Arabidopsis* stock centers and (2) the mutants are often null alleles. T-DNA insertion mutants have been extensively used in reverse genetics and in studies of genetic interactions in *Arabidopsis*.

Studies on genetic interactions between two non-allelic mutants often provide insights into the functions of the two genes and the relative positions of the genes in a genetic pathway [77, 78]. Phenotypes of a mutant can be suppressed or enhanced by mutations in other genes. Synergistic genetic enhancement between two mutants often suggests that the two genes have overlapping functions or participate in parallel

pathways [77]. If the two mutants are not null alleles and the two genes have no sequence homology, synergistic enhancement can also suggest that the two genes function in the same pathway [79]. Genetic suppression of the phenotypes of one mutant by a mutation in another gene could be achieved through several mechanisms [78]. A mutant could be rescued if the general machinery of transcription and/or translation is altered. For example, a mutation that converts a sense codon to the stop codon UAG in a gene can be suppressed if the anti-codon in Trp-tRNA is mutated from CCA to CUA. Additionally, genetic suppression could also take place if the suppressor removes toxic proteins or metabolic intermediates. A mutant can also be suppressed if protein interactions or gene dosages are altered. Genetic screens for enhancers and suppressors for mutants have led to the discoveries of the regulatory mechanisms of major signaling and metabolic pathways.

In general, the phenotypes of a mutation are suppressed when an extragenic suppressor is present. Removal of the suppressor leads to the restoration of the original mutant phenotypes. In this paper, we report an unexpected phenomenon that phenotypes of a T-DNA insertion mutant are partially suppressed by another T-DNA insertion at another locus. Remarkably, the suppressed phenotypes could be stably transmitted for generations even in the absence of the suppressor T-DNA insertion. We crossed an auxin biosynthesis mutant *yuc1-1* to a floral mutant *ag-TD* in order to generate the *yuc1-1 ag-TD* double mutants for analyzing the roles of auxin in flower development. Both *yuc1-1* and *ag-TD* are T-DNA insertion mutants (Figure 2.1A) and both are loss-of- function, recessive mutants. The *YUC1* gene encodes a flavin-containing monooxygenase involved in auxin biosynthesis [11, 14, 15]. The *yuc1-1* mutant has no obvious developmental defects because of the existence of other homologous *YUC* genes in *Arabidopsis* [14]. *AGAMOUS* (*AG*) is an essential gene for reproductive organ formation in *Arabidopsis* [80]. The *ag-TD* mutant displays the characteristic ag loss-of-function phenotypes including

the transformation of stamens into petals, loss of floral meristem determinacy, and a lack of carpels and stamens [80]. Surprisingly, none of the *ag-TD* plants in the F2 population displayed the typical *ag-TD* phenotypes, regardless of the presences of *yuc1-1*. We demonstrate that suppression of *ag-TD* is mediated by trans-interaction between the T-DNA insertions in *yuc1-1* and *ag-TD*. Although gene silencing mediated by trans-interaction between two T-DNA insertions has been well documented [81], it has never been reported previously that such a trans-interaction among T-DNA insertions can lead to the restoration of gene functions inactivated by the same T-DNA insertions. We show that suppression of intronic T-DNA insertional mutants is frequently induced by other T-DNA insertions, suggesting that caution is needed when intronic T-DNA mutants are used in *Arabidopsis*.

2.3 Results

2.3.1 Suppression of an *agamous* T-DNA Insertion Mutant by *yuc1-1*

To investigate the mechanisms of local auxin biosynthesis in specifying flower development, we combined the auxin biosynthesis mutant *yucca1* (*yuc1*) [14] with a known floral homeotic mutant *agamous* (*ag*) [80]. We chose the recessive T-DNA insertion mutants *ag-TD* and *yuc1-1* because both mutants are in the Columbia background. In both *ag-TD* and *yuc1-1*, the T-DNA is inserted in an intronic region Figure 2.1A). The *yuc1-1* does not show obvious developmental defects [14], but *ag-TD* fails to produce any stamens and carpels (Figure 2.1). We crossed *ag-TD*$^{+/-}$ to *yuc1-1* and genotyped the F1 plants to select the *ag-TD*$^{+/-}$ *yuc1-1*$^{+/-}$ plants (Figure 2.1B), which did not have obvious defects as expected. We let the F1 *ag-TD*$^{+/-}$ *yuc1-1*$^{+/-}$ plants self-pollinate and collected the F2 seeds (Figure 2.1B). We analyzed the F2 population in order to identify the *ag-TD yuc1-1* double mutants. Unexpectedly, none of the *ag-TD* plants

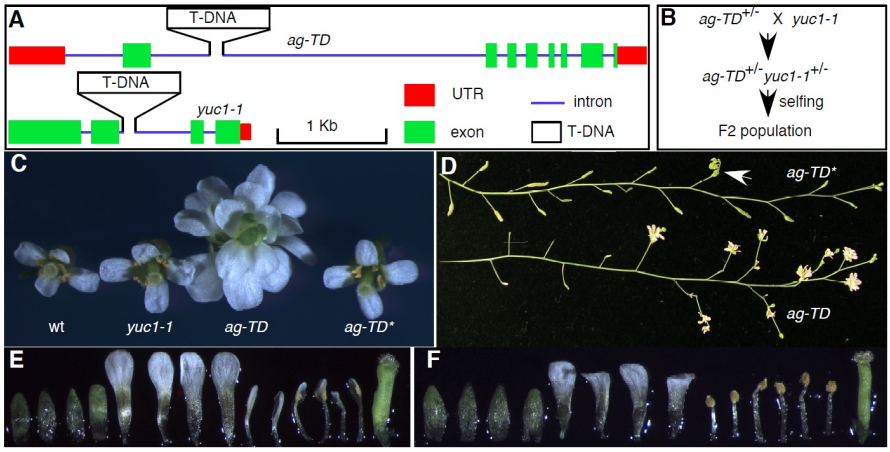

Figure 2.1: Suppression of *ag-TD* by Crossing *ag-TD*$^{+/-}$ to *yuc1-1*. (A) A diagrammatic presentation of the two T-DNA insertion mutants: *yuc1-1* and *ag-TD*. (B) The crossing scheme. The *ag-TD*$^{+/+}$ *yuc1-1*$^{+/-}$ F1 plants were discarded. (C) Suppression of the floral defects in *ag-TD* in the F2 population. From left to right: WT, *yuc1-1*, *ag-TD*, and *ag-TD**. (D) Phenotypic difference between *ag-TD* and *ag-TD** inflorescence. (E) Production of petal-like stamens in *ag-TD**. (F) Normal floral organs in *ag-TD**.

displayed the typical *ag* phenotypes, indicating that *ag-TD* phenotypes were partially suppressed (Figure 2.1C). We named the plants with *ag-TD* genotype but without *ag* flower phenotypes as *ag-TD** (Figure 2.1C). Note that *ag-TD** is still homozygous for the T-DNA insertion as shown in Figure 2.1A, but the *AG* function is no longer inactivated by the T-DNA insertion in *ag-TD**. The *ag-TD** plants were fertile and produced viable seeds (Figure 2.1D). The suppression of *ag-TD* was only partial, because some *ag-TD** flowers still contained petal-like stamens (Figure 2.1E) and indeterminate flowers (Figure 2.1D). However, the majority of *ag-TD** flowers had flower with four sepals, four petals, and one gynoecium consisting of two fused carpels (Figure 2.1F).

2.3.2 The *yuc1-1* Is Not Required in the F2 Population for *ag-TD** Phenotypes

We genotyped the F2 plants from the cross between *ag-TD* and *yuc1-1* for the presence of *ag-TD* and *yuc1-1*. Among the 176 F2 individual plants, 56 were *ag-TD*,

indicating that the T-DNA insertion at the AG locus segregated normally. Among the *ag-TD* plants, 43 did not contain T-DNA insertion at *YUC1*, 13 were *yuc1-1*$^{+/-}$, and zero were *yuc1-1*. Because both *AG* and *YUC1* are on chromosome IV and they are about 15 cM apart, it was expected that very few *ag-TD yuc1-1* would be observed in the F2 population. Floral defects in all of the *ag-TD* plants in the F2 population were partially suppressed. Overall, 80% of the *ag-TD YUC1* plants were suppressed well enough to be fertile. We noticed that all of the *ag-TD*$^{-/-}$ *yuc1-1*$^{+/-}$ plants were able to set seeds, suggesting that the presence of the *yuc1-1* mutation enhanced the suppression. However, the continued presence of the *yuc1-1* mutation was not required to suppress *ag-TD*.

2.3.3 The *ag-TD** Is Genetically Stable

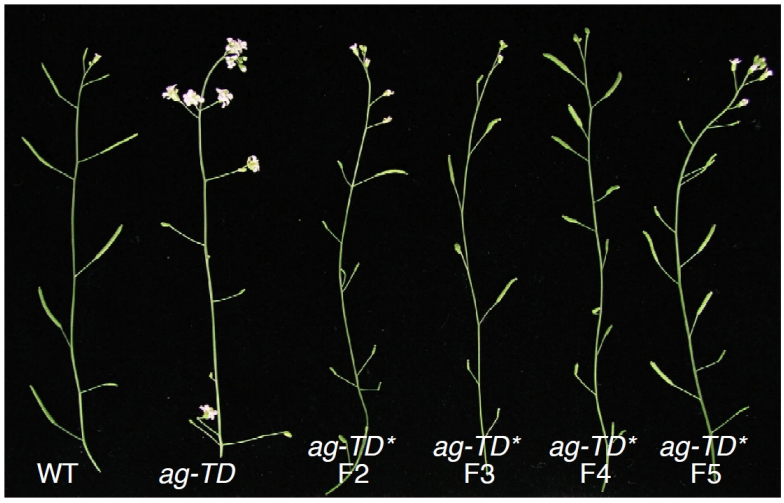

Figure 2.2: Inheritability of *ag-TD**. The *ag-TD** has been transmitted for five generations. Note that the fifth generation of *ag-TD** produced more seeds than the earlier generations of *ag-TD**.

To test whether *ag-TD** phenotypes could be stably transmitted, we let the *ag-TD** plants self-fertilize and studied the progeny for five generations. All of the progeny of *ag-TD** was fertile in every generation and set a good number of seeds. We also noticed that the later generation of *ag-TD** produced more seeds than the earlier generation of

*ag-TD** (Figure 2.2). We concluded that, once *ag-TD* was converted to *ag-TD**, the *ag-TD** does not spontaneously revert to *ag-TD* over generations (Figure 2.2).

We crossed *ag-TD** to wild-type (WT) Columbia (Col) and let the F1 plants self-pollinate to generate an F2 population for analysis of the genotypes and phenotypes. Among the 98 plants analyzed, 23 were homozygous for the T-DNA insertion at the *AG* locus and all of the *ag-TD* plants displayed the *ag-TD** phenotypes, indicating that *ag-TD** is very stable.

2.3.4 The *ag-TD** Is Able to Convert *ag-TD* to *ag-TD**

We tested whether *ag-TD** could induce similar changes in *ag-TD*. We crossed *ag-TD** to *ag-TD*$^{+/}$ plants and half of the resulting F1 plants were homozygous with the T-DNA insertion as expected. The F1 plants that presumably had the *ag-TD**/*ag-TD* genotype were fertile and set a good number of seeds. We further analyzed the F2 plants generated from *ag-TD**/*ag-TD* selfing. Among the 68 F2 plants analyzed, 66 plants behaved like *ag-TD**. Two plants had weak *ag-TD* phenotypes and did not set seeds. Our data suggest that *ag-TD** has the capacity to convert *ag-TD* into *ag-TD**.

2.3.5 The *ag-TD** Cannot Suppress Non-T-DNA *ag* Alleles

We have shown that *ag-TD** allele induced the conversion of *ag-TD* into *ag-TD**. We investigated whether *ag-TD** could also restore the *AG* functions in other non-T-DNA *ag* mutant alleles. We used the strong *ag-3* mutant and the weak *ag-4* mutant alleles for the experiments (Figure 2.2A). Both *ag-3* and *ag-4* carried point mutations at splice junction sites (Figure 2.2A) [82, 83]. We crossed *ag-TD** to *ag-3*$^{+/-}$, and the resulting F1 *ag-TD**/*ag-3* plants still displayed the typical ag mutant phenotypes and were sterile, suggesting that *ag-TD** could not rescue *ag-3*. When we crossed *ag-TD** to the weak

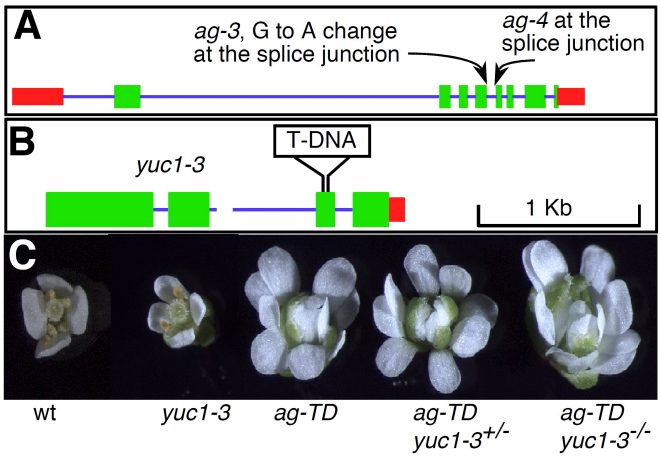

Figure 2.3: Suppression of *ag* Involves Special Alleles of *ag* and *yuc*. (A) The two non-T-DNA alleles of *ag* used in this study. (B) Allele of *yuc1-3*. *yuc1-3* has a T-DNA insertion in the third exon. (C) The *ag-TD* was not suppressed by *yuc1-3*.

ag-4$^{+/-}$ plants, the *ag-TD*/ag-4* plants were partially fertile. Normally, the *ag-4* plants produce some stamens and carpel-like structures, but are sterile in our growth conditions. The *ag-TD*/ag-4* plants could set seeds and their phenotypes were intermediate when compared to *ag-TD** and *ag-4* plants. We further analyzed the F2 population produced from selfing the *ag-TD*/ag-4* plants. All of the homozygous *ag-TD* plants from the F2 population displayed the same phenotypes as those of *ag-TD**. The *ag-TD*/ag-4* plants in the F2 population were fertile, but all of the *ag-4* plants were sterile. Our data indicate that *ag-TD** could not rescue non-T-DNA *ag* mutants.

2.3.6 Conversion of *ag-TD* to *ag-TD** Depends on a Specific *yuc1* T-DNA Allele

The *ag-TD* mutant was rescued when it was crossed to *yuc1-1* (Figure 2.1). We tested whether other T-DNA insertion mutants in *yuc1* could also convert *ag-TD* to *ag-TD**. We crossed *ag-TD* to *yuc1-3* (Figure 2.3B). The *yuc1-3* contained a T-DNA insertion at the third exon in the *YUC1* gene (Figure 2.3B). Although both *yuc1-1* and

yuc1-3 were T-DNA insertion lines, they were generated using two different plasmids. The *yuc1-1* was generated using the plasmid pROK2, which renders kanamycin resistance in *Arabidopsis*. The *yuc1-3* was produced using a different plasmid that contains the *SPM transposase* gene and the *BAR* gene.

We genotyped the F2 population generated from selfing *ag-TD*$^{+/-}$ *yuc1-3*$^{+/-}$ to identify *ag-TD* plants. All of the *ag-TD* plants in the F2 population displayed the typical *ag-TD* phenotypes regardless of the existence of *yuc1-3* mutation and none of the *ag-TD* plants set any seeds (Figure 2.3C). We also isolated *ag-TD yuc1-3* plants from the progeny of a single *ag-TD*$^{+/-}$ *yuc1-3* plant and the double mutants behaved like *ag-TD*. These results suggest that inactivation of *YUC1* is not sufficient to trigger the suppression of *ag-TD* and that the suppressor and the suppressed T-DNA mutants need to be generated from similar plasmids.

2.3.7 Production of Full-Length *AG* cDNA Using mRNAs from *ag-TD* and *ag-TD**

We investigated whether the *ag-TD* to *ag-TD** conversion is caused by an increased expression of *AG* in *ag-TD**. We designed PCR primers to amplify the portion of *AG* cDNA starting from the start codon to the stop codon. To our surprise, *ag-TD* produced the full-length *AG* cDNA, suggesting that *ag-TD* is a partial loss-of-function mutant. We sequenced the *AG* cDNA from WT plants, *ag-TD*, and *ag-TD**, and discovered that there were no structural differences among the cDNAs from the analyzed genotypes. It is difficult to compare the expression levels of *AG* in WT and in *ag-TD* using RTPCR or Northern blot because the floral structures are quite different for the two genotypes. We used RNA in situ hybridization to detect the expression levels of *AG* in WT, *ag-TD*, and *ag-TD**. The *AG* expression in *ag-TD* was weaker than that in WT, but *ag-TD** clearly had more *AG* expression than *ag-TD*, suggesting that the conversion of

ag-TD to *ag-TD** correlates with an increased *AG* mRNA level in *ag-TD** (Figure 2.4A).

2.3.8 Kanamycin Resistance Gene Is Silenced in *ag-TD**

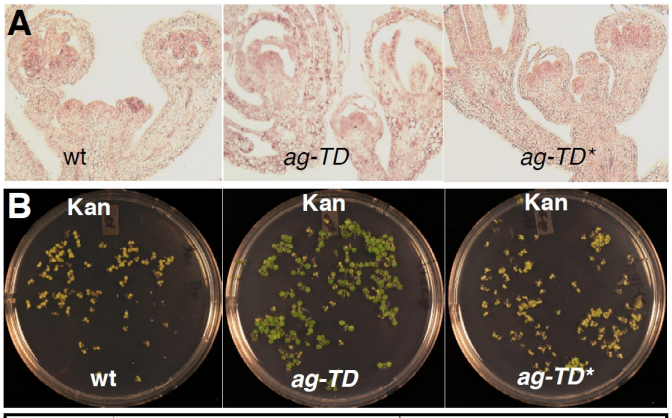

Phenotypes of T1 Plants	Number of plants (Total = 25)	Percentage
Strong *ag-TD* like	6	24
Weak *ag-TD** (no seeds)	8	32
Strong *ag-TD** (with seeds)	11	44

Figure 2.4: Suppression of *ag-TD* Is Probably Mediated by *Trans*-Interaction between Two T-DNA Insertions. (A) In situ analysis of *AG* expression in WT, *ag-TD*, and *ag-TD**. (B) Conversion of *ag-TD* to *ag-TD** correlates with the loss of kanamycin resistance. (C) Conversion of *ag-TD* to *ag-TD** can be achieved by the introduction of a T-DNA fragment that expresses the *NPT II* gene. About 75% of the T1 plants with *ag-TD* genotype did not show the typical *ag* phenotypes.

We hypothesized that perhaps the partial restoration of *AG* function in *ag-TD** might be caused by structural changes in DNA/chromatin in or near the T-DNA insertion. Such DNA/chromatin structural modifications might also alter the expression of the *Neomycin phosphotransferase II* (*NPT II*) gene, which renders plants resistant to kanamycin, within the T-DNA fragment. The *NPT II* gene in the T-DNA insertion made *ag-TD* plants resistant to kanamycin (Figure 2.4B) and, accordingly, about 25% of the progeny from *ag-TD*$^{+/-}$ plants were kanamycin-sensitive, suggesting that *ag-TD*

contains a single T-DNA insertion. In contrast, all of the *ag-TD** plants were kanamycin-sensitive (Figure 2.4B), although the *NPT II* gene still existed in *ag-TD**. These data suggest that transcripts from the T-DNA fragment are also affected by the epigenetic modifications that suppressed *ag-TD*.

2.3.9 Suppression of *ag-TD* by *Trans*-Interactions between T-DNA Loci

The observation that kanamycin resistance was lost in *ag-TD** suggested that *trans*-interactions between the T-DNA fragment in *yuc1-1* locus and the T-DNA in *ag-TD* may be responsible for the suppression of *ag-TD*. To test this hypothesis, we transformed *ag-TD*$^{+/-}$ plants with a construct that expressed both the *NPT II* and the *BAR* gene (Figure 2.4C). Transformants were selected on basta-containing media. Among the 26 T1 plants with *ag-TD* genotype, 76% were partially suppressed and 44% were fertile (Figure 2.4C), demonstrating that introduction of another T-DNA insertion that expresses *NPT II* gene is sufficient to suppress *ag-TD*. The suppression of *ag-TD* is likely mediated by *trans*-interactions among T-DNA insertions.

2.3.10 Suppression of T-DNA Mutants by Other T-DNA Insertions Is Not Rare

We have demonstrated that *ag-TD* is suppressed by *yuc1-1* and also by transforming a T-DNA fragment into *ag-TD*. We investigated whether other T-DNA insertion mutants can also be suppressed by similar T-DNA interactions. We crossed *yuc1-1* to *cob-TD*, which also contains a T-DNA insertion in the large intron (Figure 2.5A). The *COB* gene encodes a glycosylphosphatidylinositol (GPI) anchored protein and plays an important role in cellulose microfibril orientation in *Arabidopsis* [84, 85]. Inactivation

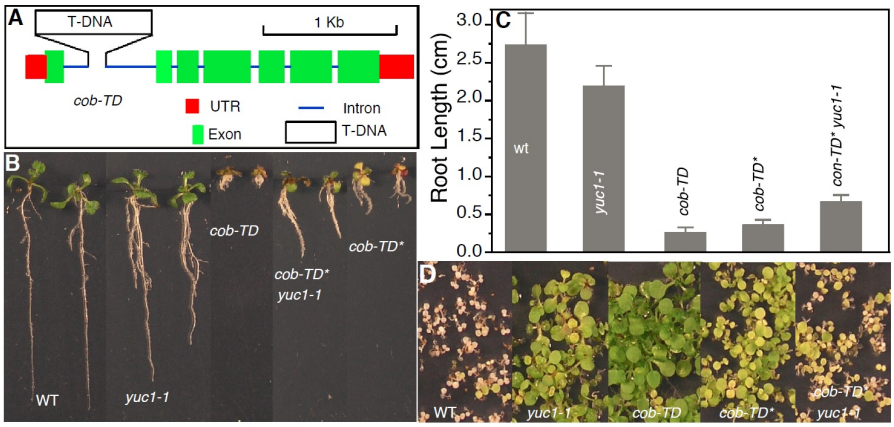

Figure 2.5: Partial Suppression of *cob-TD* by *yuc1-1*. (A) The *cob-TD* mutant with a T-DNA insertion in the large intron. (B) Suppression of *cob-TD* in the F2 population from a cross between *cob-TD* and *yuc1-1*. (C) Increased root length in *cob-TD**. (D) The conversion of *cob-TD* to *cob-TD** correlated with the loss of kanamycin resistance.

of *COB* by the T-DNA insertion led to very short roots and other defects (Figure 2.5B). However, all of the *cob-TD* plants in the F2 plants from the cross between *yuc1-1* and *cob-TD* had longer roots than the original *cob-TD* lines, indicating that *yuc1-1* also converted *cob-TD* to *cob-TD**, which was partially suppressed (Figure 2.5). The presence of *yuc1-1* made the suppression of *cob-TD* better (Figure 2.5B). This result is consistent with the observation that the *ag* phenotypes in *ag-TD yuc1-1*$^{+/-}$ were better suppressed than those in *ag-TD* alone. Interestingly, the conversion of *cob-TD* to *cob-TD** also led to the loss of kanamycin resistance (Figure 2.5D).

2.4 Discussion

In this paper, we presented the analyses of an unexpected epigenetic phenomenon in *Arabidopsis*. We showed that some *Arabidopsis* T-DNA mutants were stably suppressed by T-DNA insertions in other non-homologous loci. We proposed that a T-DNA insertion in one locus could trigger undefined epigenetic modifications at a different T-DNA insertion site. The epigenetic modifications in the T-DNA mutants were heritable

in the absence of the T-DNA suppressor. Because T-DNA mutants have been widely used in reverse genetics and in analyzing genetic interactions in *Arabidopsis*, this work suggests that we should be cautious about intronic T-DNA mutants.

2.4.1 Suppression Reported in this Work Violates Rules of Mendelian Genetics

When *ag-TD* was crossed to *yuc1-1*, all of the *ag-TD* plants in the F2 population were partially suppressed no matter whether *yuc1-1* was present or not, although the presence of *yuc1-1* rendered better suppression (Figure 2.1). The *ag-TD** not only could be stably transmitted for many generations in the absence of *yuc1-1* (Figure 2.2), but also had the ability to trigger new epigenetic suppressions in *ag-TD*. There are many similarities between the epigenetic suppression of T-DNA mutants and paramutation, a well-studied epigenetic phenomenon in Maize [86–89]. In paramutation, one allele (*B'*) causes heritable changes in another allele (*B-I*) of the same locus. Both the conversions of *B-I* to *B'* and *ag-TD* to *ag-TD** were triggered by a cross. Once *B-I* is converted to *B'*, the new *B'* from *B-I* can be stably transmitted. We have shown that *ag-TD** could also be stable for many generations (Figure 2.2). The newly converted *B'* can convert *B-I* to *B'* and we showed that *ag-TD** can convert *ag-TD* to *ag-TD**. The end results of paramutation appear to be unidirectional because it is always that *B-I* is converted to *B'*. In the cases of T-DNA suppression that we have analyzed, the suppression appeared to be one-directional as well. When *ag-TD** was crossed with *ag-TD*, *ag-TD* was always converted to *ag-TD**.

2.4.2 Epigenetic Suppression of T-DNA Mutants Is Triggered by *Trans*-Interaction between T-DNA Insertions

Several lines of evidence support the hypothesis that the conversion of *ag-TD* to *ag-TD** is probably caused by *trans*-interaction between T-DNA insertions. First, *ag-TD* mutant displays strong kanamycin resistance whereas *ag-TD** is kanamycin-sensitive (Figure 2.4). It has been demonstrated that *trans*-inactivation between homologous genes causes the loss of antibiotic resistance in T-DNA insertion mutants [81]. The T-DNA insertions in both *yuc1-1* and *ag-TD* are from the same plasmid; therefore, the *NPT II* transcripts from the T-DNA insertion at the *yuc1-1* locus have the capacity to induce the silencing of the *NPT II* gene in the T-DNA fragment at the *ag-TD* locus. Second, the conversion of *ag-TD* to *ag-TD** could also be achieved by transforming *ag-TD*$^{+/-}$ plants with a construct that expresses *NPT II* from the 35S promoter (Figure 2.4C).

We propose that transcripts such as the *NPT II* mRNA from the T-DNA insertions in *yuc1-1* and *ag-TD* interact *in trans* to cause the silencing of *NPT II*. It has been well documented that trans T-DNA interactions can lead to the silencing of homologous genes [81]. What is very unusual is that the silencing of the genes located in the T-DNA fragments such as *NPT II* is correlated with the restoration of the gene function inactivated by the T-DNA insertion.

It is often hypothesized that intronic T-DNA insertions disrupt gene function because transcripts cannot be properly spliced. However, some genes have very large introns that are spliced out properly from the primary transcripts, suggesting that other factors may also contribute to the inactivation of gene function by intronic T-DNA insertions. When a T-DNA fragment is inserted into an intron of a gene, the primary transcript from the gene contains the entire intron plus the T-DNA fragment if the transcription is not prematurely terminated within the T-DNA region. Therefore, it is

conceivable that transcripts from the T-DNA fragment such as the *NPT II* transcript may be able to form a partial duplex with the primary transcript when the *NPT II* gene is transcribed from the opposite direction. Such a duplex may affect proper processing of the primary transcript or even lead to degradation of the transcript. When those T-DNA-generated reverse transcripts are silenced by transcripts from another homologous T-DNA insertion (a process very similar to co-suppression), the duplex between the *NPT II* transcript and the primary transcript would be resolved. Consequently, the intronic T-DNA mutants are partially suppressed and the *NPT II* gene is silenced. We recognize that the *NPT II* transcript from the T-DNA insertion is similar to long intronic non-coding RNA, which causes epigenetic changes and affects gene expression levels [90].

Our findings indicated that intronic T-DNA insertion mutants can be easily suppressed by *trans*-interaction with another T-DNA. Therefore, the use of intronic T-DNA insertion mutants sometimes may lead to incorrect interpretations. We would like to point out that *trans*-interaction with another T-DNA insertion may not be the only trigger that is capable of causing the suppression of the phenotypes of an intronic T-DNA mutant. Environmental factors may also be able to cause the suppression of T-DNA mutants. For example, the intronic T-DNA insertion mutant *opr3* has long been recognized as a null allele and it produced no detectable Jasmonic acids (JAs) following wounding and looper infestation [91]. However, recently it was shown that the same *opr3* mutant became activated upon fungal infection and accumulated substantial levels of JAs. It was suggested that splicing of the T-DNA-containing intron might be responsible for the reactivation of *OPR3* [91]. In light of our findings, it is also possible that epigenetic modifications induced by fungal infection may play a role. Our study indicates that we should be careful about the use of intronic T-DNA mutants because some intronic T-DNA insertion mutants may undergo epigenetic changes that complicate interpretations of genetic interactions in *Arabidopsis*.

2.5 Methods

The T-DNA insertion mutants *cob-TD* and *yuc1-3* were obtained from the ABRC at Ohio. The *ag-TD* was from Dr Yanofsky. The *yuc1-1* was previously described [14,26]. For genotyping T-DNA mutants, we used PCR-based methods as previously described [76]. The gene-specific primers for genotyping *ag-TD* were 5'- ACGGCGTACCAATCGGAGCTAGGAGGA -3' and 5'- TCTAGCTAGTTTCACCTTATTCACTCTC -3'. Primers for genotyping *yuc1-1* and *yuc1-3* were 5'- GGTTCATGTGTTGCCAAGGGA -3' and 5'- CCTGAAGCCAAGTAGGCACGTT -3'. Gene-specific primers for *cob-TD* were 5'- TCCACTCCTCCTTCAAGCAAAGC -3' and 5'- CCATTTCATTGTAATGTTGCCTTC -3'. The T-DNA specific primer for genotyping *ag-TD*, *cob-TD*, and *yuc1-1* was JMLB1 (5'- GGCAATCAGCTGTTGCCCGTCTCACTGGTG -3'). T-DNA primer for *yuc1-3* was Spm32 (5'- TACGAATAAGAGCGTCCATTTTAGAGTGA -3'). RNA in situ hybridization was performed as described previously [14].

2.6 Funding

This work is partially supported by the N.I.H. R01GM068631 to Y.Z. and the N.S.F. Plant Genome DBI-0820729 to Y.Z.

2.7 Acknowledgments

We would like to thank Drs Marty Yanofsky, Juan Jose Ripoll, and Bing Ren for valuable discussions. We thank Dr Marty Yanofsky, Dr Juan Jose Ripoll, Miss Allison Zhao, and members of the Zhao lab for critical reading of the manuscript. No conflict of interest declared.

Chapter 2 in full, is a reprint of the material as it appears in Molecular Plant, 2013,

Gao, Yangbin; Zhao, Yunde. The dissertation/thesis author was a primary investigator and author of this paper.

Chapter 3

Self-processing of ribozyme-flanked RNAs into guide RNAs in vitro and in vivo for CRISPR-mediated genome editing

3.1 Abstract

CRISPR/Cas9 uses a guide RNA (gRNA)molecule to execute sequence-specific DNA cleavage and it has been widely used for genome editing in many organisms. Modifications at either end of the gRNAs often render Cas9/gRNA inactive. So far, production of gRNA in vivo has only been achieved by using the U6 and U3 snRNA promoters. However, the U6 and U3 promoters have major limitations such as a lack of cell specificity and unsuitability for in vitro transcription. Here, we present a versatile method for efficiently producing gRNAs both in vitro and in vivo. We design an artificial gene named *RGR* that, once transcribed, generates an RNA molecule with ribozyme

sequences at both ends of the designed gRNA. We show that the primary transcripts of *RGR* undergo self-catalyzed cleavage to generate the desired gRNA, which can efficiently guide sequence-specific cleavage of DNA targets both in vitro and in yeast. *RGR* can be transcribed from any promoters and thus allows for cell- and tissue-specific genome editing if appropriate promoters are chosen. Detecting mutations generated by CRISPR is often achieved by enzyme digestions, which are not very compatible with high-throughput analysis. Our system allows for the use of universal primers to produce any gRNAs in vitro, which can then be used with Cas9 protein to detect mutations caused by the gRNAs/CRISPR. In conclusion, we provide a versatile method for generating targeted mutations in specific cells and tissues, and for efficiently detecting the mutations generated.

3.2 Introduction

The CRISPR/Cas9 system (Clustered Regularly Interspaced Short Palindromic Repeats/CRISPR-associated endonuclease Cas9) has been shown to mediate efficient genome editing in human cells [92,93], mice [94], rat [95], zebrafish [96,97], *Caenorhabditis elegans* [98], *Drosophila* [99], yeast [92,100], *Arabidopsis* [101], and crop plants [101–103]. CRISPR/Cas9 relies on RNA-guided DNA cleavage to generate double-stranded breaks [104]. CRISPR provides a very simple approach for targeted gene disruption and targeted gene insertion. To disrupt a gene by CRISPR, only two components are needed: (1) the Cas9 protein that contains the nuclease domains, and (2) the guide RNA (gRNA) that provides sequence specificity to the target DNA. The first 20-nucleotide sequence at the 5'-end of the gRNA is complementary to the target sequence and it provides the specificity for the CRISPR/ Cas9 system [104]. The 3' portion of the gRNA forms certain secondary structures and is required for Cas9 activities. The

gRNA brings the Cas9 nuclease to the specific target and subsequently Cas9 generates double-stranded breaks in the target DNA at the protospacer-adjacent motif (PAM) site. Non-homologous end-joining repair of the double-stranded breaks often leads to deletions or small insertions that disrupt the target DNA.

There are two major challenges in using CRISPR for targeted mutagenesis: (1) production of the gRNAs, and (2) analysis of the CRISPR-generated mutations. The first 20- nucleotide sequence of the gRNA is used to guide targeted DNA cleavage. Additional bases at the 5'-end of gRNA or other modifications may abolish the gRNA's ability to guide DNA cleavage by Cas9 [104]. RNAs transcribed by RNA polymerase II (pol II), which is the polymerase responsible for the production of the majority of mRNAs, cannot be used as gRNAs because they undergo extensive processing and modification at both ends. Additionally, most mRNAs are actively transported from the nucleus into the cytoplasm after transcription, while the Cas9/gRNA only has access to the genomic DNA inside the nucleus. Most of the well-characterized promoters are transcribed by pol II and have not been used to produce gRNA for CRISPR. Therefore, promoters such as U3 and U6, which are transcribed by the RNA polymerase III (pol III) were previously chosen to produce gRNA in various organisms. There are many limitations to U6- or U3-based gRNA production. First, U6 snRNA and U3 snRNA are housekeeping genes and they are ubiquitously expressed. Therefore, they cannot be used to generate gRNAs with cell or tissue specificity. Second, the U6 and U3 promoters in many organisms have not been characterized, making it difficult to choose the correct U6/U3 promoters for CRISPR. Third, the U6 and U3 promoters are not suitable for routine in vitro production of gRNAs because RNA pol III is not commercially available. Furthermore, the U6 and U3 promoters limit the CRISPR target sequences to $G(N)_{20}GG$ and $A(N)_{20}GG$, respectively. Improved methods for producing gRNAs in vivo are needed in order to conduct targeted mutagenesis with spatial and temporal control in a wide

range of organisms.

The second challenge in using CRISPR for genome editing is detecting and analyzing the mutations generated. Mutations are often detected by enzyme digestion of a PCR product that contains the target region, followed by DNA sequencing. Restriction digestion can only work when a restriction site is altered and many useful mutations may not be detected by restriction digestion. CEL I-based enzyme digestion can also be used to detect mutations [105]. However, CRISPR often generates many different mutations in a tissue or an organism, making a CEL I-based method less effective. We believe that the best way to detect mutations caused by CRISPR is to use the specific gRNA and Cas9 protein to digest the PCR products that contain the target sequence [104]. However, such a method requires an easy and efficient way to produce gRNAs in vitro.

In this paper, we present a method that successfully overcomes the aforementioned challenges in using CRISPR for genome editing. We take advantage of the nuclease activity of ribozymes [106, 107] to design an artificial gene *RGR* (Ribozyme-gRNA-Ribozyme). We hypothesize that the primary transcripts of *RGR* undergo self-catalyzed cleavage to precisely release the designed gRNA. We show that gRNA is specifically released from the primary transcripts of *RGR* by self-processing in vitro. The produced gRNA efficiently guides Cas9-mediated cleavage of target DNA in vitro. Furthermore, we introduce the *RGR* gene into yeast under the control of the *alcohol dehydrogenase 1* (*ADH1*) promoter, which is transcribed by pol II, and we observe the targeted DNA cleavage in yeast. Our results demonstrate that production of gRNAs is no longer limited to a specialty promoter such as the U6 promoter, thereby enabling us to conduct genome editing with spatial and temporal precision if proper promoters are chosen. In addition, we demonstrate that the target sequences are no longer limited to $G(N)_{20}GG$ or $A(N)_{20}GG$ because our method does not require the specific G or A for transcription initiation for gRNA production as is the case for U6 and U3 promoters. We also show that the

efficient production of gRNAs by in vitro transcription from a commonly used promoter such as SP6 makes it very easy to use gRNA and Cas9 to detect mutations caused by CRISPR/Cas9.

3.3 Results

3.3.1 Design an RNA molecule with self-processing capacity for g-RNA production

We took advantage of the nuclease activities of ribozymes that catalyze the cleavage at a specific site within an RNA molecule. We designed an RNA molecule (pre-gRNA) that was predicted to undergo self-catalyzed processing (Figure 3.1A). The RNA molecule we designed contained a Hammerhead (HH) type ribozyme [108] at the 5'-end, a gRNA that targets a *green fluorescent protein* (*GFP*) gene in the middle, and a hepatitis delta virus (HDV) ribozyme [109] at the 3'-end (Figure 3.1A). After the self-cleavage at the predicated sites, the mature gRNA was released (Figure 3.1A). The gRNA was predicted to guide Cas9 to cut DNA at the targeted sites (Figure 3.1B). By altering only the first six nucleotides of the HH ribozyme, our design can be employed to generate gRNAs that target any DNA sequence with a PAM site (NGG). Previous CRISPR targets were limited to either $G(N)_{20}GG$ or $A(N)_{20}GG$.

3.3.2 Production of a gRNA by in vitro transcription and self-processing

The designed pre-gRNA molecule can be generated by in vitro transcription of the corresponding DNA sequence, which we named the Ribozyme-gRNA-Ribozyme (*RGR*) gene (Figure 3.2A). We placed the *RGR* gene under the control of the SP6 promoter and

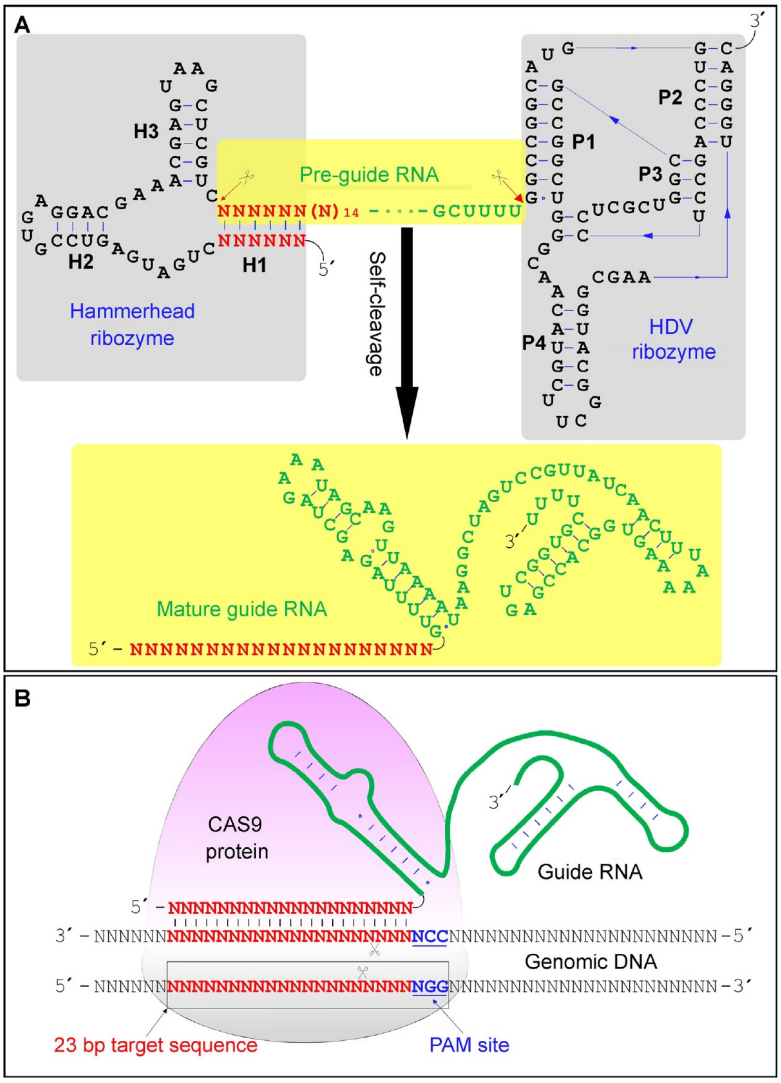

Figure 3.1: The schematic design of a self-processing RNA molecule for gRNA production. (A) The modular structure of the pre-gRNA, which contains a Hammerhead ribozyme at the 5' -end, the sequence-specific gRNA portion in the middle (shaded yellow), and a HDV ribozyme at the 3' -end. The predicted secondary structures of both ribozymes are shown. The hairpin (stem) regions in the Hammerhead ribozyme are labeled H1, H2, and H3. P1, P2, P3, and P4 refer to the hairpin regions in the HDV ribozyme. The pre-gRNA undergoes self-catalyzed processing to release the mature gRNA. The 5'-end (in red) of the mature gRNA is complementary to the target sequences and the 3'-end (in green) is universal for all gRNAs in this work. (B) Schematic representation of gRNA and Cas9-mediated cleavage of target DNA. Note that the target sequence contains the NGG PAM site, which is not in the gRNA.

conducted in vitro transcription using the commercially available SP6 RNA polymerase.

As shown in Figure 3.2B, the primary transcripts of the *RGR* were self-processed into

several RNA bands. The smallest RNA band was the predicted gRNA (Figure 3.2B). We introduced mutations in the HH ribozyme and in the HDV ribozyme individually to disrupt their self-processing ability. We also mutated the two ribozymes simultaneously. We then tested the self-processing ability of the mutated pre-gRNAs (Figure 3.2B, Lanes 2, 3, and 4, respectively). Disruption of the two ribozymes simultaneously led to a complete failure to self-process the transcripts (Figure 3.2B, Lane 4). Inactivation of the HH ribozyme (5'-end) blocked the separation of the 5'-end ribozyme from the rest of the RNA molecule, but did not affect the processing of the 3'-end HDV ribozyme (Figure 3.2B, Lane 2). On the other hand, mutations in the HDV ribozyme only disrupted the removal of the 3'-end portion of the pre-gRNA molecule (Figure 3.2B, Lane 3). We noticed that the processing ability of the HDV ribozyme was not as strong as that of the HH ribozyme because partial cleavage directed by the HDV ribozyme was observed (Figure 3.2B, Lanes 1 and 2).

3.3.3 Guide RNA molecules produced in vitro guided specific cleavage of the target DNA

We next investigated whether the gRNA molecules produced from in vitro transcription and self-processing have the ability to guide Cas9 to perform sequence-specific cleavage of the target DNA in vitro. When the gRNA, Cas9, and the PCR fragment containing the target sequence were mixed and incubated for 60 min, we observed efficient and complete cleavage of the target DNA (Figure 3.2C, Lane 1). The cleavage appeared to be specific because the sizes of the resulting DNA fragments were the same as predicted. We discovered that unprocessed pre-gRNA molecules generated from the in vitro transcription of the mutated RGR gene failed to guide the cleavage of the targeted sequences (Figure 3.2C, Lane 4). Removal of the HDV ribozyme alone was also insufficient to support Cas9 digestion (Figure 3.2C, Lane 2). However, gRNA with the

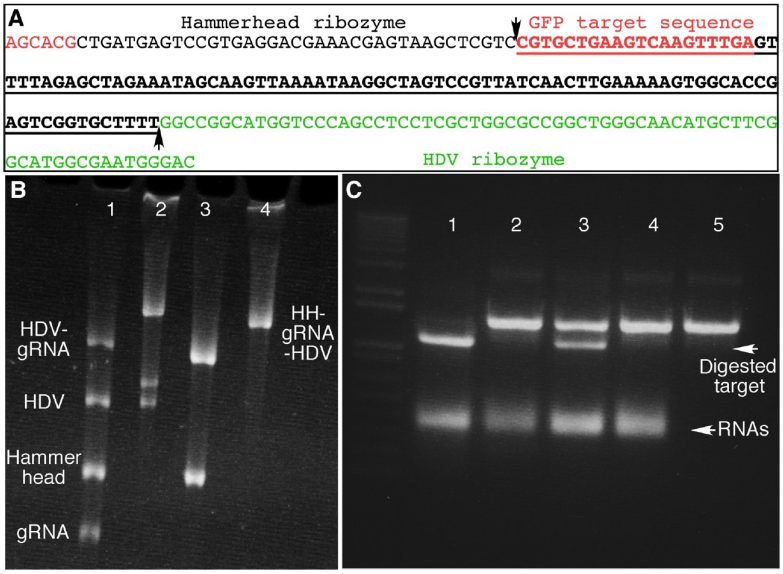

Figure 3.2: gRNA production and gRNA-mediated specific cleavage of a DNA target in vitro. (A) DNA sequence of the artificial gene *RGR* that encodes the pre-gRNA. The first six nucleotides (in red) of the Hammerhead (HH) ribozyme must be complementary to the first six nucleotides of the target sequence (in red). The entire mature gRNA sequence is in bold and is underlined. The HDV ribozyme is in green. The two arrows mark the cleavage sites for the ribozyme-catalyzed reactions. (B) Analysis of the self-processing capacity of transcripts generated by in vitro transcription. The primary transcripts are 416 bp long (extra bases are added to both ends of the pre-gRNA during in vitro transcription). The predicted size of mature gRNA is 100 bp, the length from the transcription initiation site to the Hammerhead cleavage site is 131 bp, and the length from the HDV cleavage site to the end is 185 bp. Lane 1: gRNA is released from the pre-gRNA with both functional ribozymes. Note that the cleavage of the HDV ribozyme is incomplete. Lane 2: the Hammerhead ribozyme is mutated, which does not prevent the processing of the 3'-end of HDV ribozyme. However, the processing of HDV ribozyme is incomplete. Lane 3: the HDV ribozyme is mutated and only the Hammerhead ribozyme is released. The self-processing of the 5'-end of the pre-gRNA is complete, but no mature gRNA is released. Lane 4: both Hammerhead and HDV ribozymes are mutated and no self-processing is observed. (C) The gRNA-mediated cleavage of target DNA in vitro. The PCR fragment of the *GFP* gene is used as a substrate for gRNA/Cas9 digestion. gRNA released from wild-type pre-gRNA leads to a complete digestion of the target DNA (Lane 1). However, RNAs from pre-gRNAs with mutations in the Hammerhead ribozyme fail to guide the target cleavage (Lanes 2 and 4). Interestingly, the gRNA with the 3'-end HDV ribozyme mutated is still partially active (Lane 3).

HDV ribozyme at the 3'-end still retained sufficient activity to guide Cas9 to cut target DNA (Figure 3.2C, Lane 3). The gRNAs used in the assays were not purified, suggesting

that the free ribozymes and other components from the in vitro transcription did not interfere with the Cas9/gRNA-mediated cleavage. These results bode well for using this method in vivo, where many other RNAs and proteins exist.

3.3.4 Guide RNAs produced from the ADH1 promoter guide specific DNA cleavage in yeast

We next tested whether our method for producing a self-processing RNA molecule to generate a gRNA could succeed in vivo. We placed the *RGR* gene under the control of the ADH1 promoter, which is transcribed by pol II (Figure 3.3A). The transcripts of the *RGR* gene contained the gRNA portion that was designed to target the *GFP* gene (Figure 3.3A). We introduced the plasmid along with another Cas9-expressing plasmid to a yeast strain that harbors a *GFP* gene in its chromosomes and that is brightly fluorescent (*Figure 3*B). We first analyzed whether our constructs disrupted the fluorescence displayed in the yeast cells. The yeast cells that harbored the plasmids failed to produce any fluorescence, indicating that the *GFP* gene had likely been disrupted in the cells (Figure 3.3B). Interestingly, partially processed pre-gRNA with the HDV remaining at the 3'-end displayed significant activity in vitro (Figure 3.2C, Lane 3). However, such an RNA molecule did not function in yeast as we did not observe any silencing of the GFP signal when the HDV was mutated in the pre-gRNA (data not shown).

We extracted the genomic DNA from the yeast cells and amplified the *GFP* gene by PCR. The PCR fragments were resistant to Cas9/gRNA digestion (Figure 3.3C). By sequencing, we found that deletion mutations were generated in the *GFP* gene as was expected for CRISPR-mediated mutations (Figure 3.3D).

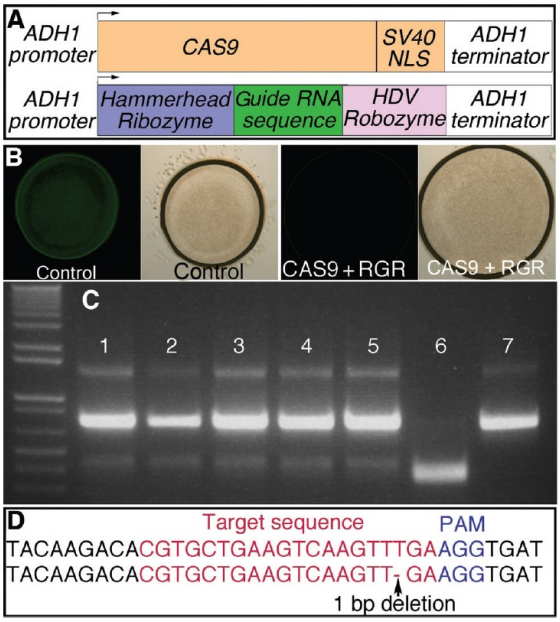

Figure 3.3: ADH1 promoter-driven expression of the pre-gRNA is sufficient to guide Cas9-mediated disruption of a target gene in yeast. (A) Schematic representation of the constructs that express Cas9 and the pre-gRNA. (B) Yeast cells that harbor the *GFP* gene display bright green fluorescence (left). The DIC image of the control is also shown. Expression of the Cas9 and the gRNA silences the fluorescence of GFP (right two panels). (C) PCR fragments of the *GFP* gene amplified from the genomic DNA of different yeast clones expressing *Cas9* and *RGR*. The GFP fragments are resistant to Cas9/gRNA in vitro cleavage, indicating that the target sites in the *GFP* gene have likely been mutated. Lanes 1-5: PCR fragments amplified from different yeast colonies. Lane 6: wild-type *GFP* fragment as a positive control. Lane 7: no gRNA was added. (D) DNA sequencing confirms that the *GFP* gene is mutated by expressing *Cas9* and the pre-gRNA in yeast. The target sequence and the 1 bp deletion are indicated (red). The PAM site (blue) is also marked.

3.4 Discussion

We demonstrate that gRNAs can be efficiently produced in vitro and in vivo from essentially any promoters when the primary transcripts are flanked by self-cleaving ribozymes. The produced gRNAs can guide Cas9-mediated specific cleavage of DNA targets both in vitro and in vivo. This work opens the door to conducting more sophisticated CRISPR-mediated genome editing in many organisms. Because gRNAs can now be produced using tissue-specific promoters, hormone-responsive promoters, environ-

mental signal-regulated promoters, and other well-characterized promoters; this work lays the foundation for studying the roles of specific genes in various developmental and pathological processes. For example, temporal control of gRNA production is necessary when sequential disruption of different genes is preferred, which cannot be achieved by modulating the Cas9 expression alone. Additionally, when multiplex gene targeting is desired, different *RGR* genes can be expressed as a single transcript under one single promoter. Furthermore, gRNA and Cas9 together enable us to cut specific DNA in vitro, thus greatly enhancing our ability to manipulate DNA in vitro.

There are two main structural differences between the gRNAs produced in this work and the gRNAs generated using U6 and U3 promoters. First, gRNAs transcribed from U6 and U3 promoters have a triphosphate group at the 5'-end whereas gRNAs generated from self-processing of the pre-gRNAs have a hydroxyl group at the 5'-end. Second, the 3'-end of the gRNAs reported in this work is 2',3'-cyclic phosphate while transcripts from U6 or U3 often end with hydroxyl groups at both 2' and 3' positions. Although both types of gRNAs possess the ability to guide the cleavage of target DNA in vivo, the structural features in the ends of our gRNAs may have advantages. For example, our gRNAs may be more stable because some nucleases require the 5'-terminal phosphate group for specific cleavage [110].

We have shown that we can effectively use Cas9 as a restriction enzyme in vitro to cut specific DNA sequences that complement the 20 nucleotides of the 5'-end of the gRNA. Because we have shown that the specific gRNAs can be easily produced from in vitro transcription (Figure 3.2), we can now generate specific Cas9 sites in DNA molecules to facilitate routine molecular cloning. This application is especially useful when no other restriction enzyme sites are available in the region. Another application we have successfully demonstrated in this work is using Cas9/gRNA to detect the mutations generated by CRISPR (Figure 3.3C).

Our system has the potential for automation and high-throughput production of gRNAs, thus laying the foundation for systematically knocking out every single gene in an organism using CRISPR technology. Because the *RGR* genes we designed mainly differ in the 20-nucleotide sequence encoding for the specific portion of the gRNA, every *RGR* gene can potentially be amplified by PCR with a pair of universal primers. If the SP6 or T7 promoter sequences are included in the primers, we can easily transcribe all of the *RGR* genes and produce the corresponding gRNAs using commercially available RNA polymerases (Figure 3.2). Amplification and in vitro transcription can be programmed for automation if thousands of different gRNAs are needed.

Only one construct is needed for generating a specific gRNA in vitro and in vivo. The construct can be transformed into a cell/organism to generate targeted modifications in the genome. The same construct also serves as the DNA template for amplifying the RGR gene using universal primers. The PCR fragments can be used for in vitro transcription to produce gRNAs, which along with Cas9 can be used for detecting mutations generated by the same gRNA.

3.5 Materials and Methods

3.5.1 Design ribozyme-flanked gRNAs

The gRNA sequence except for the target sequence was adapted from [93]. The sequence in the *GFP* gene targeted by the Cas9/gRNA in this study was 5'- CGTGCT-GAAGTCAAGTTTGAAGG -3', with the first 20 bp as the beginning of the gRNA. At the 5'-end of the gRNA was a HH ribozyme, and at the 3'-end of the gRNA was a HDV ribozyme. The design of both ribozymes was based on the work of Avis et al. (2012) [111]. The mutated HH ribozyme (mHH) had a 13 bp deletion at its 5'-end, which affected the H1 and H2 stem-loop region as well as the conserved CUGANGA

domain of the HH ribozyme (Figure 3.1). The mutated HDV ribozyme (mHDV) had a 15 bp deletion at its 3'-end, which affected the P2 and P4 region (Figure 3.1). Four different ribozyme-flanked gRNAs (pre-gRNA) were generated by overlapping PCR reactions: HH-gRNA-HDV (referred as Full), mHH-gRNA-HDV (referred as mHH), HH-gRNA-mHDV (referred as mHDV), and mHH-gRNA-mHDV (referred as mm).

3.5.2 Cloning, expression, and purification of Cas9

The human-codon-optimized *Cas9c* gene template was a generous gift from Luhan Yang (G. Church Laboratory, Harvard University). The *Cas9* gene was cloned into pET28a plasmid in order to express the N-terminally His-tagged Cas9 protein. The pET28a-Cas9 plasmid was transformed into BL21(DE3) (Invitrogen, Carlsbad, CA, United States). One single colony harboring pET28a-Cas9 was inoculated into 5 mL of Luria-Bertani (LB) media and grown at 250 rpm, 37 °C for 7 h. All of the 5 mL culture was transferred into 50 mL of LB and then grown overnight at 250 rpm, 17 °C. Of the overnight culture, 50 mL was transferred into pre-chilled 1000 mL of Terrific Broth (TB) media, and the resulting culture was grown at 250 rpm, 17 °C for 24 h. When the OD600 reached 1, the cells were chilled on ice for 30 min. Isopropylthio-β-galactoside was then added to the final concentration of 1 mmol/L, and $MgCl_2$ was added to the final concentration of 10 mmol/L. The cells were then grown at 250 rpm, 17 °C for 48 h before harvesting.

Cells were collected by centrifugation at 5000 rpm for 10 min. Cells were then frozen at -80 °C for 30 min, followed by thawing on ice for 15 min. Cells were re-suspended in 18 mL lysis buffer (50 mmol/L HEPES, pH 7.5, 300 mmol/L NaCl, 10 mmol/L imidazole). Lysozyme was added to the final concentration of 1 mg/mL. Cells were incubated on ice for 30 min and DTT was added to the final concentration of 2 mmol/L. Cells were then lysed by sonication on ice for 80 s.

His-tagged Cas9 protein was purified from the cell lysate using Ni-NTA Agarose from Qiagen, Hilden, Germany following the manufacturer's instructions. The wash buffer contained 50 mmol/L HEPES, pH 7.5, 300 mmol/L NaCl, 20 mmol/L imidazole and the elution buffer contained 50 mmol/L HEPES, pH 7.5, 300 mmol/L NaCl, 250 mmol/L imidazole. The buffer was then exchanged to Cas9 storage buffer (20 mmol/L HEPES, pH 7.5, 150 mmol/L KCl, and 1 mmol/L TCEP) using the PD-10 Desalting Columns (GE Healthcare Life Sciences, Waltham, MA, United States). The purified protein was kept at 4 °C.

3.5.3 Yeast strains and constructs

The yeast strain LPY16936 expressing GFP as a C-terminal fusion protein of the *GDH1* gene was used for the Cas9/gRNA in vivo assay. The yeast strain LPY142 was used as a negative control for GFP fluorescence imaging. Both yeast strains were gifts from Bessie Xue Su (L. Pillus Laboratory, UCSD).

To express Cas9 in yeast cells, the *Cas9* gene with SV40 NLS signal at its C-terminal was cloned into the H*ind*III sites in the pACT2 vector (Leu selection marker) between the ADH1 promoter and ADH1 terminator. The sequence between the H*ind*III sites, including the region for the GAL4 activation domain, was removed. To express ribozyme-flanked gRNAs, the DNA fragment corresponding to the designed pre-gRNA molecules was cloned into pRS316 (Ura selection marker) between the B*am*HI and E*co*RI sites by overlapping PCR. The pACT2-Cas9 and pRS316-pre-gRNA constructs were sequentially transformed into LPY16936.

3.5.4 In vitro transcription for gRNA production

The templates for in vitro transcription were amplified by PCR from pRS316-pre-gRNA constructs using common primers 5'- GTCACTATTTAGGTGACACTATA-GAAGCGCCTCGTCATTGTTCTCGTTCC -3' and 5'- ACGTATCTACCAACGATTT-GACC -3'. In vitro transcription was carried out at 40 °C for 3 h in a total volume of 50 μL with 700 ng purified DNA template, 2 μL of SP6 RNA polymerase (19U/μL, Promega, Madison, WI, United States), 0.5 mmol/L rNTPs, 1X Transcription Optimized Buffer (Promega), 10 mmol/L DTT and 1 μL of RNasin Ribonuclease Inhibitor (Promega). 1 μL of 500 mmol/L EDTA was added to each tube to terminate the reactions. The RNA transcripts were not further purified. Of the in vitro transcription products, 4 μL were analyzed by electrophoresis in 12% denaturing urea polyacrylamide gels. The RNA bands were stained with ethidium bromide and visualized using a UV transilluminator.

3.5.5 In vitro cleavage assay using Cas9 protein and gRNA

For each in vitro cleavage assay, approximately 100 ng of purified PCR products were digested with 0.2 μL of the purified Cas9 and 0.8 μL of the gRNA from the in vitro transcription reaction in 1X cleavage buffer (20 mmol/L HEPES pH 7.5, 150 mmol/L KCl, 1 mmol/L TCEP, and 10 mmol/L $MgCl_2$) in a total volume of 20 μL, at 37 °C for 60 min. The reaction was stopped by adding 2 μL of 10% SDS, and was then chilled on ice for 2 min, and centrifuged at 13,000 rpm for 2 min. The supernatant was analyzed by 1%-1.5% agarose gel electrophoresis. The DNA bands were stained with ethidium bromide and visualized using a UV transilluminator.

3.5.6 Green Fluorescent Protein fluorescent imaging of yeast

To observe the collective GFP fluorescence of yeast cells in different constructs, each yeast strain harboring the corresponding plasmids (if any) were grown in SD-Ura-Leu media overnight. The OD600 of each strain was measured (around 1.0) and concentrated to the OD600 of 20 in 50% glycerol. The 0.15 μL concentrated culture of each strain was carefully spotted onto ProbeOn Precleaned slides (Fisher Biotech, Waltham, MA, United States), covered and photographed under a DIC or fluorescent microscope (10X objective lens).

3.6 Acknowledgments

We would like to thank Luhan Yang (G. Church Laboratory, Harvard University) and Bessie Xue Su (L. Pillus Laboratory, UCSD) for materials and reagents. This work was supported by NIH R01GM068631 to Y.Z.

Chapter 3 in full, is a reprint of the material as it appears in Journal of Integrative Plant Biology, 2014, Gao, Yangbin; Zhao, Yunde. The dissertation/thesis author was a primary investigator and author of this paper.

Chapter 4

Auxin Binding Protein 1 (*ABP1*) is not required for either auxin signaling or *Arabidopsis* development

4.1 Abstract

Auxin binding protein 1 (ABP1) has been studied for decades. It has been suggested that ABP1 functions as an auxin receptor and has an essential role in many developmental processes. Here we present our unexpected findings that ABP1 is neither required for auxin signaling nor necessary for plant development under normal growth conditions. We used our ribozyme-based CRISPR technology to generate an *Arabidopsis abp1* mutant that contains a 5-bp deletion in the first exon of *ABP1*, which resulted in a frameshift and introduction of early stop codons. We also identified a T-DNA insertion *abp1* allele that harbors a T-DNA insertion located 27 bp downstream of the ATG start codon in the first exon. We show that the two new abp1 mutants are null alleles. Surprisingly, our new *abp1* mutant plants do not display any obvious

developmental defects. In fact, the mutant plants are indistinguishable from wild-type plants at every developmental stage analyzed. Furthermore, the *abp1* plants are not resistant to exogenous auxin. At the molecular level, we find that the induction of known auxin-regulated genes is similar in both wild-type and *abp1* plants in response to auxin treatments. We conclude that *ABP1* is not a key component in auxin signaling or *Arabidopsis* development.

4.2 Introduction

The auxin binding protein 1 (ABP1) was first isolated from maize plants based on its ability to bind auxin [112]. The crystal structure of ABP1 demonstrated clearly that ABP1 has an auxin-binding pocket and, indeed, binds auxin [113]. However, the elucidation of the physiological functions of ABP1 has been challenging because the first reported *abp1* T-DNA insertion mutant in *Arabidopsis* was not viable [114]. Nevertheless, *ABP1* has been recognized as an essential gene for plant development and as a key component in auxin signaling [115–120]. Because viable *abp1* null mutants in *Arabidopsis* were previously unavailable, alternative approaches have been used to disrupt ABP1 function in *Arabidopsis* to determine the physiological roles of the protein. Cellular immunization approaches were used to generate *ABP1* knockdown plants [121, 122]. Inducible overexpression of the single chain fragment variable regions (scFv12) of the anti-ABP1 monoclonal antibody mAb12 both in cell lines and in *Arabidopsis* plants presumably neutralizes the endogenous ABP1 activities [121, 122]. Two such antibody lines, SS12S and SS12K, have been widely used in many ABP1-related studies [115, 117, 120–122]. The results obtained from the characterization of the antibody lines suggest that ABP1 regulates cell division, cell expansion, meristem activities, and root development [115, 117, 121, 123, 124]. Transgenic plants that overexpress *ABP1*

antisense RNA were also used to elucidate the physiological functions of *ABP1* [115,121]. Moreover, missense point mutation alleles of abp1 have also been generated through the *Arabidopsis* TILLING project. One such TILLING mutant, named *abp1-5*, harbors a mutation (His94 >Tyr) in the auxin-binding pocket and has been widely used in many ABP1-related studies [115, 119, 120]. Previous studies based on the antisense lines, antibody lines, and *Arabidopsis* mutant alleles have led to the conclusion that ABP1 is essential for embryogenesis, root development, and many other developmental processes. However, the interpretation of results generated by using the *ABP1* antisense and antibody lines are not straightforward and off-target effects have not been completely ruled out. We believe that characterization of *abp1* null plants is urgently needed to unambiguously define the roles of ABP1 in auxin signaling and in plant development.

In the past several years, studies of the presumed ABP1-mediated auxin signal transduction pathway were carried out in several laboratories. It has been hypothesized that ABP1 is an auxin receptor mediating fast, nongenomic effects of auxin [115,117,123, 124], whereas the TIR1 family of F-box protein/auxin receptors are responsible for auxin-mediated gene regulation [125,126]. One of the proposed functions of ABP1 is to regulate subcellular distribution of PIN auxin efflux carriers [117,120,124]. Furthermore, a recent report suggests that a cell surface complex consisting of ABP1 and transmembrane receptor-like kinases functions as an auxin receptor at the plasma membrane by activating the Rho-like guanosine triphosphatases (GTPases) (ROPs) in an auxin-dependent manner [119]. ROPs have been reported to play a role in regulating cytoskeleton organization and PIN protein endocytosis [116, 117]. However, it is important to unequivocally determine the biological processes that require ABP1 before extensive efforts are directed toward elucidating any ABP1-mediated signaling pathways.

In this paper, we generate and characterize new *abp1* null mutants in *Arabidopsis*. We are interested in elucidating the molecular mechanisms by which auxin regulates

flower development because our previously identified auxin biosynthetic mutants display dramatic floral defects [14, 15, 127]. Because *ABP1* was reported as an essential gene and ABP1 binds auxin [113, 114], we decided to determine whether ABP1 plays a role in flower development. We used our recently developed ribozyme-based CRISPR gene editing technology [128] to specifically inactivate *ABP1* during flower development. Unexpectedly, we recovered a viable *abp1* mutant (*abp1-c1*, c stands for alleles generated by using CRISPR) that contains a 5-bp deletion in the first exon of ABP1. We also isolated a T-DNA *abp1* allele (*abp1-TD1*) that harbors a T-DNA insertion in the first exon of *ABP1*. We show that both *abp1-c1* and *abp1-TD1* are null mutants. Surprisingly, the mutants were indistinguishable from wild-type (WT) plants at all of the developmental stages we analyzed. Our data clearly demonstrate that *ABP1* is not an essential gene and that ABP1 does not play a major role in auxin signaling and Arabidopsis development under normal growth conditions.

4.3 Results and Discussion

4.3.1 Generation of Loss-of-Function *abp1* Mutants in *Arabidopsis* Using CRISPR Technology

In an attempt to determine the roles of ABP1 in *Arabidopsis* flower development, we used the latest CRISPR technology [128] to specifically knockout the *ABP1* gene during *Arabidopsis* flower development. We designed a ribozyme-guide RNA-ribozyme (RGR) unit that specifically targets a stretch of DNA in the first exon of *ABP1* gene (Figure 4.1). The RGR unit was placed under the control of the strong constitutive *CaMV 35S* promoter. Primary transcripts of *RGR* undergo self-processing to release the mature functional guide RNA (gRNA) as we demonstrated [128]. We controlled the

expression of the Cas9 nuclease by using the *APETALA 1* (*AP1*) promoter (Figure 4.1A). We expected that the gRNA would bring the Cas9 protein to the *ABP1* target site where it will generate double-stranded breaks. Deletions and insertions will be produced during nonhomologous end joining repair of the double-stranded break. We hypothesized that the gene editing will take place only during flower development as the expression of the Cas9 nuclease is under the control of a floral meristematic promoter.

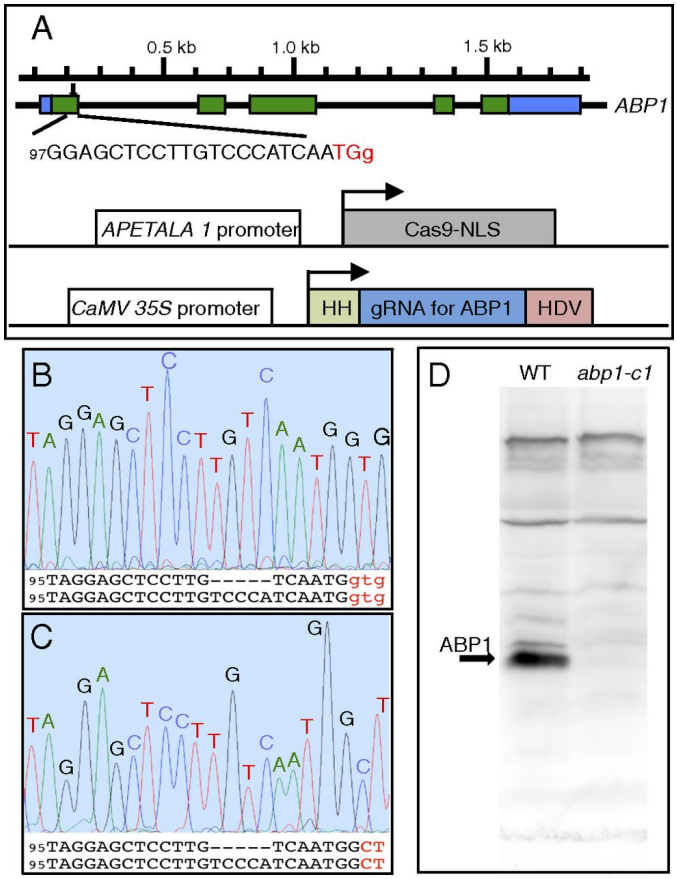

Figure 4.1: Generation of a null allele of *abp1* mutant using the ribozyme-based CRISPR gene editing technology. (A) A schematic description of the CRISPR construct that contains a Cas9 expression cassette and a CaMV 35S promoter controlled gRNA production unit. (B) A 5-bp deletion was detected in genomic DNA of *abp1-c1* mutants. The intron sequences are in lowercase and in red. (C) The *abp1-c1* cDNA also contained the same 5-bp deletion. (D) There was no detectable ABP1 protein in *abp1-c1* as shown in this Western blot image.

We were disappointed that no obvious floral defects were observed in the T1

transgenic plants that contained the expression cassettes for *Cas9* and the *RGR*. We then grew T2 plants to identify homozygous *Cas9*/*RGR* insertion plants, which may have higher efficiency of editing *ABP1* because of potentially higher expression of *RGR* and *Cas9* in the homozygous lines. Unexpectedly, we recovered T2 plants that are homozygous *abp1* deletion mutant plants (named *abp1-c1*). The *abp1-c1* contains a 5-bp deletion in the first exon (Figure 4.1B). The deletion presumably leads to a frameshift and would generate premature stop codons. Therefore, *abp1-c1* is likely a null mutant. Because our *abp1-c1* results appear to contradict a previous report that a T-DNA insertion abp1 mutant was embryo lethal [114], we hypothesized that perhaps the Cas9 protein or the CRISPR construct or an off-target site mutation partially rescued the presumed embryo lethal phenotypes of *abp1-c1*. We then backcrossed the *abp1-c1* to WT plants to segregate out the CRISPR construct and potential off-target background mutations. We genotyped the F2 population generated from the backcross and identified *Cas9* free, *abp1-c1* homozygous plants. It was clear that *abp1-c1* plants were not embryo lethal. The mutation in *abp1-c1* was stable and transmitted to next generations in a Mendelian fashion (Figure 4.2).

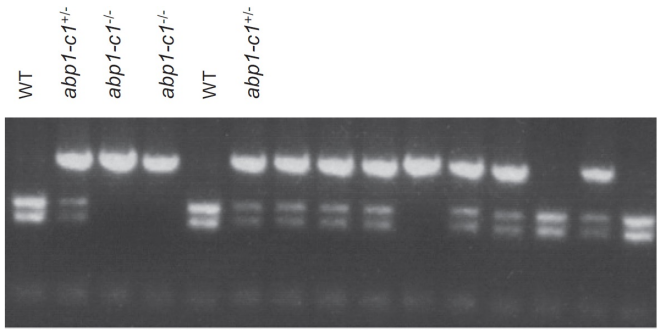

Figure 4.2: The CRISPR allele of *abp1* is stably transmitted to next generations according to Mendel genetics. Ninety-six progenies from a single *abp1-c1*$^{+/}$ plant were genotyped by using methods described in the text. The gel picture shows the patterns of WT, heterozygous, and homozygous *abp1-c1* samples. The actual number of plants for each genotype is shown in parentheses.

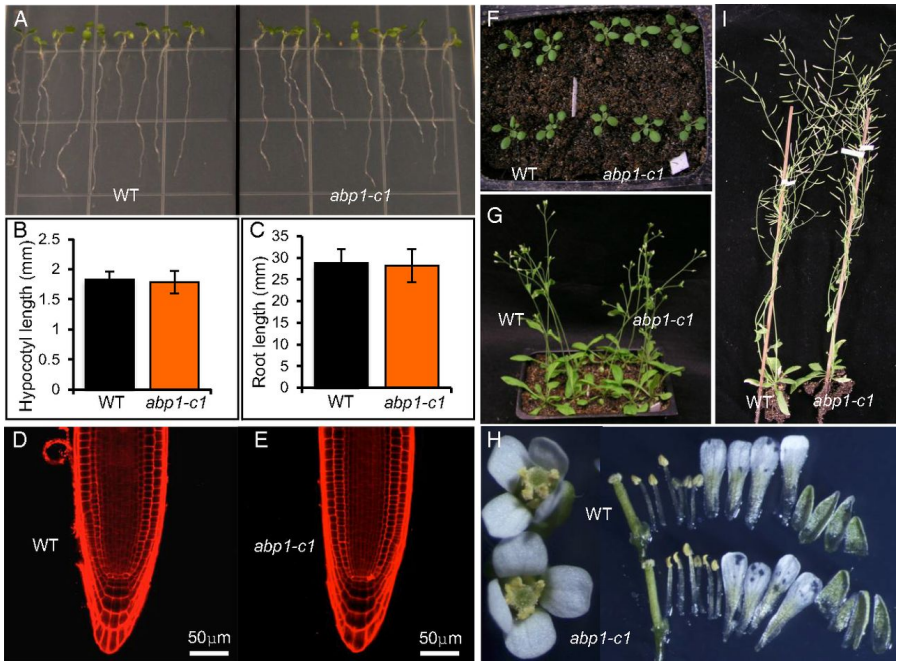

Figure 4.3: The *abp1-c1* and WT plants display no significant differences at various developmental stages. (A) Seven-day-old seedlings on regular MS plates. (B and C) Hypocotyl length and root length of 7-d-old WT and *abp1-c1* seedlings. Shown are average SD (n = 50). (D and E) Root cell shape of 7-d-old WT and *abp1-c1*. (F, G, and I) Phenotype of WT and *abp1-c1* at juvenile stage (F), floral transition stage (G), and mature plant stage (I). (H) Flowers and floral organs of WT and *abp1-c1*.

4.3.2 The *abp1-c1* Mutant Is a Null Allele

The 5-bp deletion in the first exon is predicted to cause a frameshift and to introduce several early stop codons. Because our results were not consistent with what was previously reported regarding an *abp1* null mutant, we investigated whether the 5-bp deletion in *ABP1* might generate cryptic splicing junctions that might still lead to the production of functional *ABP1* mRNA and ABP1 protein. We extracted mRNA from *abp1-c1* and WT plants, and amplified *ABP1* cDNAs by RT-PCR. The *ABP1* cDNA from WT plants was the same as reported [114]. The *ABP1* cDNAs from *abp1-c1* all contained the 5-bp deletion (Figure 4.1C). The mutant *abp1-c1* cDNA contained several premature stop codons and was unlikely to produce a functional ABP1 protein. To further

demonstrate that our *abp1-c1* is a null allele, we performed a Western blot by using anti-ABP1 polyclonal antibody [119]. The results in Figure 4.1D show that the antibody detected ABP1 and several nonspecific bands. Although both the WT and *abp1-c1* lanes had the same nonspecific bands, the ABP1 band in *abp1-c1* sample was clearly missing, demonstrating that the *abp1-c1* is a null mutant.

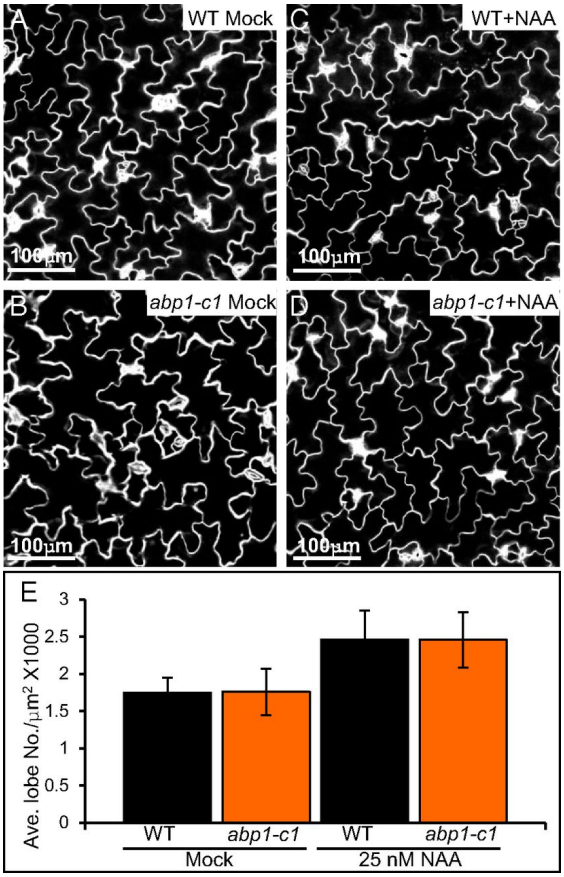

Figure 4.4: Pavement cell development in *abp1-c1* and WT. Confocal images of cotyledon pavement cells of WT (A and C) and *abp1-c1* (B and D) with auxin (C and D) and without auxin (A and B) treatments. Five-day-old light-grown seedlings were transferred to MS plates with or without 25 nM NAA for 2 d. Samples were treated with 5 μg/mL FM1-43 (Life Technologies; F-35355) for 30 min before confocal imaging. (E) Quantification of pavement cell lobes. One hundred fifty cells for each treatment and each genotype were quantified. Images were gridded to 25 of 20,000 μm^2 squares by using ImageJ before counting. Error bars are SD.

4.3.3 The *abp1-c1* Plants Are Indistinguishable from WT Plants

In previous studies, *ABP1* knockdown was associated with a number of developmental defects including changes in root and hypocotyl elongation, leaf expansion, and maintenance of the root meristem [115, 121, 122, 129–132]. To determine whether *abp1-c1* plants exhibited any of these defects, we compared them to WT plants grown under the same growth conditions. As shown in Figure 4.3A, light grown *abp1-c1* seedlings looked similar to WT seedlings. Both WT and *abp1-c1* plants had similar hypocotyl lengths (Figure 4.3B). Hypocotyl elongation is sensitive to changes in auxin concentration or auxin response [11, 133]. The length of primary roots of *abp1-c1* seedlings was also like that of WT plants (Figure 4.3A and C), and the cellular organization of primary roots of the mutant, including the meristem, appeared similar to that of WT plants (Figure 4.3D and E). We did not observe any alterations of cell size or changes in spatial arrangement of the different cell types (Figure 4.3D and E). The microscopic structure of *abp1-c1* roots is not different from that of WT plants. At young adult stages, *abp1-c1* plants developed normally and appeared as healthy as WT plants (Figure 4.3F). WT plants and *abp1-c1* plants had similar flowering time (Figure 4.3G). Flowers of *abp1-c1* had the same numbers of floral organs as WT flowers (Figure 4.3H). Lastly, mature *abp1-c1* plants and WT plants had similar architecture and *abp1-c1* plants were as fertile as WT plants (Figure 4.3I). Dark-grown seedlings of the ABP1 antibody lines were partially de-etiolated with short hypocotyls and lacked an apical hook [122]. However, the *abp1-5* weak allele was indistinguishable from WT when grown in total darkness [134]. Because dark-grown conditions vary little from laboratory to laboratory, we tested whether *abp1-c1* displayed any phenotypes in the dark. Dark-grown *abp1-c1* appeared similar to WT seedlings in terms of hypocotyl length and the formation of an apical hook (Figure 4.5).

One of the key phenotypic readouts of *abp1* knockdown or weak alleles in previous studies is a reduction of pavement cell interdigitation [119, 120]. The reduction

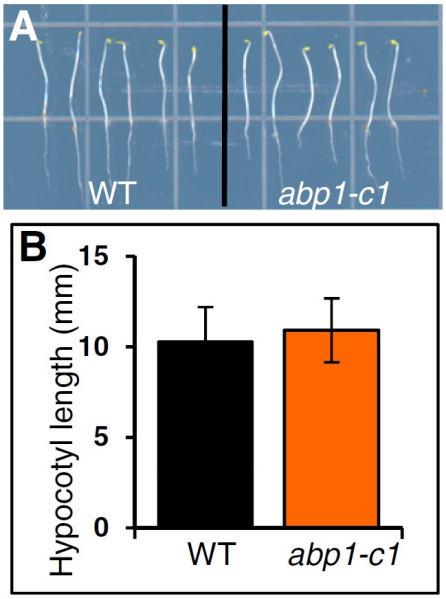

Figure 4.5: The *abp1-c1* seedlings grown in the dark were similar to WT grown under the same conditions. (A) Four-day-old seedlings grown in total darkness: WT (Left) and *abp1-c1* (Right). Note that both WT and the mutant had an apical hook. (B) Quantification of hypocotyl length of dark-grown seedlings.

of interdigitation in *abp1* knockdown lines or *abp1-5* cannot be rescued by exogenous auxin [119, 120]. We analyzed pavement cell interdigitation in both WT and *abp1-c1* with and without auxin treatments (Figure 4.4). In the absence of exogenous auxin, *abp1-c1* and WT showed the same levels of pavement cell interdigitation (Figure 4.4). Auxin treatments slightly increased interdigitation of pavement cells in both WT and *abp1-c1* (Figure 4.4). We did not observe any differences between *abp1-c1* and WT plants in terms of pavement cell interdigitation.

Overall, the *abp1-c1* plants were indistinguishable from WT plants at the various developmental stages we analyzed, demonstrating that *ABP1* probably does not play a major role in *Arabidopsis* development under normal growth conditions.

4.3.4 The *abp1-c1* Plants Are Not Auxin Resistant

Several studies have reported changes in auxin response in *ABP1* knockdown lines [129, 130]. We used a classic root elongation assay [135] to determine whether *abp1-c1* had altered sensitivity to exogenous auxin. We tested both the natural auxin indole-3-acetic acid (IAA) and the synthetic auxin 1-naphthaleneacetic acid (NAA), because ABP1 has been reported to have a higher affinity for NAA than IAA [136]. In the presence of increasing concentrations of auxin in the growth media, primary roots of WT plants became progressively shorter (Figure 4.6). Both auxins also inhibited the elongation of primary roots of *abp1-c1* (Figure 4.6). The dose-response curves to IAA treatments for WT and *abp1-c1* were almost superimposable, indicating that there was not a significant difference between WT and *abp1-c1* plants in response to auxin treatments (Figure 4.6A). Similar results were also observed when NAA was used in the treatments (Figure 4.6B).

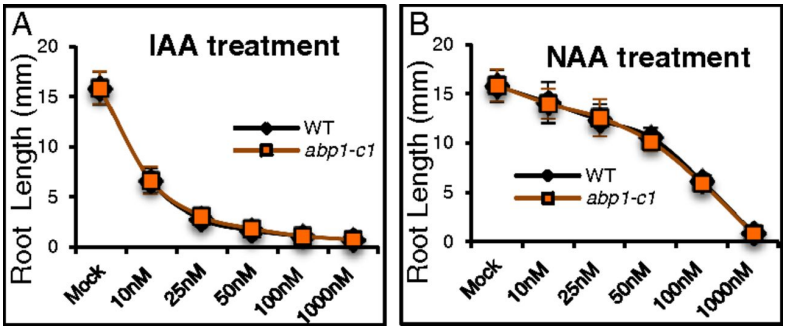

Figure 4.6: Effects of auxin treatments on *abp1-c1* root elongation. Quantification of root elongation of WT and *abp1-c1* with various concentrations of IAA (A) or NAA (B) for 2 d. Shown are average SD (n = 50).

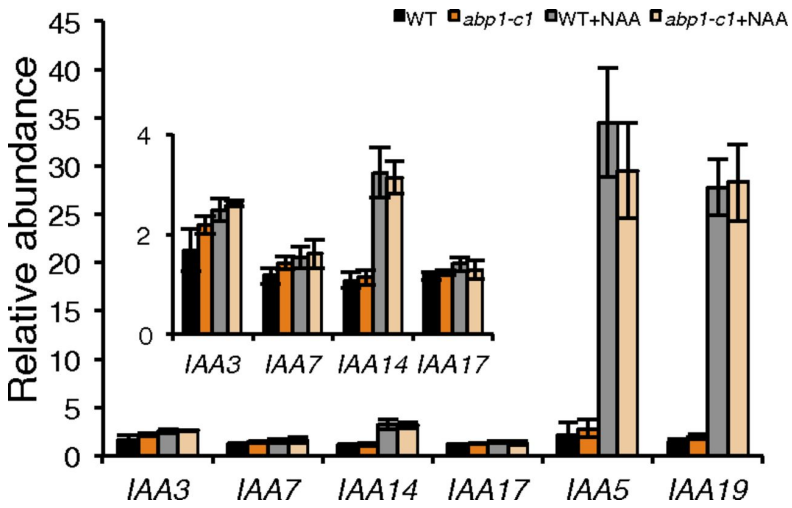

Figure 4.7: *AUX/IAA* transcripts abundance in *abp1-c1* with NAA treatments. Light grown, 7-d-old seedlings were treated with or without 1 μM NAA for 2 h and were collected for RNA extraction. For each genotype and treatment, five biological replicates were performed. Expression of *IAA3*, *IAA7*, *IAA14*, and *IAA17* with reduced y axis are shown as inset. Error bars are SD.

4.3.5 The *abp1-c1* and WT Plants Respond to Auxin Similarly at the Molecular Level

Although ABP1 was suggested to mainly function in nongenomic pathways, several studies have reported that reduction in ABP1 function affects auxin-regulated gene expression [121,129,130]. Furthermore, it was recently reported that ABP1 regulates the degradation of AUX/IAA proteins [118]. Therefore, we analyzed the expression levels of a set of well-characterized auxin inducible genes in both *abp1-c1* and WT plants with and without auxin treatments to determine whether disruption of *ABP1* affects auxin signaling. The tested auxin responsive genes were induced by auxin in WT plants (Figure 4.7). The same set of auxin-inducible genes was also induced in *abp1-c1* plants (Figure 4.7). The overall expression levels of the genes in *abp1-c1* and WT were similar, indicating that disruption of *ABP1* did not affect auxin-mediated gene expression.

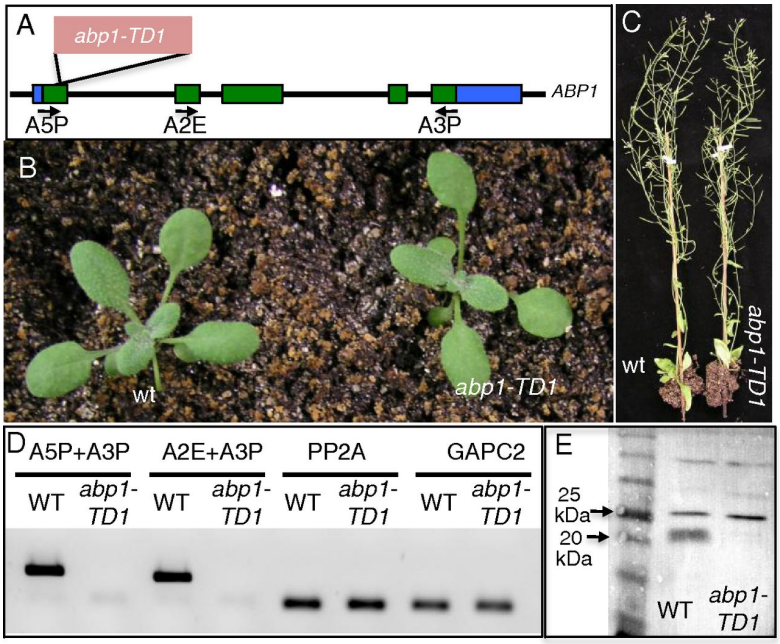

Figure 4.8: Identification of a T-DNA insertion null allele of *abp1*. (A) Schematic presentation of the T-DNA insertion site in *abp1-TD1*. The T-DNA insertion is 27 bp downstream of ATG start codon of the first exon. (B) *abp1-TD1* is viable and does not have obvious developmental defects. (C) *abp1-TD1* is fertile and similar to WT in size. (D) RT-PCR results indicate that *abp1-TD1* plants do not produce *ABP1* mRNA. The A5P and A3P pair amplifies the full length *ABP1* cDNA from the start codon to the stop codon. The A2E and A3P primers amplify the *ABP1* cDNA that does not contain the sequences of the first exon. The positions of the PCR primers are schematically indicated in the panel A. The RT-PCR products were amplified with 45 saturated cycles and loaded onto 1.2% agarose gel. (E) A Western blot image indicates that *abp1-TD1* lacked ABP1 protein. The band between 25 and 20 kDa in WT lane is ABP1, which has a predicted size of 22 kDa.

4.3.6 A New T-DNA *abp1* Null Mutant Was Not Embryo Lethal and Displayed No Obvious Developmental Defects

We have provided clear evidence that *abp1-c1* is a null mutant and that *abp1-c1* plants do not display any obvious defects at the various developmental stages we analyzed. Further, the *abp1-c1* plants did not show altered auxin responses. Because of the lack of any visible and molecular phenotypes in *abp1-c1*, it is difficult to completely rule out the possibility that a tightly-linked unknown *abp1* suppressor may have completely

masked the effects of *abp1* mutation. We believe that analysis of additional alleles of *abp1* that were generated by using non-CRISPR methods will help us to further confirm our findings. We obtained a T-DNA insertion mutant from the *Arabidopsis* stock center (Figure 4.8). The mutant (*abp1-TD1*) had a T-DNA insertion at 27 bp downstream of the ATG start codon in the first exon (Figure 4.8A). Interestingly, the T-DNA insertion site was close to the previously reported embryonic lethal T-DNA insertion mutant, which had an insertion at 51 bp from the ATG [114]. The *abp1-TD1* plants were viable and displayed no obvious differences from WT plants (Figure 4.8B). At the mature stage, *abp1-TD1* and WT were similar in size and both were fertile (Figure 4.8C). We investigated whether *abp1-TD1* still produced *ABP1* mRNA by RT-PCR analysis. We first used a pair of primers (A5P + A3P, please see Table 4.1 for primers used in this study) (Figure 4.86A) that can amplify the entire ORF from ATG start codon to the TAA stop codon. It was clear that the primers efficiently amplified the *ABP1* cDNA from WT samples, whereas no *ABP1* cDNA was amplified in the *abp1-TD1* sample (Figure 4.8D). We then used another pair of primers (A2E and A3P) (Figure 4.8A) to determine whether *abp1-TD1* can produce partial *ABP1* mRNA, which might still produce functional ABP1 protein. As shown in Figure 4.8D, *abp1-TD1* did not produce such partial mRNA. Moreover, our Western blot analysis (Figure 4.8E) indicated that *abp1-TD1* is a null allele. The finding that *abp1-TD1* was viable, normal, and fertile further supports the conclusions that *ABP1* is not essential.

In summary, the new *abp1* mutants presented in this paper offer the genetic materials needed to unambiguously define the physiological roles of *ABP1*. The mutants are viable, stable, and more importantly, they are nulls. Moreover, the mutants are generated by using different methods and the *abp1-c1* and *abp1-TD* harbor different types of mutations. Our results clearly demonstrate that plants do not need *ABP1* for auxin signaling and for their growth and development under normal growth conditions.

At this point, the reasons for the differences between the phenotype of our mutants and previously described *ABP1* knockdown lines are not clear. However, both cellular immunization and antisense approaches can be susceptible to off-target effects. For example, a recent study in zebrafish showed that 80% knockdown mutants induced by Morpholinos (antisense) were not recapitulated by true null mutants [137].

4.4 Materials and Methods

4.4.1 Plant Materials

The *abp1-TD1* (SK21825) was obtained from the *Arabidopsis* stock center. All plants were grown under long-day conditions (16-h light and 8-h darkness) at 22 °C if not otherwise specified. For hypocotyl and root length measurements, seedlings were grown on Murashige and Skoog (MS) media containing 1% sucrose under long-day conditions on vertical plates for 7 d. The plates were scanned, and NIH Image J software was used to quantify hypocotyl and root lengths.

4.4.2 Generation of *abp1-c1* using CRISPR technology

Our ribozyme-based CRISPR technology was described [128]. WT *Arabidopsis* plants, Columbia-0 ecotype, were transformed with the CRISPR construct by floral dipping. The *abp1-c1* plants were identified at the T2 stage.

4.4.3 Genotyping *abp1* Mutants

The T-DNA insertion mutant was genotyped by using a PCR-based method described [76, 138]. Genotyping primers for *abp1-TD1* were as follows: ABP1-U409F, ABP1-586R, and the T-DNA specific primer pSKTAIL-L3 (please see Table 4.1). For

genotyping *abp1-c1*, we amplified an *ABP1* fragment by PCR using the following two primers: ABP1-U409F and ABP1-586R. The resulting PCR product was digested with the restriction enzyme B*sl*I, which cuts WT PCR product once and does not cut the mutant band (Figure 4.2).

Table 4.1: Primers used in this study

Name	Sequences
ABP1-5P (A5P)	ATGATCGTACTTTCTGTTGGTTCC
ABP1-3P (A3P)	TTAAAGCTCGTCTTTTTGTGATTCT
ABP-2E (A2E)	TTGCCAATCGTGAGGAATATTAG
pSKTAIL-L3	ATACGACGGATCGTAATTTGTCG
ABP1-U409F	CCTCATCACACAACAAAGTCACTC
ABP1-586R	GGAGCCAGCAACAGTCATGTG
IAA3qPCR-F	TGGATGCTCATTGGTGATGT
IAA3qPCR-R	CAACCCAAGCACAGACAGAG
IAA5qPCR-F	TCCGCTCTGCAAATTCTGTTCG
IAA5qPCR-R	ACGATCCAAGGAACATTTCCCAAG
IAA7qPCR-F	TCGGCCAACTTATGAACCTC
IAA7qPCR-R	CTTCTCCTTGGGAACAGCAG
IAA14qPCR-F	GAAGCAGAGGAGGCAATGAG
IAA14qPCR-R	CCCATGGTAAAGGAGCTGAA
IAA17qPCR-F	GGTTTCCTGCCAAAAATCAA
IAA17qPCR-R	TTTGCCCATGGTAAAAGAGC
IAA19qPCR-F	GGTGACAACTGCGAATACGTTACCA
IAA19qPCR-R	CCCGGTAGCATCCGATCTTTTCA
PP2A (At1g69960)-F	TAACGTGGCCAAAATGATGC
PP2A (At1g69960)-R	GTTCTCCACAACCGCTTGGT
GAPC2 (At1g13440)-F	TTGGTGACAACAGGTCAAGCA
GAPC2 (At1g13440)-R	AAACTTGTCGCTCAATGCAATC

4.4.4 Western Blot

Plant extracts were loaded onto SDS/PAGE gels. The gel was run until bromophenol blue was approximately 1 cm above the bottom of the gel, and the proteins were transferred to a PVDF membrane. The membrane was blocked in 5% (wt/vol) nonfat

milk overnight at 4 °C and with anti-ABP1 antibody at room temperature for 3 h. The membranes were washed in TBST (20 mM Tris, 150 mM NaCl, pH = 8.0 plus 0.05% Tween 20) three times, incubated with goat anti-rabbit secondary antibody for 3 h, and washed in TBST three times. Results were visualized by ECL Plus Western Blotting Detection System (Amersham; RPN2232).

4.4.5 Analysis of Auxin Responses

Five-day-old seedlings grown on MS plates were transferred to MS plates containing various concentrations of IAA or NAA, or mock. The root tips of seedlings were marked. After grown vertically for 2 d, plates were scanned. The root elongation that occurred during the 2-d period, and hypocotyl length was measured by using NIH ImageJ.

To analyze auxin-induced gene expression, 7-d-old seedlings were treated with or without 1 μM NAA for 2 h. Five biological replicates were prepared for both WT and *abp1-c1* mutant, with or without the treatment. Total RNAs were extracted by using the RNeasy Plant Mini Kit (Qiagen; 74904) according to the instructions from the manufacturer. RNA samples were treated with DNase and purified before performing quantitative RT-PCR. PCR primers are listed in Table 4.1.

4.5 Acknowledgments

We thank Dr. Alan Jones for kindly providing us the ABP1 antibody. This work was supported by NIH Grants R01GM068631 (to Y. Zhao) and R01GM43644 (to M.E.), National Science Foundation (Plant Genome Grant DBI-0820729 (to Y. Zhao), the Gordon and Betty Moore Foundation (M.E.), and the Howard Hughes Medical Institute (M.E.).

Chapter 4 in full, is a reprint of the material as it appears in Proceedings of the National Academy of Sciences, 2015, Gao, Yangbin; Zhang, Yi; Zhang, Da; Dai, Xinhua; Estelle, Mark; Zhao, Yunde. The dissertation/thesis author was a primary investigator and author of this paper.

Chapter 5

Identification and Characterization of *IAMH1* Gene In Biosynthesis of Plant Hormone Auxin

5.1 Abstract

Plant hormone auxin is a small-molecule growth regulator that is involved in almost every aspect of plant life. In *Arabidopsis* plants, the major active form of auxin, indole-3-acetic acid (IAA), could be synthesized through many different pathways via different intermediates. The two-step auxin biosynthesis by YUC and TAA family proteins has recently been established as the main auxin biosynthesis pathway using indole-3-pyruvic acid (IPA) as the intermediate. IAA could also be synthesized from other intermediates found in *Arabidopsis*, such as tryptamine (TAM), indole-3-acetaldoxime (IAOx) and indole-3-actamide (IAM). Although genes capable of converting IAM into IAA in *Arabidopsis* have been discovered, their knockouts do not confer IAM resistance, indicating the presence of other genes responsible for the auxin-overproduction phenotype

in IAM-treated plants. In this paper, we report the identification of the *IAMH1* gene, which is involved in converting IAM into IAA in *Arabidopsis*. We show that *iamh1* point mutation lines are resistant to IAM treatment. we also demonstrated that IAMH1 could convert IAM into IAA both in vitro and in vivo. The expression pattern of *IAMH1* gene is also examined, and its expression is found in various tissues and stages of *Arabidopsis* plants. We also identified another close homolog of *IAMH1*, the *IAMH2* gene. Interestingly, *IAMH2* gene appears as a tandem repeat on the chromosome with *IAMH1* gene. To better understanding the function of *IAMH* genes, we generated *iamh2* mutants in the *iamh1* background using ribozyme-based CRISPR genome-editing technology and we identified two lines in *iamh1* background with different *iamh2* mutations. The possible interactions between auxin-overproduction mutant *sur1* and *iamh1* mutant are also examined.

5.2 Introduction

Auxin plays essential roles in many aspects of plant growth and development [1]. Auxin concentrations in plant cells need to be tightly controlled so that plants can grow properly in response to developmental and environmental signals. Plants have evolved a complex network to effectively modulate auxin concentrations. Auxin biosynthesis, degradation, and transport all contribute to establishing proper auxin concentrations in cells [11, 14, 15, 27, 139, 140]. Recent studies have shown that spatially and temporally regulated auxin biosynthesis is involved in determining almost all of the major developmental processes including embryogenesis, seedling growth, vascular pattern formation, and flower development [14, 15, 141]. Understanding the molecular mechanisms of auxin biosynthesis provides the necessary tools for effectively modulating auxin levels in plants, thus allowing us to improve agriculturally important traits such as branching and root

architecture.

Auxin is generally believed to be synthesized through both tryptophan (Trp)-dependent and Trp-independent pathways [1]. Very little is known about the Trp-independent pathway. Only recently a report demonstrates that the cytosolic indole synthase (INS) is a key enzyme in the elusive Trp-independent pathway and that mutants defective in INS functions display phenotypes during early embryogenesis [142]. Trp-dependent pathways have not been fully elucidated either. It has been proposed that Trp may be converted to IAA, the main natural auxin in plants, through several routes [1]. Trp can be metabolized into tryptamine (TAM) and indole-3-pyruvate (IPA) by PLP-dependent decarboxylases and aminotransferases, respectively. It is also known that Trp can be converted into indole-3-acetaldoxime (IAOx) by CYP79B2 and CYP79B3 P450 monooxygenases [45]. Moreover, plants also produce indole-3-acetamide (IAM) and indole-3-acetonitrile (IAN) from Trp [7]. All of the aforementioned Trp metabolites including TAM, IPA, IAOx and IAM have been proposed as intermediates for auxin biosynthesis in plants. However, so far only IPA has been firmly established as an important auxin biosynthetic intermediate in plants [16, 25, 26]. Disruption of either IPA biosynthesis or metabolism in *Arabidopsis*, maize, and rice leads to dramatic developmental defects [14, 15, 22, 23, 26, 28, 38, 143]. It has been shown that Trp is converted into IAA using IPA as the intermediate in two steps in the so-called TAA/YUC pathway [144]. Trp is first metabolized into IPA by the TAA family of aminotransferases and subsequently the YUC family of monooxygenases catalyzes the conversion of IPA into IAA [144]. The TAA/YUC pathway is evolutionary conserved among plant species and it is required for all of the major developmental processes in *Arabidopsis*. Therefore, the TAA/YUC pathway has been recognized as a major auxin biosynthesis pathway.

The roles of the other Trp metabolites in auxin biosynthesis and plant development have not been fully resolved. IAOx has long been recognized as a potential

auxin biosynthesis precursor. Over accumulation of IAOx in *Arabidopsis* by either overexpressing the biosynthetic enzyme CYP79B2 or by inactivating IAOx metabolizing enzymes such as SUR1 and SUR2 leads to auxin overproduction [9, 45, 145]. Although IAOx can be metabolized into IAA in *Arabidopsis*, the exact mechanisms by which IAOx is converted into IAA are not understood at present. It is generally accepted that IAOx probably is not a major intermediate for auxin biosynthesis for two reasons. First, complete elimination of IAOx production in *Arabidopsis* by knocking out both *CYP79B2* and *B3* does not lead to dramatic developmental defects. Second, IAOx is only produced in limited number of plant species that produce indolic glucosinolates [7].

The biosynthetic route for IAOx is well understood, but the reactions from IAOx to IAA have not been elucidated. In contrast, enzymes responsible for converting other Trp metabolites such as IAN into IAA are known [13], but the biosynthetic route for IAN and IAM are not understood. IAN can be converted into IAA in plants when added to plant growth media. It was shown more than a decade ago that IAN is converted into IAA by a family of nitrilases [13]. Mutations in *nitrilase 1* (*nit1*) in *Arabidopsis* render the mutant resistant to exogenous IAN [13]. Under normal growth conditions, *nit1* mutants do not display obvious developmental defects probably because of the compensatory effects provided by NIT1 homologs in *Arabidopsis*. It is still an outstanding question whether nitrilases and IAN play an important in auxin biosynthesis and plant development.

IAM was the first definitively identified intermediate used in Trp-dependent auxin biosynthesis pathways in bacteria. Plant pathogens such as agrobacterium and pseudomonas synthesize auxin from Trp when they infect plants [39, 146, 147]. The bacteria-produced auxin alters the growth and developmental patterns of the infected plant cells so that the pathogens can use the plant cells to produce carbon- and nitrogen- rich compounds for their growth. The pathogens convert Trp into IAM using the bacterial iaaM Trp-2-monooxygenase and subsequently the pathogen-encoded hydrolase iaaH converts

IAM to IAA [39, 146, 147]. *Arabidopsis* and other plants produce IAM in the absence of a bacteria infection, suggesting that plants may use IAM as an auxin biosynthetic intermediate as well. Furthermore, IAM was proposed as an intermediate in a route that converts IAOx into IAA [7]. It is well known that *Arabidopsis* and other plants have the capacity to convert IAM into IAA. Overexpression of *iaaM* in *Arabidopsis*, petunia, and tobacco led to auxin overproduction phenotypes [10, 148, 149]. It is hypothesized that plant hydrolases can convert IAM produced by the *iaaM* transgene to generate IAA. Bioinformatic analyses have identified a small family of IAM hydrolases named as amidases that share significant homology to the bacterial iaaH proteins [40, 150, 151]. *Arabidopsis AMIDASE I* (*AMI1*) has been shown to have the capacity to hydrolyze IAM into IAA in vitro and in *Arabidopsis* [151]. However, the amidase mutants do not display much reduced sensitivity to exogenous IAM [151], suggesting that plants probably also use other unidentified hydrolases to convert IAM to IAA. Identification of additional enzymes that are responsible for converting IAM to IAA will help us to unambiguously determine whether IAM is a key auxin biosynthetic intermediate in plants and whether IAM-derived auxin plays an important role in plant growth and development. Understanding of how IAM is converted into IAA in plants will also clarify whether IAM is an important intermediate in metabolizing IAOx into IAA.

In this paper, we present the identification of two homologous genes that encode hydrolases responsible for converting IAM to IAA in *Arabidopsis*. We conducted a genetic screen for mutants that displayed reduced sensitivity to exogenous IAM. We mapped one of the strong IAM-resistant mutants to chromosome IV and discovered that the mutant contained a G to A conversion that generated a premature stop codon in the gene At4g37550, which encodes a predicted hydrolase. We named At4g37550 *IAMH1* (*IAM HYDROLASE 1*). We demonstrated that *IAMH1* had the capacity to convert IAM into IAA both in vitro and in Ar*abidopsis*. Furthermore, we show that IAMH1 was

localized in the cytosol and *IAMH1* is almost ubiquitously expressed in the shoot and root tip. Interestingly, *Arabidopsis* genome contains two copies of the *IAMH* genes and the two genes are arranged as tandem repeats on the chromosome IV. We found that disruption of either *IAMH* gene lead to a decreased sensitivity to IAM. We successfully used the latest CRISPR genome editing technology to generate mutations in the *IAMH2* gene in the *iamh1-1* mutant background. *Arabidopsis* plants lacked any IAMH activities were resistant to IAM, but did not display any obvious growth and developmental defects, suggesting that the IAM-derived auxin is not required for *Arabidopsis* development under normal growth conditions. The work identified the main enzymes for hydrolyzing IAM to IAA in *Arabidopsis* and clarified the roles of IAM in auxin biosynthesis and plant development.

5.3 Results and Discussion

5.3.1 IAM promotes plant growth and activates the auxin reporter DR5-GUS

IAM is the key intermediate used by some plant pathogenic bacteria to synthesize auxin (Figure 5.1A) [39, 146, 147]. The two-step pathway catalyzed by the bacterial iaaM and iaaH effectively converts Trp into IAA (Figure 5.1A). The *iaaM* gene has been widely used to genetically modulate auxin levels in plants [10, 14, 149]. *Arabidopsis* seedlings grown on IAM-containing media in the light had much elongated hypocotyls and developed epinastic cotyledons (Figure 5.1B). IAM also slightly inhibited the elongation of primary roots. IAM-treated plants resembled closely to the well-characterized *Arabidopsis* auxin overproduction mutants such as *YUC* overexpression lines and *sur1* mutants [9, 11], suggesting that IAM either activates an auxin signaling pathway directly

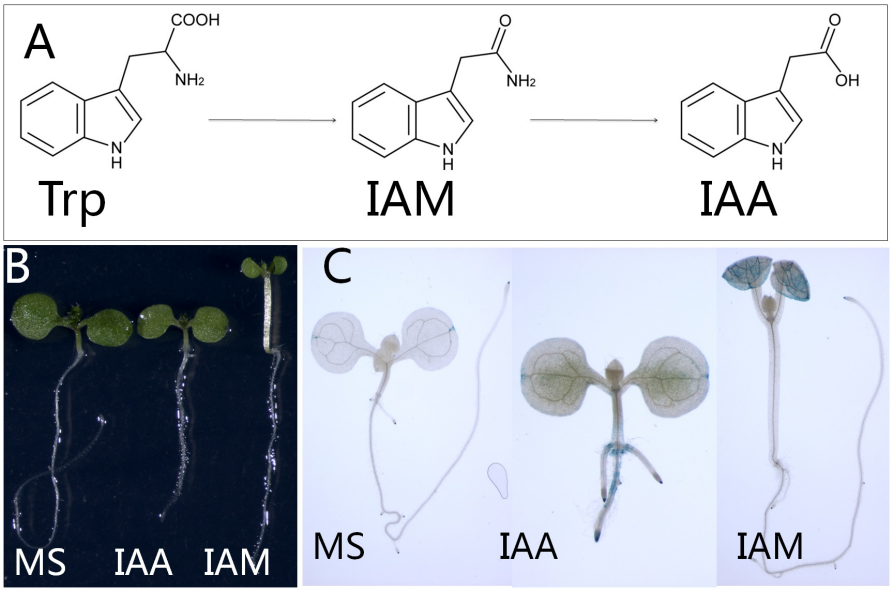

Figure 5.1: Indole-3-acetamide (IAM) is a potential auxin biosynthetic intermediate in plants and IAM treatments affect plant growth and activate auxin reporter DR5-GUS. (A) A proposed Trp-dependent auxin biosynthetic pathway using IAM as the intermediate. (B) Five-day old *Arabidopsis* seedlings grown on MS media and media containing 20 μM IAA or IAM. Note that IAA inhibits primary root elongation and IAM stimulates hypocotyl growth. (C) Activation of DR5-GUS expression by IAA and IAM. Interestingly, IAM mainly activates DR5-GUS expression in aerial tissue whereas IAA increases DR5-GUS signal in the root.

or IAM is converted into IAA, the active natural auxin. Interestingly, seedlings grown on IAA plates did not display long hypocotyls and epinastic cotyledon (Figure 5.1B). Rather IAA mainly inhibited primary root elongation and stimulated lateral root initiation and elongation (Figure 5.1B). We investigated whether IAM activated the expression of the auxin reporter DR5-GUS. As shown in Figure 5.1C, seedlings grown on IAM-containing media had much elevated expression levels of DR5-GUS in the cotyledons and true leaves compared to seedlings grown on regulate media. Activation of DR5-GUS expression in aerial part by IAM is consistent with the observation that IAM mainly stimulated hypocotyl elongation and changed the shape of cotyledons (Figure 5.1B). In contrast, IAA activated DR5-GUS expression in the roots (Figure 5.1C). Our results indicated that IAM and IAA caused different developmental phenotypes in *Arabidopsis* seedlings

(Figure 5.1B & C). The observed differences were probably caused by differences in uptake and transport of the two compounds. It is very clear that IAM treatment could activate the auxin reporter and cause phenotypes related elevated auxin levels.

5.3.2 Genetic screens for mutants resistant to IAM

Arabidopsis seedlings grown on 20 μM IAM phenocopied the *YUC* overexpression plants, which produce elevated levels of auxin due to the overexpression of the YUC flavin monooxygenase, a rate limiting enzyme in auxin biosynthesis [11, 14]. Because auxin overproduction mutants display phenotypes different from those caused by IAA treatments and because previous genetic screens for auxin resistant mutants were mainly conducted using IAA or synthetic auxin 2,4-D, we hypothesized that a genetic screen for mutants that can suppress *YUC* overexpression lines would uncover novel auxin genes. We hypothesized that such a genetic screen might be able to identify genes that are important for auxin biosynthesis, conjugation, degradation, transport or auxin signaling. Unfortunately, the *YUC* overexpression lines were not stable and the strong lines were completely sterile. Therefore, genetic screens for suppressors/enhancers of YUC overexpression lines were not feasible. Because of the strong phenotypic similarities between IAM-treated plants and *YUC* overexpression lines, we believe that genetic screens for IAM resistant mutants would mimic the screens for suppressors of YUC overexpression lines.

We mutagenized A*rabidopsis* seeds using EMS and conducted the genetic screen using 7- to 9-day old seedlings grown on 20 μM IAM under light. The putative mutants should have short hypocotyls and normal cotyledons. We screened M2 seeds from 1000 individual M1 plants and identified more than 100 putative IAM-resistant mutants, which were transplanted to soil. Among the putative mutants, many were dwarf with dark-green leaves, which are very similar to the brassinolide (BR) biosynthesis and signaling mutants.

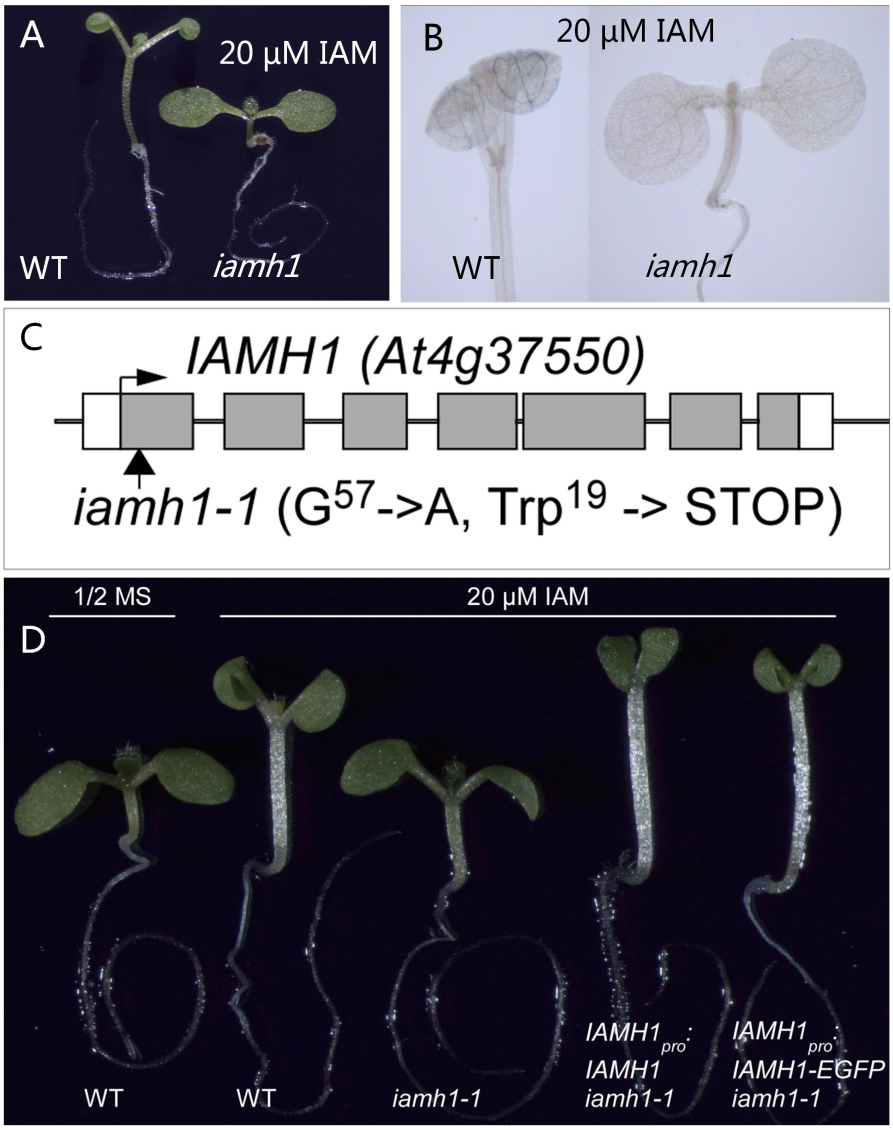

Figure 5.2: Isolation and cloning of an IAM resistant mutant(*iamh1*). Isolation of an IAM-resistant mutant, which does not have elongated hypocotyl and does not display epinastic cotyledons when grown on 20 μM IAM-containing media. (B) The expression of DR5-GUS auxin reporter is not induced by IAM treatments in the *iamh1* mutant. (C) The *iamh1* mutation was identified by map-based positional cloning. The *IAMH1* gene is At4g37550. The *iamh1-1* mutant harbors a G to A mutation in At4g37550 that results in a premature stop codon. (D)The *iamh1* phenotypes are rescued by wild type *IAMH1* cDNA or *IAMH1* cDNA fused with GFP driven by the *IAMH1* promoter.

After discarded the obvious BR-related mutants and conducted second round screens with M3 seeds, we had isolated 24 confirmed IAM-resistant mutants. One of the mutants, #483, was almost insensitive to IAM. Light grown mutant #483 had a short hypocotyl and

flat cotyledons (Figure 5.2A) when grown on 20 μM IAM. We backcrossed the mutant to Wild-Type (WT) Columbia (Col) and out-crossed it to Wild-Type (WT) Landsberg (Ler). About 25% seedlings from either F2 populations displayed the IAM resistant phenotype, suggesting that the phenotype was caused by a single locus.

We mapped the mutation in the #483 mutant to the bottom of chromosome IV and narrowed the mapping interval down to about 330 Kb region. Among the ORFs in the mapping interval, At4g37550 encodes a putative Acetamidase/Formamidase, which potentially has the hydrolase activities that can break an amide bond. We hypothesized that a mutation in At4g37550 probably would abolish the conversion of IAM into IAA, thus causing the IAM-insensitive phenotypes. We sequenced the genomic DNA of At4g37550 from the mutant #483 and identified a G to A conversion in the first exon of At4g37550 (Figure 5.2A). The mutation converted a Trp codon to a stop codon (Fig. 2A), suggesting that the mutant is likely a null allele.

To confirm that the identified mutation in the At4g37550 gene caused the observed IAM insensitive phenotype of mutant #483, we obtained a T-DNA insertion mutant of At4g37550 from the ABRC stock center. The T-DNA mutant was also resistant to IAM treatment, demonstrating that #483 mutant phenotypes were caused by disruption of At4g37550. We renamed #483 mutant *iamh1-1* (*IAM HYDROLASE 1*) and At4g37550 gene IAMH1. The T-DNA allele was named *iamh1-2*. To further demonstrate that we had identified the causal mutation in *iamh1-1*, we transformed *iamh1-1* plants with a construct that harbored a cassette that expresses At4g37550 cDNA under the control of At4g374550 promoter. As shown in Figure 5.2C, the *IAMH1* transgene fully restored the IAM sensitivity of the *iamh1-1* mutant. We also expressed an IAMH1-GFP fusion under the control of the *IAMH1* promoter in the *iamh1-1* background. The GFP fusion could also fully rescue the *iamh1-1* phenotypes. Interestingly, the complementation transgenic lines appeared to have longer hypocotyls than wild type plants grown under

the same conditions (Figure 5.2C). The differences probably were caused by a slight overexpression of the transgenes. Such an observation actually further supports the hypothesis that IAMH1 is involved in converting IAM to IAA in *Arabidopsis*.

IAMH1-like genes have been identified in all of the plant genomes that have been sequenced. IAMH1 appears to be a plant specific protein. The only animal genome that contains a close homolog of IAMH1 is the Tibetan antelope genome. However, it has not been ruled out whether the antelope gene is contaminated from a plant source. IAMH1 is highly conserved throughout the plant kingdom. For example, the maize IAMH1 homolog shares 89% amino acid sequence identity with the *Arabidopsis* IAMH1.

5.3.3 The *IAMH1* is broadly expressed and is not localized in the nucleus

We expressed the *GUS* gene driven by the *IAMH1* promoter in *Arabidopsis*. At seedling stage, the *GUS* expression was broadly distributed in cotyledons, true leaves, and root tips (Figure 5.3). At reproductive stage, *GUS* expression was observed in young flowers, gynoecia, and in inflorescences (Figure 5.3A). Expression of IAMH1-GFP fusion driven by *IAMH1* promoter showed that *IAMH1* was clearly not expressed in the nucleus (Figure 5.3B)

5.3.4 IAMH1 has the capacity to hydrolyze IAM into IAA and ammonia

Our genetic data suggest that IAMH1 functions as a hydrolase that converts IAM to IAA in *Arabidopsis*. We expressed IAMH1 as a His-tagged fusion protein in *E. coli* and purified it to homogeneity (Figure 5.4A). IAM and IAA can be easily separated on a TLC plate (Figure 5.4B). In the presences of recombinant IAMH1, IAM was converted

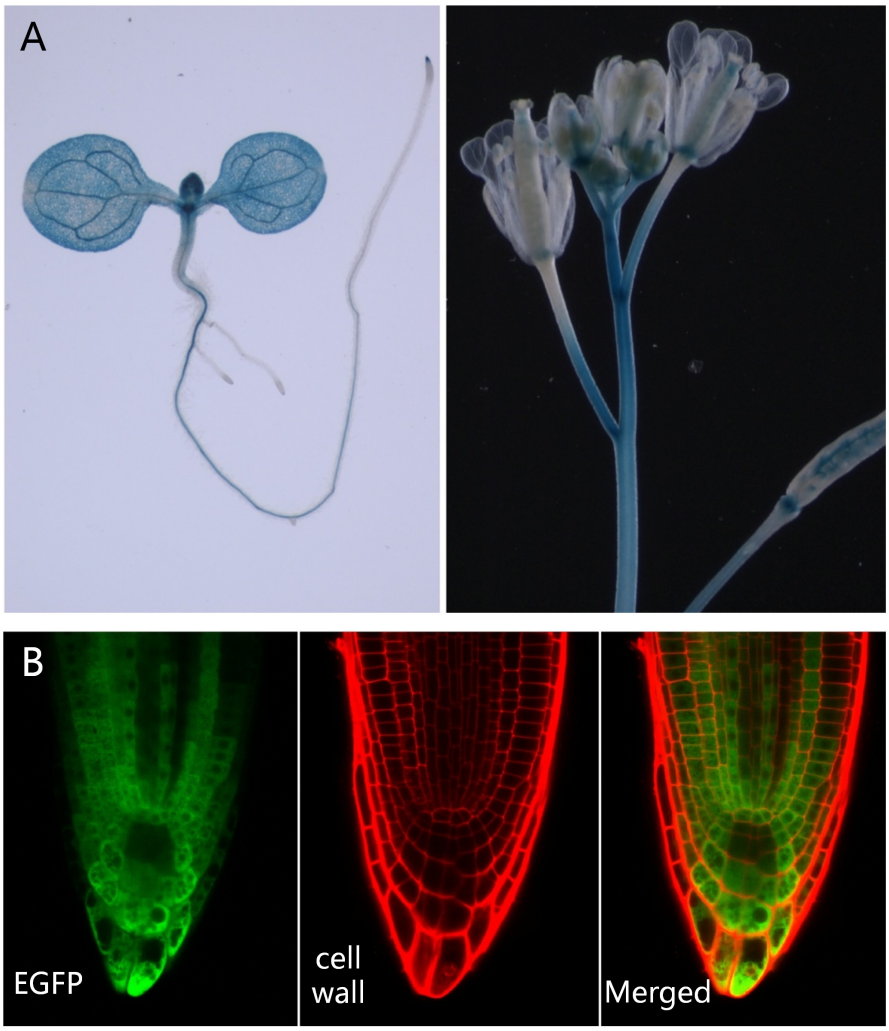

Figure 5.3: Expression pattern of *IAMH1* and sub-cellular localization of IAMH1 protein. (A) The GUS expression patterns of $IAMH1_{pro}$*:GUS* Transgenic lines. Note that the reporter has a broad expression pattern. (B) Expression of the IAMH1-EGFP fusion in *Arabidopsis* roots driven by the *IAMH1* promoter. *IAMH1* appears to be located in the cytosol.

into IAA (Figure 5.4). In contrast, heat-inactivated IAMH1 protein failed to hydrolyze IAM to IAA in vitro (Figure 5.4B). We also used a colorimetric assay and successfully detected the other product ammonia. Further quantitative analysis showed that IAMH1 was a rather slow enzyme with k_{cat} of 1.5 min^{-1} and Km for IAM as 437 μM. The in vitro data suggest that the assay conditions probably were not optimal and that additional in vivo factors might affect the catalysis. Nevertheless, our in vitro data was consistent

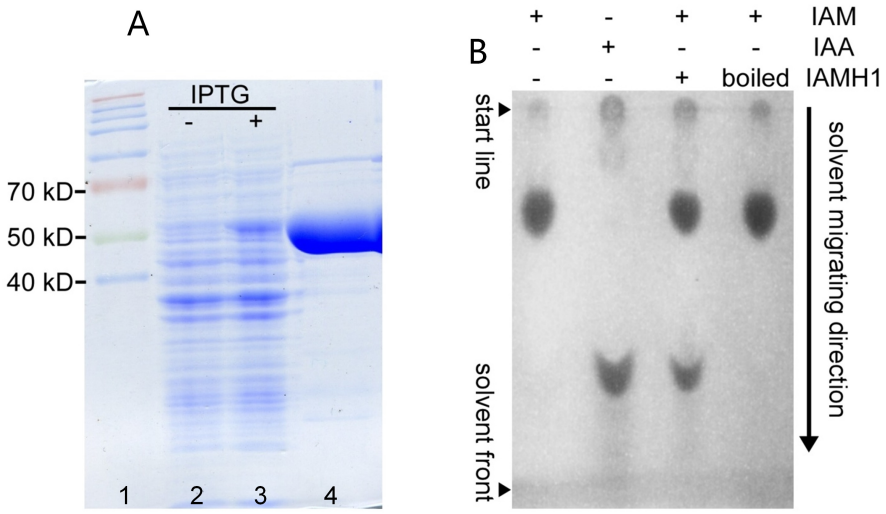

Figure 5.4: IAMH1 can hydrolyze IAM into IAA and ammonia. (A) IAMH1 with a His-tag was expressed in *E.coli* and purified to homogeneity. Lane 1: Prestained protein marker. Lane 2: *E.coli* cell lysate before IPTG induction. Lane 3: *E.coli* cell lysate after IPTG induction. Lane 4: Purified IAMH1 protein using Ni-NTA agarose. (B) IAM and IAA are separated on a TLC plate. Ammonia produced in the reaction was detected colormetrically.

with a role for IAMH1 in converting IAM into IAA in *Arabidopsis*.

5.3.5 *Arabidopsis* genome contains two copies of *IAMH* genes

Both *iamh1-1* and *iamh1-2* did not show obvious developmental defects under normal growth conditions, despite that both mutant alleles were resistant to IAM. Blastp analysis using IAMH1 protein as query identified At4g37560 as a close homolog of IAMH1 in the *Arabidopsis* genome (Figure 5.5). We named At4g37560 *IAMH2*. *IAMH2* and *IAMH1* share 90% amino acid sequence identity. Because of the high sequence homology, we hypothesized that *IAMH2* might also play an important role in converting IAM into IAA in *Arabidopsis*. Functional redundancy between *IAMH1* and *IAMH2* may explain our observation that *iamh1-1* and *iamh1-2* did not show obvious developmental defects.

We obtained a T-DNA insertion mutant from the ABRC stock center to test

Figure 5.5: *IAMH2* gene is also involved in converting IAM into IAA. (A) IAMH1 has a close homolog, IAMH2. The two genes are tandem repeats located on Chromosome IV. (B) A T-DNA insertion in *IAMH2* also caused resistance to exogenous IAM. (C) Generation of *iamh2* alleles by CRISPR. TGG in red is the PAM site for CRISPR/Cas9. The *iamh2-2* allele harbors one T insertion and *iamh2-3* contains a 20 bp deletion.

whether *iamh2* was also resistant to IAM. As shown in Figure 5.5B, *iamh2-1* had short hypocotyls and normal cotyledons when grown on 20 μM IAM whereas wild type plants developed long hypocotyls and epinastic cotyledons, demonstrating that disruption of *IAMH2* also led to IAM resistance. These data suggest that *IAMH2* likely has overlapping functions with *IAMH1*.

5.3.6 Construction of *iamh1 iamh2* double mutants

In order to assess the roles of the *IAMH* genes in auxin biosynthesis and *Arabidopsis* development, we need to inactivate both *IAMH* genes simultaneously. The two *IAMH* genes are located at Chromosome IV as tandem repeats (Figure 5.5A). It is virtually impossible to generate *iamh1 iamh2* double mutants by crossing two single mutants together because of the extremely tight linkage between the two genes. We employed our recently developed ribozyme-based CRISPR technology [128, 152] to generate *iamh2* mutations in the *iamh1-1* background. We obtained two *iamh2* alleles (Figure 5.5C): *iamh2-2* and *iamh2-3*. The *iamh2-2* contained a single bp insertion after the nucleotide 330 from the ATG start codon in the cDNA (A in the ATG start codon counts as the first nucleotide), which generated an immediate stop codon (Figure 5.5C). Therefore, *iamh2-2* is likely a null allele. The *iamh2-3* allele harbored a 20 bp deletion from nucleotide 320 to 339 in the cDNA. Such a large deletion in *iamh2-3* was also likely to completely abolish *IAMH1* function. We backcrossed both *iamh2* alleles to wild type Col plants to segregate out the CRISPR/Cas9. Both *iamh1-1 iamh2-2* and *iamh1-1 iamh2-2* double mutants were viable and fertile. In fact, we did not observe any obvious developmental defects in the *iamh* double mutants under normal plant growth conditions. Our data suggest that auxin-derived from IAM probably is not required for *Arabidopsis* growth and development under laboratory growth conditions.

5.3.7 Auxin overproduction phenotypes of *sur1* is not suppressed by *iamh1*

SUR1 is a key enzyme for indolic glucosinolate biosynthesis. Disruption of *SUR1* leads to the accumulation of IAOx, which is metabolized into IAA through an undefined pathway [9, 145]. One of the proposed intermediate in converting IAOx into IAA is

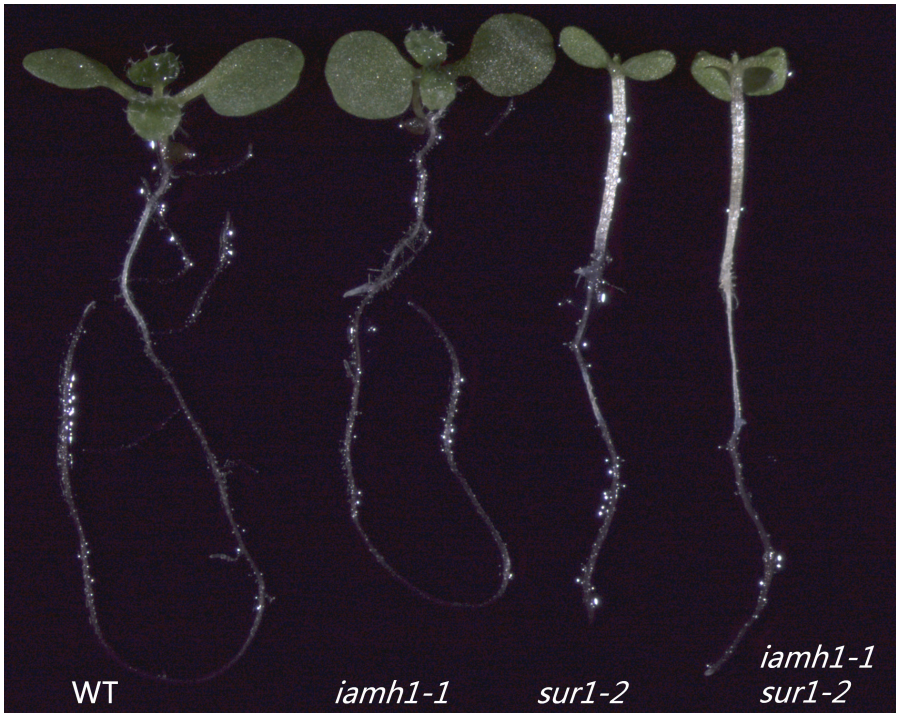

Figure 5.6: Disruption of the *IAMH1* gene could not suppress the auxin overproduction phenotypes of *sur1*. Note that the *iamh1 sur1* double mutants still have long hypocotyl and epinastic cotyledons.

IAM [7]. We introduced the *iamh1-1* mutation into *sur1-2* to test whether the auxin overproduction phenotypes of *sur1* could be suppressed by compromising the *IAMH* functions. As shown in Figure 5.6, the *iamh1-1 sur1-2* double mutants still developed long hypocotyls and epinastic cotyledons, suggesting that IAM probably is not the main intermediate for metabolizing IAOx into IAA.

In this paper, we uncovered two *IAMH* genes that encode hydrolases capable of converting IAM into IAA both in vitro and in *Arabidopsis*. Our data demonstrated that the two *IAMH* genes are the main players in metabolizing exogenous IAM into IAA. Inactivation of the *IAMH* genes renders *Arabidopsis* plants insensitive to IAM treatments. Our preliminary data indicate that *IAMH* genes do not play an essential role in *Arabidopsis* development. Further detailed characterization of the *iamh1 iamh2* double mutants is still needed to definitively determine their functions in auxin biosynthesis and

plant development. We still need to biochemically determine whether concentrations of IAA, IAM, IAN, and IAOx in the *iamh1 iamh2* double mutants are affected. The genetic interactions between the *iamh* mutants with known auxin biosynthetic mutants such as *yuc*, *taa*, and *cyp79b2 cyp79b3* will further clarify the auxin biosynthetic landscape.

5.4 Materials and Methods

5.4.1 Plant Materials and Growth Conditions

The *iamh1-2* and *iamh2-1* T-DNA mutants was obtained from the *Arabidopsis* stock center. Plants were grown under long-day conditions (16-h light and 8-h darkness) at 22 °C. Seeds were surfaced sterilized by 70% ethanol and air-dried on filter papers in the hood before placed on plates containing Murashige and Skoog (MS) media (supplemented with IAA or IAM when indicated). The plates with seeds were then incubated at 4 °C for 2 days before placed in the growth chamber. Seedlings were grown on the plates in the growth chamber until 7-9 days old, and then transfered to grow in soil if needed.

5.4.2 IAM-resistant mutant screening

WT Col plants were mutagenized using Ethyl methanesulfonate (EMS). Seeds from each mutagenized plants were harvested individually and grown on MS plates containing 20 μM IAM. WT plants would show obviously elongated hypocotyl. IAM-resistant seedlings with reduced hypocotyl length were selected and further analyzed. The *iamh1-1* mutant was backcrossed 2 times to WT Col to remove background mutations.

5.4.3 Plant Transformation

Arabidopsis plants with different genetic background were tranformed using corresponding T-DNA constructs in agrobacteria *GV3101* via floral dipping method described previously [153].

5.4.4 Constructs and Transgenic Plants

IAMH1$_{pro}$*:GUS* construct was made using pBI101.3 with the 2.8 Kb promoter region before the ATG start codon cloned before the *GUS* gene. WT Col plants were transformed and T1 plants were selected on MS plates containing kanamycin.

IAMH1$_{pro}$*:IAMH1* construct was made using pART27 with the whole 5.5 Kb genomic region, which includes the 2.8 Kb promoter region before the start codon, the 2.0 Kb region from the start codon to the stop codon and the 657 bp region after the stop codon. *iamh1-1* plants were transformed and T1 plants were selected on MS plates containing 20 μM IAM. Plants showing restored IAM sensitivity were selected as complemented lines.

IAMH1$_{pro}$*:IAMH1-EGFP* construct was made using pART27 with the 4.9 Kb genomic region (which includes the 2.8 Kb promoter region before the ATG start codon, the 2.0 Kb region from the start codon to just before the stop codon), the EGFP gene coding region, and an OCS terminator. *iamh1-1* plants were transformed and T1 plants were selected on MS plates containing 20 μM IAM. Plants showing restored IAM sensitivity were selected as complemented lines.

CRISPR construct targeting *IAMH2* gene was generated using our ribozyme-based guide RNA CRISPR system described previously [128, 152]. The CRISPR target site chosen for *IAMH2* gene was TGCAACTTGGGTCCTCTTCCAGG, which is in the second exon and the 314 to 336 bp region counting from the ATG start codon in

the cDNA. *iamh1-1* plants were transformed and T1 plants were selected on MS plates containing hygromycin. Mutant plants were identified using restriction enzyme B*sl*I (recognition site CCNNNNNNNGG) to cut PCR fragments containing the CRISPR target site amplified from the genomic DNA.

5.4.5 *iamh1-1* genotyping

Plants with *iamh1-1* mutation were genotyped using primers 5'- GATGACGCC-AAGCGTGTAAGC -3' and 5'- CTGGGAATTCAGAGGTAAGCAC -3' to amplify the genomic DNA and then digested with N*co*I. PCR products from WT plants would be cut into two fragments (0.6 Kb + 0.9 Kb) while the PCR products from the *iamh1-1* mutants would appear as a single band (1.5 Kb).

5.4.6 Beta-glucuronidase (GUS) staining

GUS staining of $IAMH1_{pro}$*:GUS* plants and *DR5-GUS* plants were performed according to the previously described protocol [154].

5.4.7 IAMH1 protein expression, purification and SDS-PAGE analysis

IAMH1 cDNA was cloned into pET28a vector, and transformed into *E. coli* strain BL21 (DE3). The IAMH1 protein is expressed at 15 °C induced by 1mM IPTG. The protein is purified via the His-tag fused on the N-terminal using Ni-NTA Agarose from Qiagen, Hilden, Germany following the manufacturer's instructions. The *E. coli* cell lysate before and after the IPTG induction as well as the purified protein were loaded onto 12% SDS-PAGE gel and stained with coomassie blue to visualize the bands.

5.4.8 IAMH1 in vitro activity assay

IAMH1 protein was tested in a buffer solution containing 50 mM NaCl, 1 mM DTT, 20 mM Tris-Cl (pH = 7.5) and 0.1 mg/mL BSA. Boiled or active IAMH1 protein was tested at the final concentration of 50 μg/mL in a total volume of 100 μL. Reaction was carried out at room temperature for 24 h. 50 μL of the reaction mix was transfered into a new tube, and acidified by adding 3 μL of 1 M HCl. After mixing, 250 μL of ethyl acetate was added and vortexed for 30 s to extract the indole derivatives. The mix was then centrifuge at 12,000 rpm for 1 min. 200 μL of the top layer was transfered to a new tube, and concentrated by spin vacuuming at 60 °C for 7 min. The concentrated samples were spotted onto a TLC plate by repeatedly spotting 1.5 μL with drying in between. Control samples of IAM or IAA were dissolved in 100% ethanol and spotted onto the TLC plate. TLC was performed in 100% ethyl acetate for 10-12 min (before the solvent front reach the top) and briefly dried in air. Then plate was visualize under UV light and the indole derivatives appeared as dark spots on the plate.

To test the ammonia produced and calculate the IAMH1 enzymatic kinetics, a colorimetric assay based on the Berthelot indophenol reaction was used [155]. For each 50 μL sample after reaction, 10 μL of 10% Phenol (ethanol solution), 2 μL of 0.5% sodium nitroprusside (SNP), 7 μL of (20% Na_3Citrate + 1% NaOH) and 2 μL of NaClO solution (12% chlorine) were sequentially added and mixed after each addition. The color was developed at room temperature for 30 min and OD640 was measured. Standard curves were produced using NH_4Cl following the same protocol.

5.4.9 Confocal imaging of root tips

Root tips of *IAMH1$_{pro}$:IAMH1-EGFP* plants were stained using Propidium Iodide and visualized using a confocal microscope. The cell contour appeared as red florescence

signal and IAMH1-EGFP fusion proteins appeared as green florescence signal.

5.5 Acknowledgments

This work was supported by NIH Grants R01GM068631 (to Y. Zhao) and National Science Foundation (Plant Genome Grant DBI-0820729 (to Y. Zhao)

Chapter 5, in part is currently being prepared for submission for publication of the material. Gao, Yangbin; Zhang, Da; Dai, Xinhua; Guo, Xiuhua; Zhao, Yunde. The dissertation/thesis author was a primary investigator and author of this material.

Appendix A

Final notes

Just as "*All roads lead to Rome*", the plants use many different intermediates via different pathways to synthesize the important plant hormone auxin. With the main auxin biosynthesis route being identified as the YUC/TAA pathway, the importance of the other pathways remains to be fully elucidated. The identification of the *IAMH* genes put one more piece in the puzzle, and more await to be discovered in the years to come.

Bibliography

[1] Yunde Zhao. Auxin biosynthesis and its role in plant development. *Annu Rev Plant Biol*, 61:49–64, 2010.

[2] A. D. Wright, M. B. Sampson, M. G. Neuffer, L. Michalczuk, J. P. Slovin, and J. D. Cohen. Indole-3-acetic acid biosynthesis in the mutant maize orange pericarp, a tryptophan auxotroph. *Science*, 254(5034):998–1000, Nov 1991.

[3] J. Normanly, J. D. Cohen, and G. R. Fink. Arabidopsis thaliana auxotrophs reveal a tryptophan-independent biosynthetic pathway for indole-3-acetic acid. *Proc Natl Acad Sci U S A*, 90(21):10355–10359, Nov 1993.

[4] S F Yang and N E Hoffman. Ethylene biosynthesis and its regulation in higher plants. *Annual Review of Plant Physiology*, 35(1):155–189, 1984.

[5] A. Sakurai and S. Fujioka. The current status of physiology and biochemistry of brassinosteroids. *Plant Growth Regulation*, 13(2):147–159, 1993.

[6] J. Ouyang, M. Chen, and J. Li. Measurement of soluble tryptophan and total indole-3-acetic acid in arabidopsis by capillary electrophoresis. *Anal Biochem*, 271(1):100–102, Jun 1999.

[7] Satoko Sugawara, Shojiro Hishiyama, Yusuke Jikumaru, Atsushi Hanada, Takeshi Nishimura, Tomokazu Koshiba, Yunde Zhao, Yuji Kamiya, and Hiroyuki Kasahara. Biochemical analyses of indole-3-acetaldoxime-dependent auxin biosynthesis in arabidopsis. *Proc Natl Acad Sci U S A*, 106(13):5430–5435, Mar 2009.

[8] J. A. BENTLEY, K. R. FARRAR, S. HOUSLEY, G. F. SMITH, and W. C. TAYLOR. Some chemical and physiological properties of 3-indolylpyruvic acid. *Biochem J*, 64(1):44–49, Sep 1956.

[9] W. Boerjan, M. T. Cervera, M. Delarue, T. Beeckman, W. Dewitte, C. Bellini, M. Caboche, H. Van Onckelen, M. Van Montagu, and D. Inzé. Superroot, a recessive mutation in arabidopsis, confers auxin overproduction. *Plant Cell*, 7(9):1405–1419, Sep 1995.

[10] C. P. Romano, P. R. Robson, H. Smith, M. Estelle, and H. Klee. Transgene-mediated auxin overproduction in arabidopsis: hypocotyl elongation phenotype

and interactions with the hy6-1 hypocotyl elongation and axr1 auxin-resistant mutants. *Plant Mol Biol*, 27(6):1071–1083, Mar 1995.

[11] Y. Zhao, S. K. Christensen, C. Fankhauser, J. R. Cashman, J. D. Cohen, D. Weigel, and J. Chory. A role for flavin monooxygenase-like enzymes in auxin biosynthesis. *Science*, 291(5502):306–309, Jan 2001.

[12] J. Normanly, P. Grisafi, G. R. Fink, and B. Bartel. Arabidopsis mutants resistant to the auxin effects of indole-3-acetonitrile are defective in the nitrilase encoded by the nit1 gene. *Plant Cell*, 9(10):1781–1790, Oct 1997.

[13] B. Bartel and G. R. Fink. Differential regulation of an auxin-producing nitrilase gene family in arabidopsis thaliana. *Proc Natl Acad Sci U S A*, 91(14):6649–6653, Jul 1994.

[14] Youfa Cheng, Xinhua Dai, and Yunde Zhao. Auxin biosynthesis by the yucca flavin monooxygenases controls the formation of floral organs and vascular tissues in arabidopsis. *Genes Dev*, 20(13):1790–1799, Jul 2006.

[15] Youfa Cheng, Xinhua Dai, and Yunde Zhao. Auxin synthesized by the yucca flavin monooxygenases is essential for embryogenesis and leaf formation in arabidopsis. *Plant Cell*, 19(8):2430–2439, Aug 2007.

[16] Kiyoshi Mashiguchi, Keita Tanaka, Tatsuya Sakai, Satoko Sugawara, Hiroshi Kawaide, Masahiro Natsume, Atsushi Hanada, Takashi Yaeno, Ken Shirasu, Hong Yao, Paula McSteen, Yunde Zhao, Ken-ichiro Hayashi, Yuji Kamiya, and Hiroyuki Kasahara. The main auxin biosynthesis pathway in arabidopsis. *Proc Natl Acad Sci U S A*, 108(45):18512–18517, Nov 2011.

[17] Xinhua Dai, Kiyoshi Mashiguchi, Qingguo Chen, Hiroyuki Kasahara, Yuji Kamiya, Sunil Ojha, Jennifer DuBois, David Ballou, and Yunde Zhao. The biochemical mechanism of auxin biosynthesis by an arabidopsis yucca flavin-containing monooxygenase. *J Biol Chem*, 288(3):1448–1457, Jan 2013.

[18] D. M. Ziegler. Flavin-containing monooxygenases: catalytic mechanism and substrate specificities. *Drug Metab Rev*, 19(1):1–32, 1988.

[19] Daniel M. Ziegler. An overview of the mechanism, substrate specificities, and structure of fmos. *Drug Metab Rev*, 34(3):503–511, Aug 2002.

[20] Jeong Im Kim, Altanbadralt Sharkhuu, Jing Bo Jin, Pinghua Li, Jae Cheol Jeong, Dongwon Baek, Sang Yeol Lee, Joshua J. Blakeslee, Angus S. Murphy, Hans J. Bohnert, Paul M. Hasegawa, Dae-Jin Yun, and Ray A. Bressan. yucca6, a dominant mutation in arabidopsis, affects auxin accumulation and auxin-related phenotypes. *Plant Physiol*, 145(3):722–735, Nov 2007.

[21] W George Lai, Nadia Farah, George A. Moniz, and Y Nancy Wong. A baeyer-villiger oxidation specifically catalyzed by human flavin-containing monooxygenase 5. *Drug Metab Dispos*, 39(1):61–70, Jan 2011.

[22] Anna N. Stepanova, Joyce Robertson-Hoyt, Jeonga Yun, Larissa M. Benavente, De-Yu Xie, Karel Dolezal, Alexandra Schlereth, Gerd Jürgens, and Jose M. Alonso. Taa1-mediated auxin biosynthesis is essential for hormone crosstalk and plant development. *Cell*, 133(1):177–191, Apr 2008.

[23] Yi Tao, Jean-Luc Ferrer, Karin Ljung, Florence Pojer, Fangxin Hong, Jeff A. Long, Lin Li, Javier E. Moreno, Marianne E. Bowman, Lauren J. Ivans, Youfa Cheng, Jason Lim, Yunde Zhao, Carlos L. Ballaré, Göran Sandberg, Joseph P. Noel, and Joanne Chory. Rapid synthesis of auxin via a new tryptophan-dependent pathway is required for shade avoidance in plants. *Cell*, 133(1):164–176, Apr 2008.

[24] Masashi Yamada, Katie Greenham, Michael J. Prigge, Philip J. Jensen, and Mark Estelle. The transport inhibitor response2 gene is required for auxin synthesis and diverse aspects of plant development. *Plant Physiol*, 151(1):168–179, Sep 2009.

[25] Anna N. Stepanova, Jeonga Yun, Linda M. Robles, Ondrej Novak, Wenrong He, Hongwei Guo, Karin Ljung, and Jose M. Alonso. The arabidopsis yucca1 flavin monooxygenase functions in the indole-3-pyruvic acid branch of auxin biosynthesis. *Plant Cell*, 23(11):3961–3973, Nov 2011.

[26] Christina Won, Xiangling Shen, Kiyoshi Mashiguchi, Zuyu Zheng, Xinhua Dai, Youfa Cheng, Hiroyuki Kasahara, Yuji Kamiya, Joanne Chory, and Yunde Zhao. Conversion of tryptophan to indole-3-acetic acid by tryptophan aminotransferases of arabidopsis and yuccas in arabidopsis. *Proc Natl Acad Sci U S A*, 108(45):18518–18523, Nov 2011.

[27] Zhigang Zhao, Yunhui Zhang, Xi Liu, Xin Zhang, Shichang Liu, Xiaowen Yu, Yulong Ren, Xiaomin Zheng, Kunneng Zhou, Ling Jiang, Xiuping Guo, Ying Gai, Chuanyin Wu, Huqu Zhai, Haiyang Wang, and Jianmin Wan. A role for a dioxygenase in auxin metabolism and reproductive development in rice. *Dev Cell*, 27(1):113–122, Oct 2013.

[28] Andrea Gallavotti, Solmaz Barazesh, Simon Malcomber, Darren Hall, David Jackson, Robert J. Schmidt, and Paula McSteen. sparse inflorescence1 encodes a monocot-specific yucca-like gene required for vegetative and reproductive development in maize. *Proc Natl Acad Sci U S A*, 105(39):15196–15201, Sep 2008.

[29] Young-Min Woo, Hee-Jin Park, Mukhamad Su'udi, Jung-Il Yang, Jong-Jin Park, Kyoungwhan Back, Yong-Mok Park, and Gynheung An. Constitutively wilted 1, a member of the rice yucca gene family, is required for maintaining water

homeostasis and an appropriate root to shoot ratio. *Plant Mol Biol*, 65(1-2):125–136, Sep 2007.

[30] Yuko Yamamoto, Noriko Kamiya, Yoichi Morinaka, Makoto Matsuoka, and Takashi Sazuka. Auxin biosynthesis by the yucca genes in rice. *Plant Physiol*, 143(3):1362–1371, Mar 2007.

[31] Kenji Fujino, Yasuyuki Matsuda, Kenjirou Ozawa, Takeshi Nishimura, Tomokazu Koshiba, Marco W. Fraaije, and Hiroshi Sekiguchi. Narrow leaf 7 controls leaf shape mediated by auxin in rice. *Mol Genet Genomics*, 279(5):499–507, May 2008.

[32] Yousef M. Abu-Zaitoon, Karina Bennett, Jennifer Normanly, and Heather M. Nonhebel. A large increase in iaa during development of rice grains correlates with the expression of tryptophan aminotransferase ostar1 and a grain-specific yucca. *Physiol Plant*, 146(4):487–499, Dec 2012.

[33] Marino Expósito-Rodríguez, Andrés A. Borges, Andrés Borges-Pérez, and José A. Pérez. Gene structure and spatiotemporal expression profile of tomato genes encoding yucca-like flavin monooxygenases: the tofzy gene family. *Plant Physiol Biochem*, 49(7):782–791, Jul 2011.

[34] Rafael Tobeña-Santamaria, Mattijs Bliek, Karin Ljung, Göran Sandberg, Joseph N M. Mol, Erik Souer, and Ronald Koes. Floozy of petunia is a flavin monooxygenase-like protein required for the specification of leaf and flower architecture. *Genes Dev*, 16(6):753–763, Mar 2002.

[35] Hong Liu, Yang-Yang Ying, Ling Zhang, Qing-Hua Gao, Jing Li, Zhen Zhang, Jing-Gui Fang, and Ke Duan. Isolation and characterization of two yucca flavin monooxygenase genes from cultivated strawberry (fragaria $\times$ ananassa duch.). *Plant Cell Rep*, 31(8):1425–1435, Aug 2012.

[36] Jeong Im Kim, Dongwon Baek, Hyeong Cheol Park, Hyun Jin Chun, Dong-Ha Oh, Min Kyung Lee, Joon-Yung Cha, Woe-Yeon Kim, Min Chul Kim, Woo Sik Chung, Hans J. Bohnert, Sang Yeol Lee, Ray A. Bressan, Shin-Woo Lee, and Dae-Jin Yun. Overexpression of arabidopsis yucca6 in potato results in high-auxin developmental phenotypes and enhanced resistance to water deficit. *Mol Plant*, 6(2):337–349, Mar 2013.

[37] Hyeong Cheol Park, Joon-Yung Cha, and Dae-Jin Yun. Roles of yuccas in auxin biosynthesis and drought stress responses in plants. *Plant Signal Behav*, 8(6):e24495, Jun 2013.

[38] Kimberly A. Phillips, Andrea L. Skirpan, Xing Liu, Ashley Christensen, Thomas L. Slewinski, Christopher Hudson, Solmaz Barazesh, Jerry D. Cohen, Simon Malcomber, and Paula McSteen. vanishing tassel2 encodes a grass-specific tryptophan

aminotransferase required for vegetative and reproductive development in maize. *Plant Cell*, 23(2):550–566, Feb 2011.

[39] T. Yamada, C. J. Palm, B. Brooks, and T. Kosuge. Nucleotide sequences of the pseudomonas savastanoi indoleacetic acid genes show homology with agrobacterium tumefaciens t-dna. *Proc Natl Acad Sci U S A*, 82(19):6522–6526, Oct 1985.

[40] Stephan Pollmann, Daniel Neu, Thomas Lehmann, Oliver Berkowitz, Tina Schäfer, and Elmar W. Weiler. Subcellular localization and tissue specific expression of amidase 1 from arabidopsis thaliana. *Planta*, 224(6):1241–1253, Nov 2006.

[41] Maik Hoffmann, Thomas Lehmann, Daniel Neu, Mathias Hentrich, and Stephan Pollmann. Expression of amidase1 (ami1) is suppressed during the first two days after germination. *Plant Signal Behav*, 5(12):1642–1644, Dec 2010.

[42] Martin de Vos, Ksenia L. Kriksunov, and Georg Jander. Indole-3-acetonitrile production from indole glucosinolates deters oviposition by pieris rapae. *Plant Physiol*, 146(3):916–926, Mar 2008.

[43] R. Carreño-Lopez, N. Campos-Reales, C. Elmerich, and B. E. Baca. Physiological evidence for differently regulated tryptophan-dependent pathways for indole-3-acetic acid synthesis in azospirillum brasilense. *Mol Gen Genet*, 264(4):521–530, Nov 2000.

[44] A. K. Hull, R. Vij, and J. L. Celenza. Arabidopsis cytochrome p450s that catalyze the first step of tryptophan-dependent indole-3-acetic acid biosynthesis. *Proc Natl Acad Sci U S A*, 97(5):2379–2384, Feb 2000.

[45] Yunde Zhao, Anna K. Hull, Neeru R. Gupta, Kendrick A. Goss, José Alonso, Joseph R. Ecker, Jennifer Normanly, Joanne Chory, and John L. Celenza. Trp-dependent auxin biosynthesis in arabidopsis: involvement of cytochrome p450s cyp79b2 and cyp79b3. *Genes Dev*, 16(23):3100–3112, Dec 2002.

[46] S. Bak and R. Feyereisen. The involvement of two p450 enzymes, cyp83b1 and cyp83a1, in auxin homeostasis and glucosinolate biosynthesis. *Plant Physiol*, 127(1):108–118, Sep 2001.

[47] Andrew W. Woodward and Bonnie Bartel. Auxin: regulation, action, and interaction. *Ann Bot*, 95(5):707–735, Apr 2005.

[48] K. Bialek, L. Michalczuk, and J. D. Cohen. Auxin biosynthesis during seed germination in phaseolus vulgaris. *Plant Physiol*, 100(1):509–517, Sep 1992.

[49] B. Bartel and G. R. Fink. Ilr1, an amidohydrolase that releases active indole-3-acetic acid from conjugates. *Science*, 268(5218):1745–1748, Jun 1995.

[50] R. T. Davies, D. H. Goetz, J. Lasswell, M. N. Anderson, and B. Bartel. Iar3 encodes an auxin conjugate hydrolase from arabidopsis. *Plant Cell*, 11(3):365–376, Mar 1999.

[51] J. Lasswell, L. E. Rogg, D. C. Nelson, C. Rongey, and B. Bartel. Cloning and characterization of iar1, a gene required for auxin conjugate sensitivity in arabidopsis. *Plant Cell*, 12(12):2395–2408, Dec 2000.

[52] Sherry LeClere, Rosie Tellez, Rebekah A. Rampey, Seiichi P T. Matsuda, and Bonnie Bartel. Characterization of a family of iaa-amino acid conjugate hydrolases from arabidopsis. *J Biol Chem*, 277(23):20446–20452, Jun 2002.

[53] Rebekah A. Rampey, Sherry LeClere, Mariusz Kowalczyk, Karin Ljung, Göran Sandberg, and Bonnie Bartel. A family of auxin-conjugate hydrolases that contributes to free indole-3-acetic acid levels during arabidopsis germination. *Plant Physiol*, 135(2):978–988, Jun 2004.

[54] B. K. Zolman, A. Yoder, and B. Bartel. Genetic analysis of indole-3-butyric acid responses in arabidopsis thaliana reveals four mutant classes. *Genetics*, 156(3):1323–1337, Nov 2000.

[55] Lucia C. Strader, Angela Hendrickson Culler, Jerry D. Cohen, and Bonnie Bartel. Conversion of endogenous indole-3-butyric acid to indole-3-acetic acid drives cell expansion in arabidopsis seedlings. *Plant Physiol*, 153(4):1577–1586, Aug 2010.

[56] Sibu Simon, Martin Kubeš, Pawel Baster, Stéphanie Robert, Petre Ivanov Dobrev, Jiří Friml, Jan Petrášek, and Eva Zažímalová. Defining the selectivity of processes along the auxin response chain: a study using auxin analogues. *New Phytol*, 200(4):1034–1048, Dec 2013.

[57] Lucia C. Strader, Dorthea L. Wheeler, Sarah E. Christensen, John C. Berens, Jerry D. Cohen, Rebekah A. Rampey, and Bonnie Bartel. Multiple facets of arabidopsis seedling development require indole-3-butyric acid-derived auxin. *Plant Cell*, 23(3):984–999, Mar 2011.

[58] L. Michalczuk and R. S. Bandurski. Enzymic synthesis of 1-o-indol-3-ylacetyl-beta-d-glucose and indol-3-ylacetyl-myo-inositol. *Biochem J*, 207(2):273–281, Nov 1982.

[59] A. J. Leznicki and R. S. Bandurski. Enzymic synthesis of indole-3-acetyl-1-o-beta-d-glucose. ii. metabolic characteristics of the enzyme. *Plant Physiol*, 88:1481–1485, 1988.

[60] A. J. Leznicki and R. S. Bandurski. Enzymic synthesis of indole-3-acetyl-1-o-beta-d-glucose. i. partial purification and characterization of the enzyme from zea mays. *Plant Physiol*, 88:1474–1480, 1988.

[61] Genji Qin, Hongya Gu, Yunde Zhao, Zhiqiang Ma, Guanglu Shi, Yue Yang, Eran Pichersky, Haodong Chen, Meihua Liu, Zhangliang Chen, and Li-Jia Qu. An indole-3-acetic acid carboxyl methyltransferase regulates arabidopsis leaf development. *Plant Cell*, 17(10):2693–2704, Oct 2005.

[62] G. Hagen, G. Martin, Y. Li, and T. J. Guilfoyle. Auxin-induced expression of the soybean gh3 promoter in transgenic tobacco plants. *Plant Mol Biol*, 17(3):567–579, Sep 1991.

[63] Z. B. Liu, T. Ulmasov, X. Shi, G. Hagen, and T. J. Guilfoyle. Soybean gh3 promoter contains multiple auxin-inducible elements. *Plant Cell*, 6(5):645–657, May 1994.

[64] Paul E. Staswick, Bogdan Serban, Martha Rowe, Iskender Tiryaki, Marién T. Maldonado, Mitsa C. Maldonado, and Walter Suza. Characterization of an arabidopsis enzyme family that conjugates amino acids to indole-3-acetic acid. *Plant Cell*, 17(2):616–627, Feb 2005.

[65] Paul Staswick. Plant hormone conjugation: a signal decision. *Plant Signal Behav*, 4(8):757–759, Aug 2009.

[66] Paul E. Staswick. The tryptophan conjugates of jasmonic and indole-3-acetic acids are endogenous auxin inhibitors. *Plant Physiol*, 150(3):1310–1321, Jul 2009.

[67] Alexander Walz, Seijin Park, Janet P. Slovin, Jutta Ludwig-Müller, Yoshie S. Momonoki, and Jerry D. Cohen. A gene encoding a protein modified by the phytohormone indoleacetic acid. *Proc Natl Acad Sci U S A*, 99(3):1718–1723, Feb 2002.

[68] Jennifer Normanly. Approaching cellular and molecular resolution of auxin biosynthesis and metabolism. *Cold Spring Harb Perspect Biol*, 2(1):a001594, Jan 2010.

[69] D. M. Reinecke and R. S. Bandurski. Oxindole-3-acetic acid, an indole-3-acetic acid catabolite in zea mays. *Plant Physiol*, 71(1):211–213, Jan 1983.

[70] A. Ostin, M. Kowalyczk, R. P. Bhalerao, and G. Sandberg. Metabolism of indole-3-acetic acid in arabidopsis. *Plant Physiol*, 118(1):285–296, Sep 1998.

[71] Kenji Kai, Junko Horita, Kyo Wakasa, and Hisashi Miyagawa. Three oxidative metabolites of indole-3-acetic acid from arabidopsis thaliana. *Phytochemistry*, 68(12):1651–1663, Jun 2007.

[72] Wendy Ann Peer, Yan Cheng, and Angus S. Murphy. Evidence of oxidative attenuation of auxin signalling. *J Exp Bot*, 64(9):2629–2639, Jun 2013.

[73] Ales Pencík, Biljana Simonovik, Sara V. Petersson, Eva Henyková, Sibu Simon, Kathleen Greenham, Yi Zhang, Mariusz Kowalczyk, Mark Estelle, Eva Zazímalová, Ondrej Novák, Göran Sandberg, and Karin Ljung. Regulation of auxin homeostasis and gradients in arabidopsis roots through the formation of the indole-3-acetic acid catabolite 2-oxindole-3-acetic acid. *Plant Cell*, 25(10):3858–3870, Oct 2013.

[74] F. Samson, V. Brunaud, S. Balzergue, B. Dubreucq, L. Lepiniec, G. Pelletier, M. Caboche, and A. Lecharny. Flagdb/fst: a database of mapped flanking insertion sites (fsts) of arabidopsis thaliana t-dna transformants. *Nucleic Acids Res*, 30(1):94–97, Jan 2002.

[75] Allen Sessions, Ellen Burke, Gernot Presting, George Aux, John McElver, David Patton, Bob Dietrich, Patrick Ho, Johana Bacwaden, Cynthia Ko, Joseph D. Clarke, David Cotton, David Bullis, Jennifer Snell, Trini Miguel, Don Hutchison, Bill Kimmerly, Theresa Mitzel, Fumiaki Katagiri, Jane Glazebrook, Marc Law, and Stephen A. Goff. A high-throughput arabidopsis reverse genetics system. *Plant Cell*, 14(12):2985–2994, Dec 2002.

[76] José M. Alonso, Anna N. Stepanova, Thomas J. Leisse, Christopher J. Kim, Huaming Chen, Paul Shinn, Denise K. Stevenson, Justin Zimmerman, Pascual Barajas, Rosa Cheuk, Carmelita Gadrinab, Collen Heller, Albert Jeske, Eric Koesema, Cristina C. Meyers, Holly Parker, Lance Prednis, Yasser Ansari, Nathan Choy, Hashim Deen, Michael Geralt, Nisha Hazari, Emily Hom, Meagan Karnes, Celene Mulholland, Ral Ndubaku, Ian Schmidt, Plinio Guzman, Laura Aguilar-Henonin, Markus Schmid, Detlef Weigel, David E. Carter, Trudy Marchand, Eddy Risseeuw, Debra Brogden, Albana Zeko, William L. Crosby, Charles C. Berry, and Joseph R. Ecker. Genome-wide insertional mutagenesis of arabidopsis thaliana. *Science*, 301(5633):653–657, Aug 2003.

[77] L. Guarente. Synthetic enhancement in gene interaction: a genetic tool come of age. *Trends Genet*, 9(10):362–366, Oct 1993.

[78] J. Hodgkin. *Genetic suppression*, volume 1-13. Wormbook, 2005.

[79] Youfa Cheng, Genji Qin, Xinhua Dai, and Yunde Zhao. Npy genes and agc kinases define two key steps in auxin-mediated organogenesis in arabidopsis. *Proc Natl Acad Sci U S A*, 105(52):21017–21022, Dec 2008.

[80] M. F. Yanofsky, H. Ma, J. L. Bowman, G. N. Drews, K. A. Feldmann, and E. M. Meyerowitz. The protein encoded by the arabidopsis homeotic gene agamous resembles transcription factors. *Nature*, 346(6279):35–39, Jul 1990.

[81] Lucia Daxinger, Ben Hunter, Mazhar Sheikh, Vincent Jauvion, Virginie Gasciolli, Hervé Vaucheret, Marjori Matzke, and Ian Furner. Unexpected silencing effects from t-dna tags in arabidopsis. *Trends Plant Sci*, 13(1):4–6, Jan 2008.

[82] T. Jack, L. Sieburth, and E. Meyerowitz. Targeted misexpression of agamous in whorl 2 of arabidopsis flowers. *Plant J*, 11(4):825–839, Apr 1997.

[83] X. Chen and E. M. Meyerowitz. Hua1 and hua2 are two members of the floral homeotic agamous pathway. *Mol Cell*, 3(3):349–360, Mar 1999.

[84] G. Schindelman, A. Morikami, J. Jung, T. I. Baskin, N. C. Carpita, P. Derbyshire, M. C. McCann, and P. N. Benfey. Cobra encodes a putative gpi-anchored protein, which is polarly localized and necessary for oriented cell expansion in arabidopsis. *Genes Dev*, 15(9):1115–1127, May 2001.

[85] Jae-Heung Ko, Jeong Hoe Kim, Sastry S. Jayanty, Gregg A. Howe, and Kyung-Hwan Han. Loss of function of cobra, a determinant of oriented cell expansion, invokes cellular defence responses in arabidopsis thaliana. *J Exp Bot*, 57(12):2923–2936, 2006.

[86] R. A. Brink, E. D. Styles, and J. D. Axtell. Paramutation: directed genetic change. paramutation occurs in somatic cells and heritably alters the functional state of a locus. *Science*, 159(3811):161–170, Jan 1968.

[87] A. P. Wolffe and M. A. Matzke. Epigenetics: regulation through repression. *Science*, 286(5439):481–486, Oct 1999.

[88] Karl F Erhard, Jr, Jennifer L. Stonaker, Susan E. Parkinson, Jana P. Lim, Christopher J. Hale, and Jay B. Hollick. Rna polymerase iv functions in paramutation in zea mays. *Science*, 323(5918):1201–1205, Feb 2009.

[89] Vicki L. Chandler. Paramutation's properties and puzzles. *Science*, 330(6004):628–629, Oct 2010.

[90] Jae Bok Heo and Sibum Sung. Vernalization-mediated epigenetic silencing by a long intronic noncoding rna. *Science*, 331(6013):76–79, Jan 2011.

[91] E Wassim Chehab, Se Kim, Tatyana Savchenko, Daniel Kliebenstein, Katayoon Dehesh, and Janet Braam. Intronic t-dna insertion renders arabidopsis opr3 a conditional jasmonic acid-producing mutant. *Plant Physiol*, 156(2):770–778, Jun 2011.

[92] Le Cong, F Ann Ran, David Cox, Shuailiang Lin, Robert Barretto, Naomi Habib, Patrick D. Hsu, Xuebing Wu, Wenyan Jiang, Luciano A. Marraffini, and Feng Zhang. Multiplex genome engineering using crispr/cas systems. *Science*, 339(6121):819–823, Feb 2013.

[93] Prashant Mali, Luhan Yang, Kevin M. Esvelt, John Aach, Marc Guell, James E. DiCarlo, Julie E. Norville, and George M. Church. Rna-guided human genome engineering via cas9. *Science*, 339(6121):823–826, Feb 2013.

[94] Dali Li, Zhongwei Qiu, Yanjiao Shao, Yuting Chen, Yuting Guan, Meizhen Liu, Yongmei Li, Na Gao, Liren Wang, Xiaoling Lu, Yongxiang Zhao, and Mingyao Liu. Heritable gene targeting in the mouse and rat using a crispr-cas system. *Nat Biotechnol*, 31(8):681–683, Aug 2013.

[95] Wei Li, Fei Teng, Tianda Li, and Qi Zhou. Simultaneous generation and germline transmission of multiple gene mutations in rat using crispr-cas systems. *Nat Biotechnol*, 31(8):684–686, Aug 2013.

[96] Nannan Chang, Changhong Sun, Lu Gao, Dan Zhu, Xiufei Xu, Xiaojun Zhu, Jing-Wei Xiong, and Jianzhong Jeff Xi. Genome editing with rna-guided cas9 nuclease in zebrafish embryos. *Cell Res*, 23(4):465–472, Apr 2013.

[97] Woong Y. Hwang, Yanfang Fu, Deepak Reyon, Morgan L. Maeder, Shengdar Q. Tsai, Jeffry D. Sander, Randall T. Peterson, J-R Joanna Yeh, and J Keith Joung. Efficient genome editing in zebrafish using a crispr-cas system. *Nat Biotechnol*, 31(3):227–229, Mar 2013.

[98] Changchun Chen, Lorenz A. Fenk, and Mario de Bono. Efficient genome editing in caenorhabditis elegans by crispr-targeted homologous recombination. *Nucleic Acids Res*, 41(20):e193, Nov 2013.

[99] Xingjie Ren, Jin Sun, Benjamin E. Housden, Yanhui Hu, Charles Roesel, Shuailiang Lin, Lu-Ping Liu, Zhihao Yang, Decai Mao, Lingzhu Sun, Qujie Wu, Jun-Yuan Ji, Jianzhong Xi, Stephanie E. Mohr, Jiang Xu, Norbert Perrimon, and Jian-Quan Ni. Optimized gene editing technology for drosophila melanogaster using germ line-specific cas9. *Proc Natl Acad Sci U S A*, 110(47):19012–19017, Nov 2013.

[100] James E. DiCarlo, Julie E. Norville, Prashant Mali, Xavier Rios, John Aach, and George M. Church. Genome engineering in saccharomyces cerevisiae using crispr-cas systems. *Nucleic Acids Res*, 41(7):4336–4343, Apr 2013.

[101] Zhengyan Feng, Botao Zhang, Wona Ding, Xiaodong Liu, Dong-Lei Yang, Pengliang Wei, Fengqiu Cao, Shihua Zhu, Feng Zhang, Yanfei Mao, and Jian-Kang Zhu. Efficient genome editing in plants using a crispr/cas system. *Cell Res*, 23(10):1229–1232, Oct 2013.

[102] Jin Miao, Dongshu Guo, Jinzhe Zhang, Qingpei Huang, Genji Qin, Xin Zhang, Jianmin Wan, Hongya Gu, and Li-Jia Qu. Targeted mutagenesis in rice using crispr-cas system. *Cell Res*, 23(10):1233–1236, Oct 2013.

[103] Qiwei Shan, Yanpeng Wang, Jun Li, Yi Zhang, Kunling Chen, Zhen Liang, Kang Zhang, Jinxing Liu, Jianzhong Jeff Xi, Jin-Long Qiu, and Caixia Gao. Targeted genome modification of crop plants using a crispr-cas system. *Nat Biotechnol*, 31(8):686–688, Aug 2013.

[104] Rachel E. Haurwitz, Martin Jinek, Blake Wiedenheft, Kaihong Zhou, and Jennifer A. Doudna. Sequence- and structure-specific rna processing by a crispr endonuclease. *Science*, 329(5997):1355–1358, Sep 2010.

[105] C. A. Oleykowski, C. R. Bronson Mullins, A. K. Godwin, and A. T. Yeung. Mutation detection using a novel plant endonuclease. *Nucleic Acids Res*, 26(20):4597–4602, Oct 1998.

[106] W. G. Scott, J. B. Murray, J. R. Arnold, B. L. Stoddard, and A. Klug. Capturing the structure of a catalytic rna intermediate: the hammerhead ribozyme. *Science*, 274(5295):2065–2069, Dec 1996.

[107] S. Nakano, D. M. Chadalavada, and P. C. Bevilacqua. General acid-base catalysis in the mechanism of a hepatitis delta virus ribozyme. *Science*, 287(5457):1493–1497, Feb 2000.

[108] H. W. Pley, K. M. Flaherty, and D. B. McKay. Three-dimensional structure of a hammerhead ribozyme. *Nature*, 372(6501):68–74, Nov 1994.

[109] A. R. Ferré-D'Amaré, K. Zhou, and J. A. Doudna. Crystal structure of a hepatitis delta virus ribozyme. *Nature*, 395(6702):567–574, Oct 1998.

[110] Jong-Eun Park, Inha Heo, Yuan Tian, Dhirendra K. Simanshu, Hyeshik Chang, David Jee, Dinshaw J. Patel, and V Narry Kim. Dicer recognizes the 5' end of rna for efficient and accurate processing. *Nature*, 475(7355):201–205, Jul 2011.

[111] SC Walker JM Avis, GL Conn. *Recombinant and In Vitro RNA Synthesis: Methods and Protocols*, chapter Cis-acting ribozymes for the production of RNA in vitro transcripts with defined 5' and 3' ends, pages 83–98. Springer Science, 2012.

[112] A M Jones. Auxin-binding proteins. *Annual Review of Plant Physiology and Plant Molecular Biology*, 45(1):393–420, 1994.

[113] Eui-Jeon Woo, Jacqueline Marshall, James Bauly, Jin-Gui Chen, Michael Venis, Richard M. Napier, and Richard W. Pickersgill. Crystal structure of auxin-binding protein 1 in complex with auxin. *EMBO J*, 21(12):2877–2885, Jun 2002.

[114] J. G. Chen, H. Ullah, J. C. Young, M. R. Sussman, and A. M. Jones. Abp1 is required for organized cell elongation and division in arabidopsis embryogenesis. *Genes Dev*, 15(7):902–911, Apr 2001.

[115] Xu Chen, Laurie Grandont, Hongjiang Li, Robert Hauschild, Sébastien Paque, Anas Abuzeineh, Hana Rakusová, Eva Benkova, Catherine Perrot-Rechenmann, and Jiří Friml. Inhibition of cell expansion by rapid abp1-mediated auxin effect on microtubules. *Nature*, 516(7529):90–93, Dec 2014.

[116] Xu Chen, Satoshi Naramoto, Stéphanie Robert, Ricardo Tejos, Christian Löfke, Deshu Lin, Zhenbiao Yang, and Jiří Friml. Abp1 and rop6 gtpase signaling regulate clathrin-mediated endocytosis in arabidopsis roots. *Curr Biol*, 22(14):1326–1332, Jul 2012.

[117] Stéphanie Robert, Jürgen Kleine-Vehn, Elke Barbez, Michael Sauer, Tomasz Paciorek, Pawel Baster, Steffen Vanneste, Jing Zhang, Sibu Simon, Milada Čovanová, Kenichiro Hayashi, Pankaj Dhonukshe, Zhenbiao Yang, Sebastian Y. Bednarek, Alan M. Jones, Christian Luschnig, Fernando Aniento, Eva Zažímalová, and Jiří Friml. Abp1 mediates auxin inhibition of clathrin-dependent endocytosis in arabidopsis. *Cell*, 143(1):111–121, Oct 2010.

[118] Alexandre Tromas, Sébastien Paque, Vérène Stierlé, Anne-Laure Quettier, Philippe Muller, Esther Lechner, Pascal Genschik, and Catherine Perrot-Rechenmann. Auxin-binding protein 1 is a negative regulator of the scf(tir1/afb) pathway. *Nat Commun*, 4:2496, 2013.

[119] Tongda Xu, Ning Dai, Jisheng Chen, Shingo Nagawa, Min Cao, Hongjiang Li, Zimin Zhou, Xu Chen, Riet De Rycke, Hana Rakusová, Wuyi Wang, Alan M. Jones, Jiří Friml, Sara E. Patterson, Anthony B. Bleecker, and Zhenbiao Yang. Cell surface abp1-tmk auxin-sensing complex activates rop gtpase signaling. *Science*, 343(6174):1025–1028, Feb 2014.

[120] Tongda Xu, Mingzhang Wen, Shingo Nagawa, Ying Fu, Jin-Gui Chen, Ming-Jing Wu, Catherine Perrot-Rechenmann, Jiří Friml, Alan M. Jones, and Zhenbiao Yang. Cell surface- and rho gtpase-based auxin signaling controls cellular interdigitation in arabidopsis. *Cell*, 143(1):99–110, Oct 2010.

[121] Nils Braun, Joanna Wyrzykowska, Philippe Muller, Karine David, Daniel Couch, Catherine Perrot-Rechenmann, and Andrew J. Fleming. Conditional repression of auxin binding protein1 reveals that it coordinates cell division and cell expansion during postembryonic shoot development in arabidopsis and tobacco. *Plant Cell*, 20(10):2746–2762, Oct 2008.

[122] Sébastien Paque, Grégory Mouille, Laurie Grandont, David Alabadí, Cyril Gaertner, Arnaud Goyallon, Philippe Muller, Catherine Primard-Brisset, Rodnay Sormani, Miguel A. Blázquez, and Catherine Perrot-Rechenmann. Auxin binding protein1 links cell wall remodeling, auxin signaling, and cell expansion in arabidopsis. *Plant Cell*, 26(1):280–295, Jan 2014.

[123] Karine M. David, Daniel Couch, Nils Braun, Spencer Brown, Jeanne Grosclaude, and Catherine Perrot-Rechenmann. The auxin-binding protein 1 is essential for the control of cell cycle. *Plant J*, 50(2):197–206, Apr 2007.

[124] Chao Wang, Xu Yan, Qian Chen, Nan Jiang, Wei Fu, Bojun Ma, Jianzhong Liu, Chuanyou Li, Sebastian Y. Bednarek, and Jianwei Pan. Clathrin light chains regulate clathrin-mediated trafficking, auxin signaling, and development in arabidopsis. *Plant Cell*, 25(2):499–516, Feb 2013.

[125] Nihal Dharmasiri, Sunethra Dharmasiri, and Mark Estelle. The f-box protein tir1 is an auxin receptor. *Nature*, 435(7041):441–445, May 2005.

[126] Xu Tan, Luz Irina A. Calderon-Villalobos, Michal Sharon, Changxue Zheng, Carol V. Robinson, Mark Estelle, and Ning Zheng. Mechanism of auxin perception by the tir1 ubiquitin ligase. *Nature*, 446(7136):640–645, Apr 2007.

[127] Youfa Cheng, Genji Qin, Xinhua Dai, and Yunde Zhao. Npy1, a btb-nph3-like protein, plays a critical role in auxin-regulated organogenesis in arabidopsis. *Proc Natl Acad Sci U S A*, 104(47):18825–18829, Nov 2007.

[128] Yangbin Gao and Yunde Zhao. Self-processing of ribozyme-flanked rnas into guide rnas in vitro and in vivo for crispr-mediated genome editing. *Journal of Integrative Plant Biology*, 56(4):343–349, 2014.

[129] Alexandre Tromas, Nils Braun, Philippe Muller, Tatyana Khodus, Ivan A. Paponov, Klaus Palme, Karin Ljung, Ji-Young Lee, Philip Benfey, James A H. Murray, Ben Scheres, and Catherine Perrot-Rechenmann. The auxin binding protein 1 is required for differential auxin responses mediating root growth. *PLoS One*, 4(9):e6648, 2009.

[130] Yunus Effendi, Steffen Rietz, Urs Fischer, and Günther F E. Scherer. The heterozygous abp1/abp1 insertional mutant has defects in functions requiring polar auxin transport and in regulation of early auxin-regulated genes. *Plant J*, 65(2):282–294, Jan 2011.

[131] Yunus Effendi, Noel Ferro, Corinna Labusch, Markus Geisler, and Günther F E. Scherer. Complementation of the embryo-lethal t-dna insertion mutant of auxin-binding-protein 1 (abp1) with abp1 point mutated versions reveals crosstalk of abp1 and phytochromes. *J Exp Bot*, 66(1):403–418, Jan 2015.

[132] Jisheng Chen and Zhenbiao Yang. Novel abp1-tmk auxin sensing system controls rop gtpase-mediated interdigitated cell expansion in arabidopsis. *Small GTPases*, page e29711, Jun 2014.

[133] C. E. Collett, N. P. Harberd, and O. Leyser. Hormonal interactions in the control of arabidopsis hypocotyl elongation. *Plant Physiol*, 124(2):553–562, Oct 2000.

[134] Yunus Effendi, Alan M. Jones, and Günther F E. Scherer. Auxin-binding-protein1 (abp1) in phytochrome-b-controlled responses. *J Exp Bot*, 64(16):5065–5074, Nov 2013.

[135] C. Lincoln, J. H. Britton, and M. Estelle. Growth and development of the axr1 mutants of arabidopsis. *Plant Cell*, 2(11):1071–1080, Nov 1990.

[136] M. Löbler and D. Klämbt. Auxin-binding protein from coleoptile membranes of corn (zea mays l.). ii. localization of a putative auxin receptor. *J Biol Chem*, 260(17):9854–9859, Aug 1985.

[137] Fatma O. Kok, Masahiro Shin, Chih-Wen Ni, Ankit Gupta, Ann S. Grosse, Andreas van Impel, Bettina C. Kirchmaier, Josi Peterson-Maduro, George Kourkoulis, Ira Male, Dana F. DeSantis, Sarah Sheppard-Tindell, Lwaki Ebarasi, Christer Betsholtz, Stefan Schulte-Merker, Scot A. Wolfe, and Nathan D. Lawson. Reverse genetic screening reveals poor correlation between morpholino-induced and mutant phenotypes in zebrafish. *Dev Cell*, 32(1):97–108, Jan 2015.

[138] Stephen J. Robinson, Lily H. Tang, Brent Ag Mooney, Sheldon J. McKay, Wayne E. Clarke, Matthew G. Links, Steven Karcz, Sharon Regan, Yun-Yun Wu, Margaret Y. Gruber, Dejun Cui, Min Yu, and Isobel A P. Parkin. An archived activation tagged population of arabidopsis thaliana to facilitate forward genetics approaches. *BMC Plant Biol*, 9:101, 2009.

[139] L. Gälweiler, C. Guan, A. Müller, E. Wisman, K. Mendgen, A. Yephremov, and K. Palme. Regulation of polar auxin transport by atpin1 in arabidopsis vascular tissue. *Science*, 282(5397):2226–2230, Dec 1998.

[140] Ottoline Leyser. Auxin distribution and plant pattern formation: how many angels can dance on the point of pin? *Cell*, 121(6):819–822, Jun 2005.

[141] Qingguo Chen, Xinhua Dai, Henrique De-Paoli, Youfa Cheng, Yumiko Takebayashi, Hiroyuki Kasahara, Yuji Kamiya, and Yunde Zhao. Auxin overproduction in shoots cannot rescue auxin deficiencies in arabidopsis roots. *Plant Cell Physiol*, 55(6):1072–1079, Jun 2014.

[142] Bing Wang, Jinfang Chu, Tianying Yu, Qian Xu, Xiaohong Sun, Jia Yuan, Guosheng Xiong, Guodong Wang, Yonghong Wang, and Jiayang Li. Tryptophan-independent auxin biosynthesis contributes to early embryogenesis in arabidopsis. *Proc Natl Acad Sci U S A*, 112(15):4821–4826, Apr 2015.

[143] Takanori Yoshikawa, Momoyo Ito, Tsuyoshi Sumikura, Akira Nakayama, Takeshi Nishimura, Hidemi Kitano, Isomaro Yamaguchi, Tomokazu Koshiba, Ken-Ichiro Hibara, Yasuo Nagato, and Jun-Ichi Itoh. The rice fish bone gene encodes a tryptophan aminotransferase, which affects pleiotropic auxin-related processes. *Plant J*, 78(6):927–936, Jun 2014.

[144] Yunde Zhao. Auxin biosynthesis: a simple two-step pathway converts tryptophan to indole-3-acetic acid in plants. *Mol Plant*, 5(2):334–338, Mar 2012.

[145] M. Delarue, E. Prinsen, H. V. Onckelen, M. Caboche, and C. Bellini. Sur2 mutations of arabidopsis thaliana define a new locus involved in the control of auxin homeostasis. *Plant J*, 14(5):603–611, Jun 1998.

[146] L. Comai and T. Kosuge. Cloning characterization of iaam, a virulence determinant of pseudomonas savastanoi. *J Bacteriol*, 149(1):40–46, Jan 1982.

[147] C. Camilleri and L. Jouanin. The tr-dna region carrying the auxin synthesis genes of the agrobacterium rhizogenes agropine-type plasmid pria4: nucleotide sequence analysis and introduction into tobacco plants. *Mol Plant Microbe Interact*, 4(2):155–162, 1991.

[148] Bruno Mezzetti, Lucia Landi, Tiziana Pandolfini, and Angelo Spena. The defh9-iaam auxin-synthesizing gene increases plant fecundity and fruit production in strawberry and raspberry. *BMC Biotechnol*, 4:4, Mar 2004.

[149] S. Eklöf, C. Astot, F. Sitbon, T. Moritz, O. Olsson, and G. Sandberg. Transgenic tobacco plants co-expressing agrobacterium iaa and ipt genes have wild-type hormone levels but display both auxin- and cytokinin-overproducing phenotypes. *Plant J*, 23(2):279–284, Jul 2000.

[150] Stephan Pollmann, Petra Düchting, and Elmar W. Weiler. Tryptophan-dependent indole-3-acetic acid biosynthesis by 'iaa-synthase' proceeds via indole-3-acetamide. *Phytochemistry*, 70(4):523–531, Mar 2009.

[151] Stephan Pollmann, Daniel Neu, and Elmar W. Weiler. Molecular cloning and characterization of an amidase from arabidopsis thaliana capable of converting indole-3-acetamide into the plant growth hormone, indole-3-acetic acid. *Phytochemistry*, 62(3):293–300, Feb 2003.

[152] Yangbin Gao, Yi Zhang, Da Zhang, Xinhua Dai, Mark Estelle, and Yunde Zhao. Auxin binding protein 1 (abp1) is not required for either auxin signaling or arabidopsis development. *Proceedings of the National Academy of Sciences*, 112(7):2275–2280, 2015.

[153] S. J. Clough and A. F. Bent. Floral dip: a simplified method for agrobacterium-mediated transformation of arabidopsis thaliana. *Plant J*, 16(6):735–743, Dec 1998.

[154] R. A. Jefferson, T. A. Kavanagh, and M. W. Bevan. Gus fusions: beta-glucuronidase as a sensitive and versatile gene fusion marker in higher plants. *EMBO J*, 6(13):3901–3907, Dec 1987.

[155] Phillip L. Searle. The berthelot or indophenol reaction and its use in the analytical chemistry of nitrogen. a review. *Analyst*, 109:549–568, 1984.